

Photoisomerization versus Photodissociation of a Chiral Fluoroethylene Derivative. Quantum Chemistry, Dynamics and Control

Dissertation

zur Erlangung des akademischen Grades doctor rerum naturalium
(Dr. rer. nat.)



seit 1558

vorgelegt dem Rat der Chemisch-Geowissenschaftlichen Fakultät der
Friedrich-Schiller-Universität Jena

von Dipl.-Chem. Daniel Kinzel
geboren am 02.10.1982 in Erfurt, Deutschland

Gutachter:

1. Prof. Dr. Leticia González, Universität Wien, Österreich
2. apl. Prof. Dr. Michael Schmitt, Friedrich-Schiller-Universität Jena, Deutschland
3. Prof. Dr. Oliver Kühn, Universität Rostock, Deutschland

Tag der öffentlichen Verteidigung: 24.04.2013

To my family.

Abstract

In the following thesis, (4-methylcyclohexylidene) fluoromethane (4MCF) has been studied by means of quantum chemical and dynamical methods. As a model for a light-triggered molecular rotor or switch, the photochemistry of 4MCF upon irradiation into the spectroscopic $\pi\pi^*$ state in particular, has been the subject of investigation.

First, the photoisomerization around the C-C double bond and the competing elimination of hydrogen fluoride in 4MCF have been studied. Both reactions are mediated by twisted conical intersections (CoIns) around the C-C bond. Coupled potential energy surfaces (PESs) for the electronic ground state and first bright excited state of $\pi\pi^*$ character are calculated using the CASSCF method along two reaction coordinates: the torsion around the C-C bond and the concerted HF-dissociation. Wavepacket dynamics on the coupled surfaces suggest that after light irradiation, torsion in the $\pi\pi^*$ state dominates over HF dissociation. However, a spurious mixing of the $\pi\pi^*$ state with a $\pi\sigma^*$ configuration has been identified.

Consequently, more elaborated multiconfigurational *ab initio* calculations of the excited states and PESs of 4MCF provide evidence that $\pi\sigma^*$ states play an important role in the abstraction of HF. It is shown that more than the ground and valence $\pi\pi^*$ states are necessary to correctly describe the relaxation of 4MCF upon excitation to the bright $\pi\pi^*$ state. A CoIn between the $\pi\sigma^*$ and $\pi\pi^*$ states has been identified at the Franck-Condon geometry, which makes dissociation of HF, but also of individual atomic H or F, possible in the electronic excited state. This conclusion is different from all the previous studies on ethylenic systems where dissociation is postulated as a ground state reaction.

In order to unravel the most probable relaxation path for 4MCF, *ab initio* molecular dynamics (AIMD) simulations have been performed using multiconfigurational CASSCF on-the-fly calculations. The simulations showed that a preferential dissociation of atomic hydrogen is taking place after exciting population to the bright $\pi\pi^*$ state. This state is then strongly mixed with $\pi\sigma^*$ states, allowing dissociation in the electronic excited state before deactivation to the ground state occurs. A minor amount of trajectories experiences F-dissociation, followed by pyramidalization of the planar sp^2 carbons and C-C bond rupture. In contrast, the number of trajectories undergoing torsion around the double bond, and therefore *cis-trans* isomerization, is marginal. The H-abstraction reaction is ultrafast, taking place in less than 60 fs.

Henceforth, hydrogen dissociation is an unwanted competing pathway, if a torsional motion around the C-C double bond in 4MCF is to be achieved. It is shown that the excited state H dissociation can be drastically diminished on timescales long enough to initiate a torsion around the C-C double bond using the non-resonant dynamic Stark effect (NRDSE). PESs, dipoles and polarizabilities for the regarded one-dimensional reaction coordinate are calculated within the CASSCF method. The influence of the excitation and the laser control fields is then simulated using quantum dynamical wavepacket dynamics.

Thus, the present thesis shows, that the inclusion of $\pi\sigma^*$ states, besides the ground and spectroscopic $\pi\pi^*$ state, into the electronic structure and dynamical simulations is crucial for the description of the photochemistry in 4MCF, which shows a major relaxation pathway via dissociation of the molecule. Towards a functioning molecular switch or rotor, it could be shown that it is possible to diminish the destroying of 4MCF using the NRDSE upon excitation to the $\pi\pi^*$ state.

Table of Contents

Abstract	i
1 Introduction	1
2 Background on 4MCF	11
3 Methodological Background and Computational Details	15
3.1 Quantum Chemistry	16
3.1.1 Born-Oppenheimer and Potential Energy Surfaces	16
3.1.2 Solution to the Electronic TISE	17
3.2 Quantum Dynamics on Coupled Surfaces	21
3.2.1 Beyond Born-Oppenheimer: Coupled PESs	21
3.2.2 Solution to the Nuclear TDSE in the Presence of External Fields .	23
3.3 <i>Ab initio</i> Molecular Dynamics	27
4 Results	31
4.1 <i>Cis-Trans</i> Photoisomerization vs. HF-Photodissociation in 4MCF	32
4.2 The Role of $\pi\sigma^*$ States in 4MCF	42
4.3 Non-adiabatic Full-dimensional <i>ab initio</i> Molecular Dynamics for 4MCF	57
4.4 Control of Molecular Hydrogen Abstraction in 4MCF. A One-dimensional study	69
5 Summary	81
6 Zusammenfassung	85
References	93
List of Figures	101
List of Abbreviations	103
Acknowledgements	105
Curriculum vitae	107
List of Publications	111
Selbständigkeitserklärung and “Documentation of Authorship”	113

1 Introduction

“Chemistry is the science of substances - their structure, their properties, and the reactions that change them into other substances” [1]. Linus Pauling’s simple definition shows that, ever since, mankind is using chemistry to support its own development. Knowing how a certain substance is behaving under certain conditions made it possible to create, e.g. extracting metal from ores, making ceramics or fermenting of plants to make alcohol, to mention only a few. Although the amount of knowledge, that early civilizations must have had, is considerable, the underlying chemical processes were not known, and hence the available knowledge could only be considered as practical rules. Just the idea that a particular substance could be converted into another one, however, permitted humans to search for better methods and procedures that help to maximize the outcome of a desired product, i.e. to control the process. Nowadays, scientists have developed a great variety of methods, that give deep insights into the structure and properties of atoms and molecules. With this information at hand, a vast number of synthetic methodologies could be developed in order to create any kind of desired chemical species. The measure of scientific and technological progress, however, is the ability to control the outcome of all of these processes of interest [2].

The outcome of chemical reactions in particular is influenced by many parameters. On the macroscopic level, a chemical reaction is governed by the reaction equilibrium between the reactants and products formed. On that level, temperature, pressure or concentrations of the involved species can be adjusted in order to increase the yield of kinetically favoured products, while unwanted side products can be diminished. One possibility for yielding even thermodynamically unfavoured products is the use of specialized catalysts or enzymes, which control the reaction at the microscopic level. Both macroscopic and microscopic control depend on the statistical behaviour of the many-molecule system, i.e. collisions between the reactant molecules and between reactant and solvent and/or catalyst molecules. These control schemes are called passive control, since the role of the experimenter is solely to initiate the reaction under certain conditions, without having control over the evolution of the chemical species in a molecular dynamics time scale [2].

Using electro-magnetic radiation, i.e. light, offers a different and new way of understanding and controlling chemical reactions on a molecular time scale. The development and advances of laser technologies gave rise to ultra-short laser pulses that interact with a molecule within the time scale of nuclear motion, usually taking place within pico- or even femtoseconds ($1 \text{ ps} = 10^{-12} \text{ s}$ to $1 \text{ fs} = 10^{-15} \text{ s}$). Due to the temporal structure of ultra-short pulses, they can be used to monitor the real-time dynamics and the nu-

clear changes that occur within a chemical reaction, giving rise to a new research field called *femtosecond chemistry* [3, 4], and leading to the Nobel Prize for Ahmed Zewail in 1999 [5]. In the same way reaction dynamics can be monitored using laser pulses, it is also possible to use these pulses as a reactant and thus actively control the outcome of the chemical reaction itself. In particular, ultrafast processes, such as an ultrafast radiationless decay through a conical intersection (CoIn), can be now viewed and controlled within the regime of femtosecond chemistry. In general, every molecular system can be modified by a molecule-light interaction to yield a desired product, which is due to the many parameters of the laser pulse, such as color, phase, amplitude or polarization, allowing the pulse to be formed in almost any arbitrary shape. The vast possibilities of control schemes determining reaction outcomes, using selectively shaped pulses, have been addressed by many theories and experimental techniques, see e.g. [2, 6, 7] and review articles [8, 9, 10, 11, 12, 13].

Important Control Strategies: The simplest and most intuitive approach on how to use laser light to manipulate a certain chemical reaction is the mode-selective scheme. Here, the vibrational mode of the bond of interest is selectively excited by a laser with the frequency of that mode until the bond breaks. This approach can be applicable under favourable conditions [14]. Especially in large molecules, however, the photon energy, that the pulse is giving to a particular stretching mode, can quickly redistribute into the rest of the molecule via internal vibrational relaxation. Hence, mode-selective chemistry can be achieved only in cases where the bond breaking occurs faster than the internal heating of the molecule [15].

The term *coherent control of reactions* has been introduced by Brumer and Shapiro [6, 8], who proposed a control scheme which is based on the quantum nature of molecules, i.e. the wave-matter duality. The idea behind this approach is the manipulation of constructive and destructive quantum interferences that arise when the desired final states are degenerate. These states are then coupled by two continuous wave lasers with different frequencies that excite population from the initial state to the final states. Depending on the relative phase of the employed lasers, the phase of the laser interferes either constructively or destructively with the phase of the excited wavepacket in each final state, which leads to different branching behaviour of the total wavepacket at the point of degeneracy, giving rise to different product ratios. An illustration of such a process is given in Figure 1a), where the formation of one photoproduct is enhanced. In the original scheme, an infra-red (IR) pulse populates the vibrational ground as well as excited state. The population in the different vibrational states are then excited with the two lasers, with different frequencies, ω_1 and ω_2 , matching the energy difference to the final states. By adapting the

relative phase of the lasers, an excess of either product P_1 or P_2 can be created. The original scheme was simplified later on, in a way that no preliminary pulse is needed anymore. Instead, the interaction of the initial state with the final states originates from one-photon and three-photon processes [16]. Experimentalists were able to verify the capability of the Brumer-Shapiro control scheme, e.g. by controlling of photodissociation of hydrogen iodide into a proton and iodide versus atomic hydrogen and iodine [17].

In contrast to the Brumer-Shapiro quantum interference control, the *pump-dump* control scheme introduced by Tannor, Rice and Kosloff [18, 19] is performed in the time-domain rather than through phase adjusting in the frequency-domain. Additionally, instead of using continuous wave sources, here, a sequence of ultrashort laser pulses is employed, whose relative time delay is adapted to steer the evolution of a wavepacket. In general, when products are separated from the reactants by barriers in the electronic ground state, one can excite a wavepacket to an electronic excited state, which then starts to propagate on this excited state. The moving wavepacket can be dumped back after a certain time delay on the other side of the barrier to reach the product side. In cases where two or more products can be formed, the time delay between the exciting pulse (pump pulse) and the dump pulse determines which product is produced. For example, the dissociation of a model molecule ABC into either $AB + C$ or $A + BC$ can be controlled using such a pump-dump scheme, illustrated in Figure 1b). After transferring population to the $[ABC]^*$ excited state using an ultraviolet (UV) pulse, the second pulse dumps population back to the ground state. Dumping at a delay time t_1 results in products $AB + C$ and dumping at time t_2 after the pump pulse results in products $A + BC$. With the availability of femtosecond laser pulses, the pump-dump control scheme could be demonstrated experimentally in several instances, e.g. in the photofragmentation of the Na_2 -dimer [20, 21] or the reaction $Xe + I_2 \rightarrow XeI + I$ [22].

Another control strategy is to make use of the Stark effect [23], which originally describes the splitting of certain (degenerate) spectral lines in the presence of an electric field. In the above mentioned control schemes, control is achieved by manipulating the transfer of population between the multi-dimensional potential energy surfaces (PESs), that are spanned by the 3N-6 degrees of freedom for a non-linear molecule. The PESs, however, are not changed during these processes. Using a non-resonant (i.e. no population transfer occurs between PESs) strong laser field, the molecular potentials can be considerably distorted to yield dressed states or light-induced potentials (LIPS) [24]. Hence, the whole landscape, in which nuclear motion can take place, can be changed according to the field applied. This control scheme is especially interesting when CoIns, i.e. intersecting or degenerate PESs, play a major role in the reaction dynamics; points at which the wavepacket is usually branching onto different electronic surfaces and into different

directions. A strong field can then be used to split the degeneracy at that particular point (geometry) on the PESs, moving the CoIn, and thus creating a different route for the wavepacket, hence, a different outcome of the reaction (illustrated in Figure 1c). The non-resonant dynamic Stark control scheme could be experimentally demonstrated for a non-adiabatic photochemical reaction, showing substantial changes of reaction product ratios in the dissociation of IBr compared to the field-free case [25]. Furthermore, the non-resonant dynamic Stark effect (NRDSE) changes reaction pathways reversibly, and in this way the NRDSE acts as a photonic catalyst.

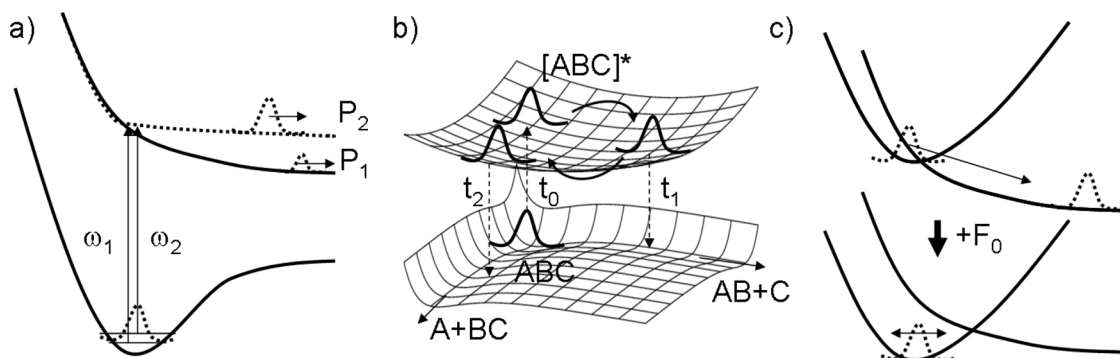


Figure 1: **a)** Brumer-Shapiro control scheme: A preliminary pulse (not shown) excites two vibrational states. From there, the transfer to the two degenerate final states is steered by the relative phase of the two control lasers with frequencies ω_1 and ω_2 ; **b)** Tannor-Rice-Kosloff pump-dump control scheme shown for a molecule ABC: At time t_0 a pump pulse creates a wavepacket in the excited state $[ABC]^*$. A dump pulse at either time t_1 or time t_2 then leads to population transfer to different exit channels in the ground state to produce either $AB + C$ or $A + BC$; **c)** Scheme for the NRDSE in 1D: A state crossing in the unperturbed PESs acts as a funnel for fast population transfer to a different state. Employing a strong field moves the crossing to another point on the PESs, creating a barrier for the fast decay. (For all cases wavepacket movement is indicated.)

In all of the above described control schemes control is achieved adapting one single parameter of the light source interacting with the reactants, e.g. the phase, the time delay, or the field amplitude. For all these approaches, exact information of field-free PESs and reaction paths is needed prior to the control experiment in order to adjust the control strategy. In contrast to single parameter control, feedback learning algorithms can be used to search the best laser parameters, that prepare specific products based on fitness information, without knowing the exact reaction path that needs to be manipulated [26]. In such an experimental setup the evaluation of the results of a chemical reaction is done by a detector, e.g. time-of-flight (TOF) mass spectrometer. According to the experimenter's target, the detector sends a feedback signal to a computer, which adjusts all kinds of pulse parameter based on a generic algorithm until the desired spec-

trogram is measured. For further details and examples, see e.g. [12, 27, 28, 29, 30]. The theoretical and purely mathematical counterpart to experimental feedback algorithms is the optimal control theory (OCT). Here, the control aim is a predefined target wavefunction at a specified final time. By using quantum-dynamical propagation methods, which solve the time-dependent Schrödinger equation, the overlap of a propagated initial wavefunction and the final target wavefunction is maximized iteratively by changing electric field parameters. OCT has been developed by Tannor, Kosloff, Rice *et al.* [18, 31] and by Rabitz *et al.* [32, 33]. For a review, further details and references the reader shall be referred to e.g. Ref. [6].

In the present thesis only single parameter control strategies will be considered since detailed knowledge of PESs and reaction paths can be obtained comparably easily in the frame of theoretical chemistry.

Molecular Rotors and Switches: As seen above, very often, the target of control is the branching of a wavepacket into different product species. However, in most of the above given examples the controlled reactions are irreversible, e.g. in photodissociation processes. Another prominent control target is photoisomerization since, commonly, isomerizations are reversible processes, and, in this way, (photon) energy can be transformed into molecular motion without destroying the molecule [34]. This property is the basis for molecular engineering in nanotechnology, where molecular switches and rotors are studied [35, 36]. Nowadays, chemists are in the ideal position to develop bottom-up approaches for the construction of nanoscale devices [37] and the shaping of such artificial machines on the molecular level is one of the major challenges in nanoscience [38]. Although functionality of such devices can be triggered in different ways, an interesting source of energy is the use of light. In fact, light-driven rotors and switches hold several advantages compared to chemically driven ones. First, the amount of energy that is put into the system can be controlled very carefully by the wavelength and intensity of the light source. Lasers provide the opportunity of working in extremely short time domains, and, therefore, it should be possible to create switches and rotatory devices that respond equally rapidly. For example, some efforts have been devoted to achieve unidirectional rotation employing femtosecond laser pulses [39]. The second advantage is that light cannot only be used to trigger a reaction, but also to monitor and to identify the outcome through several means of spectroscopy.

Examples for an artificial light driven rotor are the unidirectional rotors introduced by Feringa and co-workers, which were investigated experimentally [40, 41] as well as by means of theoretical chemistry [42, 43, 44]. Here, the photoinduced monodirectional rotation around a central carbon-carbon double bond in a chiral, helical alkene has been

reported. The olefin, also called overcrowded alkene, possesses an axial chirality due to steric hindrances that distort the aromatic plane, which in turn results helicity. In the rotary cycle, two light-induced *cis-trans* isomerizations are each associated with a 180° rotation around the carbon-carbon double bond and are each followed by thermally controlled helicity inversions, which effectively block reverse rotation, and thus ensuring the unidirectionality. Such overcrowded alkenes have also reported in the use as chiroptical switches [35, 45, 46].

Photo-induced torsion about a Carbon-Carbon Double Bond: The rotary cycles in the examples mentioned above contain a *cis-trans* isomerization of a central carbon-carbon double bond. The fact, that this kind of isomerization is utilized for many artificial rotors and switches, is inspired by the most prominent photoinduced process in the animal visual cycle. Here, the key step is the absorption of a photon by the chromophore molecule 11-*cis*-retinal which is embedded in a protein environment. The excited retinal then undergoes a rapid *cis-trans* isomerization, illustrated in Figure 2 [47, 48]. The rearrangement

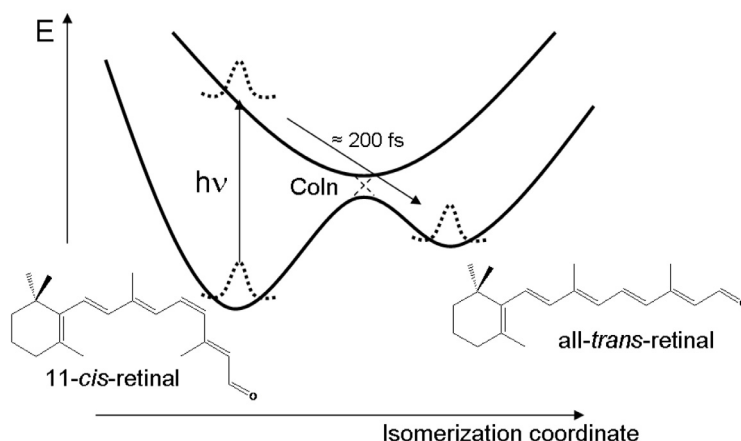


Figure 2: Illustration of the ultrafast light-triggered *cis-trans* isomerization of 11-*cis*-retinal to all-*trans*-retinal along the reaction coordinate mediating through a CoIn between the electronic ground and excited state. Wavepacket movement is indicated.

from 11-*cis*- to the all-*trans* configuration initiates the overall vision process, because the chromophore no longer fits in the protein binding pocket. A cascade of enzyme-catalyzed reactions follows, which, at the end stimulate the optic nerve. The overall visual cycle takes a couple of milliseconds. The *cis-trans* isomerization, however, is accomplished only about 200 fs after the initial absorption of the photon [47]. The involved time and size domains (200 fs and one C-C double bond, respectively) situate the eye vision event in the frame of quantum phenomena. Indeed, the high speed and the high selectivity of the isomerization are attributed to a CoIn between the electronic excited and the ground

state of retinal (schematically shown in Figure 2 in one dimension) leading to an ultrafast radiationless decay of excited population back to the ground state [49, 50]. Consequently, besides inspiring the creation of artificial molecular photon-induced devices, the isomerization of the retinal chromophore continues to attract ongoing interest within modern theoretical chemistry [51, 52] and even has been subject of several laser control studies, e.g. Refs. [53, 54, 55, 56].

Despite the fact, that molecular rotors and switches based on overcrowded alkenes as well as retinal within the natural process of vision seem to be well-functioning devices on a molecular level, an exact portrait of the underlying reaction paths is a very challenging task. Simply due to the size of the systems, an accurate description of the full-dimensional PESs, including excited states, is almost impossible to achieve. Hence, in many cases, one reduces the quantum chemical description solely to the chromophore and, thus, only to the *cis-trans* isomerization about the C-C double bond. The rest of the molecular framework, that is not connected to the central double bond, is assumed not to influence the elementary process of the isomerization itself. Yet, even the simplest system, that models the olefinic chromophore, i.e. ethylene, is very difficult to describe exactly in full-dimensionality.

In contrast to overcrowded alkenes or retinal, in the non-distorted, non-hindered double bond of ethylene, *cis-trans* isomerization occurs symmetrically. Both conformers, that are connected by a torsion of 180° around the C-C double bond, are energetically equal (see Figure 3 and cf. Figure 2). Moreover, after the photoexcitation from the electronic ground state into the optically bright $\pi\pi^*$ state, the wavepacket will move via the negative as well as positive torsion coordinate, τ , with equal results for both pathways, given the periodicity of the potential. Once irradiated, the system rapidly decays via a CoIn between

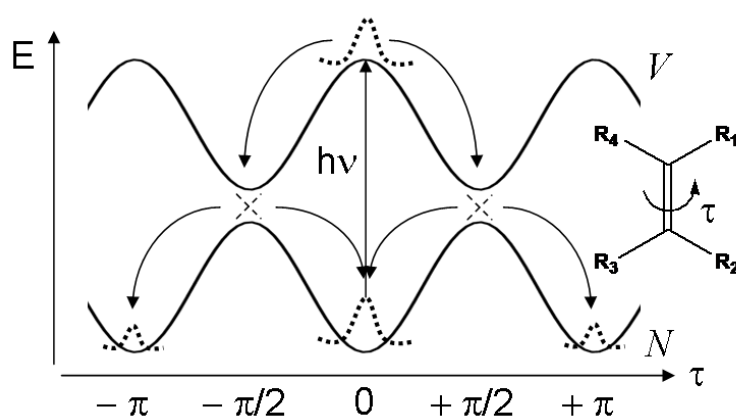


Figure 3: Symmetrical photoisomerization of a double bond. After excitation to the spectroscopic V state, both directions are equally probable. When relaxing to the ground state, N , the situation is analogous. Wavepacket motion and branching is indicated.

the excited or valence state (denoted by V , following Mulliken's notation [57]), and the electronic ground state, N [58, 59]. However, in ethylene, the torsional movement alone is not sufficient to reach the CoIn (see energy gap between excited and ground state at $\tau = 90^\circ$ in Figure 3). Actually, internal conversion between the V and N states of ethylene involves first a C-C stretching, accompanied with the torsion. Then pyramidalization of one of the methylene units [60] or hydrogen migration from one side to the other [59] lead to different CoIns on the multi-dimensional PESs connecting different relaxation pathways. Whereas the latter one is not leading to a reversible *cis-trans* isomerization, it has been pointed out, that the twisted-pyramidalized CoIn serves as the main deactivation channel to the ground state [58, 61, 62] connecting the two conformers. Additionally, more recent six-dimensional quantum dynamical simulations have identified the pyramidalization mode as the bottleneck for the radiationless decay in ethylene [63].

Despite it is tempting to use ethylene as a model for any olefinic system, caution should be taken when different substituents are added to the chromophore. For instance, quantum chemical calculations on fluoroethylene show that the torsion alone (without pyramidalization) is enough to drive the system from the V to the N state [64]. Therefore, the photoreaction dynamics of ethylene derivatives can change very much depending on the specific substituent and its position (see e.g. Ref. [65]).

Besides *cis-trans* isomerization, ethylene, as well as ethylene derivatives, can undergo photoinduced dissociation. Experimentally, it has been observed that both atomic and molecular hydrogen are eliminated in ethylene after irradiation [66, 67]. Similarly, elimination of halogen derivatives has been detected in difluoroethylenes [68, 69] and vinyl chloride [70, 71]. The reported experiments are consistent with the idea that simple olefins first deactivate to the electronic ground state via a CoIn, giving rise to a thermally hot system. The thermal energy, that the system possesses after deactivation, then causes dissociation, and therefore, justifying that classical trajectories in the electronic ground state only have been used to model photodissociation dynamics, e.g. [72, 73, 74, 75, 76]. Nonetheless, like the hydrogen migration, the dissociation pathway is irreversible and, thus, is an unwanted reaction to occur when designing molecular rotors or switches.

Goals and Structure of this Thesis: In this Thesis, (4-methylcyclohexylidene) fluoromethane (4MCF) is studied by means of accurate quantum chemical and dynamical methods. This molecule is a larger fluoroolefin that possesses axial chirality, and hence, its R and S enantiomers are connected by a torsion around the C-C double bond, see Fig. 4. Yet, it is small enough to be able to use high levels of theory in affordable computer time. In a series of papers, 4MCF has been considered as a simple model for a chiral, light-induced molecular rotor or switch [77, 78, 79]. After excitation to the bright

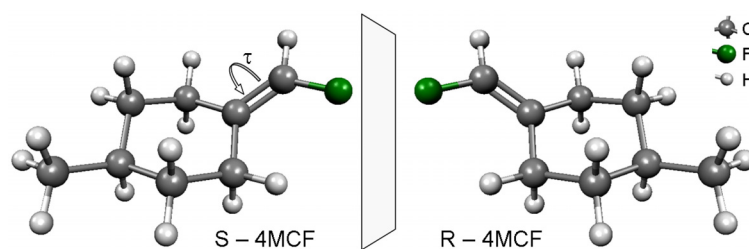


Figure 4: R- and S-enantiomers of 4MCF: mirror images, which are connected by a torsion, τ , around the double bond.

$\pi\pi^*$ state, 4MCF is expected to undergo a torsion of the CHF group around the double bond, giving rise to the two chiral stable isomers. However, similar to smaller substituted ethylenes (especially fluoroethylene), the *cis-trans* isomerization in 4MCF could compete with photodissociation of the hydrogen fluoride (HF) fragment [80], and it will be shown in this thesis, individual atomic hydrogen or atomic fluorine dissociation is at least equally possible. Therefore, the goal of this thesis is to investigate the isomerization versus the dissociation process in 4MCF. To the aim of uncovering the electronic landscape of 4MCF, PESs along the relevant coordinates using high-level quantum chemical *ab initio* calculations (state average CASSCF and multi-state CASPT2), including all electronic states playing a role in these processes, will be calculated. Moreover, dynamical simulations in reduced- as well as in full-dimensionality will be done, in order to reveal the relaxation pathways upon irradiation to the bright $\pi\pi^*$ state. The final target is to achieve an efficient molecular rotor or switch, avoiding photodissociation. Thus, with the knowledge about the PESs and the dynamical behaviour upon excitation, quantum control strategies will be employed in order to achieve controlled isomerization.

The thesis will be structured as follows: In section 2 the background information of the title molecule 4MCF and previous studies on it will be given, followed by a brief description of the quantum chemical and dynamical methods employed to study 4MCF in section 3. The results will be shown in section 4 in form of the article reprints that were published in international peer-reviewed scientific journals. A short summary of the motivation, computational details and results for each article will be given preceding the reprints of that very article. Finally, a summary in section 5 will connect all findings of the individual articles.

2 Background on 4MCF

In this section, the scientific background of the title molecule (4-methylcyclohexylidene) fluoromethane (4MCF) will be presented. The most important experimental and theoretical studies, that focus on 4MCF, and their findings of the last years will be outlined and cited, since these investigations have influenced the motivation and goals of the present thesis to a great extend.

(4-methylcyclohexylidene) fluoromethane, or 1-(fluoromethylene)-4-methyl-cyclohexane according to IUPAC nomenclature, is one of the smallest ethylene derivatives possessing axial chirality. The optical activity is due to dissymmetrically located substituents, i.e. the replacement of one vinyl hydrogen and one of the hydrogen atoms in the 4-position of the cyclohexane ring leads to a chiral system, as it is the case in 4MCF with a methyl in the 4-position and a fluorine atom in the vinyl position. The R and S enantiomers are separated by an intramolecular torsion around the C-C double bond (see Figure 4). Since a torsion implies the breaking of the double bond, both enantiomers are well separated by a high potential barrier on the electronic ground state, and thus, the molecules form stable enantiomers at room temperature, i.e. no spontaneous racemization occurs.

The scheme of the synthesis of a enantiomerically pure 4MCF is shown in Figure 5. It requires as a first step the conversion of the enantiomerically pure α -fluorinated

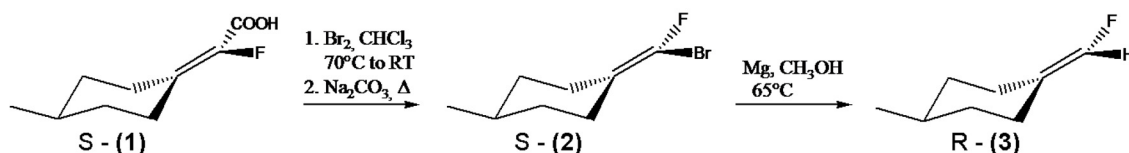


Figure 5: Scheme for the synthesis of R-4MCF

α , β -unsaturated (4-methylcyclohexylidene) fluoroacetic acid, **1**, into the (4-methylcyclohexylidene) bromofluoromethane (**2**) via a bromination-decarboxylative dehydrobromination procedure. The bromofluoro olefin, **2**, is then reduced with magnesium in methanol to give 4MCF, **3**, with an inversion of the original configuration with respect to the acid [81, 82]. Due to the fluorination at one end of the molecule, 4MCF has a high permanent dipole moment, which is the reason that 4MCF is liquid at room temperature with a boiling point of 115-116°C [81]. The recorded UV absorption spectrum identifies a single bright, vibrationally resolved $\pi\pi^*$ excitation around 6.5 eV (190 nm) [81].

In a first theoretical investigation by Kröner and co-workers, 4MCF has served as a model for strategies to selectively separate a racemic mixture into its enantiomers [83]. Based on one-dimensional PESs of N and V states along the torsional coordinate, it has

been shown, that a single linearly polarized laser pulse (IR or UV) can selectively excite one enantiomer from a racemic mixture. Later on, the one-dimensional model has been extended to include pyramidalization of one of the carbons in the double bond [77]. The mechanism for separating the enantiomers could be again demonstrated using nuclear wavepackets propagated on the two-dimensional PESs, calculated with time dependent density functional theory (TD-DFT). Here, the control scheme consists of an enantioselective IR laser pulse, that excites one quantum in the achiral pyramidalization coordinate of one enantiomer. The IR pulse is followed by an enantioselective UV laser pulse that transfers this enantiomer to the electronic excited V state, whereas the counterpart remains in the ground state. In both studies, 4MCF is assumed to be pre-oriented around a fixed axis. Hence, in a subsequent study, the above mentioned control scheme is demonstrated by dynamical simulations in all possible orientations around a fixed axis of the chiral 4MCF [78]. Due to the shown capability to selectively separate the enantiomers of 4MCF, and therefore being able to identify one or the other one, it has been suggested, that 4MCF might serve as a simple but potential chirooptical switch or rotor. For example, a IR+UV pulse control scheme has been successfully employed using the simple TD-DFT PESs of 4MCF to achieve unidirectional rotation of the CHF moiety [79]. Here, first, a few-cycle IR pulse excites the torsional vibration in the oriented 4MCF. Subsequently, a well-timed ultrashort UV pulse induces a transition from the N state to the excited V state with conservation of the angular momentum. As a consequence, the torsional motion is converted into a unidirectional intramolecular rotation, with high angular momentum.

Due to the possibility to construct a functioning small switching device based on 4MCF, some efforts have been devoted to study the detailed electronic structure and possible relaxation paths that accompany with the photoexcitation of 4MCF into the valence $\pi\pi^*$ state. Despite the fact that 4MCF represents a fairly small molecule (in light of accurate theoretical computations), there is one drawback when describing the electronic landscape. Ethylene and its derivatives, generally, show Rydberg states in the vicinity of the optical bright excitation [84], which severely complicates the description of the electronically excited states. In 4MCF, the experimental circular dichroism (CD) spectrum measured by Gedanken *et al.* [81], indeed identifies a low lying $\pi 3s$ Rydberg excitation, energetically below the $\pi\pi^*$ state. Consequently, one part of the study by Schreiber *et al.* [85] focuses on describing the vertical excitation spectrum by identifying valence and Rydberg states by means of multiconfigurational multistate CASPT2 on CASSCF wavefunctions and coupled cluster methods (RI-CC2). It has been found, that for the planar ground-state minimum structure of 4MCF (see Figure 6a), the V state is embedded in the $\pi 3s$, $\pi 3p$ Rydberg excitation series, with the $\pi 3s$ state lying below it. However, the torsion around the C-C double bond destabilizes the Rydberg states very quickly, justify-

ing that in the second part of their study, that is the localization and optimization of CoIns between the V and N states, the description of Rydberg states have been neglected.

Similar to fluoroethylene [64] or ethylene itself (see e.g. Refs. [34, 86, 87]), a series of CoIns between the ground state and the first excited state have been optimized for 4MCF by Schreiber *et al.* [85] (depicted in Fig. 6b) It has to be noted, that all of these

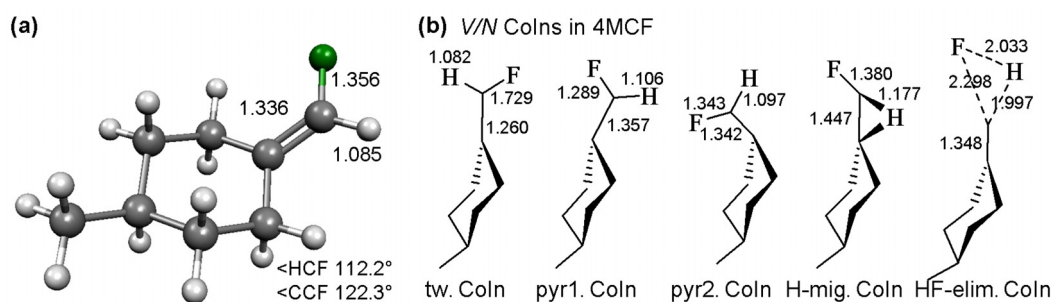


Figure 6: **a)** Structure of R-4MCF in the electronic ground state optimized at the MP2/6-31G* level of theory [85]; **b)** V/N CoIns in 4MCF: twisted CoIn, two pyramidalized CoIns, H-migration CoIn (all from Ref. [85]) and HF-elimination CoIn [80].

CoIns can only be reached via an initial twisting of the CHF group. Similar to the simple two states ethylene PESs profile (cf. Figure 3), the excited wavepacket is moving along the torsional coordinate after excitation, according to the gradient of the V state at the Franck-Condon geometry. The energy gap at the purely twisted structure ($\tau = 90^\circ$) is too big in order for the molecule to deactivate back to the ground state. Other coordinate changes are necessary to reach the point of degeneracy. In the case of the twisted CoIn, the torsion is connected with the C-C stretching mode; for the two pyramidalized CoIns, torsion is strongly coupled to the pyramidalization of the double bonded ring carbon and in case of the H-migration CoIn, torsion is connected with a bending mode of the corresponding hydrogen connected to the double bond. A couple of years later, Zilberg and co-workers have found and optimized an additional CoIn between the V and N states of 4MCF, which connects the torsional motion with a concerted dissociation of hydrogen and fluorine [80]. Henceforth, the newly found CoIn is called HF-elimination CoIn. Based on the above found CoIns between ground and excited state, it has been postulated that *cis-trans* isomerization should take place in the presence of polar solvents mediated by the twisted CoIn while in the gas phase the HF-elimination CoIn should be operative leading to HF-dissociation leaving a strongly vibrationally and rotationally excited hydrogen fluoride molecule [80]. In the present thesis, 4MCF will be studied only under gas phase conditions, and hence, the HF-elimination CoIn and the coordinates that it connects need to be incorporated in the theoretical investigation.

As it can be seen, despite 4MCF shall serve as a simple molecular rotor or switch, its full description is still very challenging. On the one hand, many coordinates seem to play an active role in the radiationless deactivation upon irradiation, i.e. many CoIns are present between the PESs of electronic excited and ground states. On the other hand, before this thesis began, the electronic description of 4MCF included only ground and $\pi\pi^*$ states (except the identification of Rydberg states in [85]), and thus concluding that any dissociation is a ground state process. Especially, with the newly found HF-elimination CoIn, however, the possibility of an excited state dissociation process cannot be neglected anymore. In general, in any event of excited state processes other than *cis-trans* isomerization, the influence of other excited valence states, e.g. $n\pi^*$ or $\pi\sigma^*$ states, on the deactivation processes might play an additional role. Concluding, before setting up any laser control scheme for a molecular switch or rotor based on 4MCF, the efficiency of the present CoIns has to be investigated, and the main deactivation path after excitation has to be identified.

3 Methodological Background and Computational Details

Within this section the underlying theoretical framework, that is used in this thesis, shall be briefly introduced. The first principle of quantum mechanics states that the wavefunction of a complete quantum mechanical system holds all the information about the very system, *i.e.* the positions of n electrons and N nuclei, \vec{r} and \vec{R} , respectively [88]. This wavefunction then satisfies a set of differential equations called the *non-relativistic time-dependent Schrödinger equation* (TDSE) as imposed by the fifth postulate of quantum mechanics [88]:

“*The wavefunction or state function of a system evolves in time according to the time-dependent Schrödinger equation.*”

$$i\hbar\frac{\partial}{\partial t}\Psi(\vec{r}, \vec{R}, t) = \hat{H}(\vec{r}, \vec{R}, t)\Psi(\vec{r}, \vec{R}, t) \quad (1)$$

where the Hamilton operator, \hat{H} , is the sum of all kinetic, \hat{T} , and potential terms, \hat{V} , as well as all time-dependent perturbations, *i.e.* dipole field interactions. In cases where the Hamilton operator is explicitly not time-dependent, one can separate the positions \vec{r} , \vec{R} from t , to obtain the *(non-relativistic) time-independent Schrödinger equation* (TISE):

$$\hat{H}(\vec{r}, \vec{R})\psi_l(\vec{r}, \vec{R}) = E_l\psi_l(\vec{r}, \vec{R}). \quad (2)$$

The solution of the TISE gives rise to the time-independent set of l wavefunctions or stationary states, Ψ_l , and the corresponding energy eigenvalues, E_l , which make up the time-independent spectrum of the system.

In general, the full description of a system of interest can be obtained by solving the corresponding differential equation, either time-dependent (eq. 1) or time-independent (eq.2). However, due to the many body problem one is facing at, the Schrödinger equations cannot be solved in an exact manner. Hence, many approximations and techniques have been introduced over the years in order to solve the above mentioned equations, each suited for particular quantum problems. In this thesis, two main problems in theoretical chemistry were treated:

- The first problem is addressed by quantum chemistry and is directly related to solving the TISE (eq. 2). In section 3.1 a further separation of the TISE into a nuclear and an electronic part will be introduced, and the creation of electronic ground as well as excited state potential energy surfaces (PESs) introducing the use of variational and perturbative multi configurational *ab initio* methods shall be described.

- The second problem treated in this thesis, is connected to the solution of the TDSE (eq. 1). In the frame of quantum dynamics the time-dependent motion of a wavepacket on several low-dimensional coupled PES is investigated. Methods used for propagating such a wavepacket in time will be described in section 3.2.

In contrast to quantum dynamics, in semi-classical molecular dynamics trajectories are propagated in time via classical Newton's equations, while the PESs, that the trajectory is feeling, are calculated on-the-fly. Section 3.3 will give an insight into this alternative methodology.

3.1 Quantum Chemistry

The aim of this section is to provide a brief description of the quantum chemical methods that were used in the present work, in order to calculate electronic PESs and to locate stationary points such as minima, transition states or conical intersections (CoIns). It shall not be the aim of this section to give a detailed description of the mathematical background to the methods themselves; it shall rather outline the chemical concepts and ideas behind the used methods. For further details the reader is referred to Refs. [89, 90, 91] as well as to the articles in sections 4.1 to 4.4 and references within.

3.1.1 Born-Oppenheimer and Potential Energy Surfaces

By separating the motion of the nuclei from the motion of the electrons the Born-Oppenheimer (or adiabatic) approximation [92] leads to a simplification of the above mentioned many-body problem when solving the TISE (eq. 2). This approximation is based upon the fact that the time scale associated with the motion of nuclei is usually much slower than that associated with electrons, leading to the conclusion that the light, fast moving electrons are immediately reacting to any change in the geometry of the nuclei.

Under these conditions the total time-independent wavefunction $\psi(\vec{r}, \vec{R})$ can be expressed as a product of a function $\psi^{nuc}(\vec{R})$, which is only dependent upon the nuclear coordinates \vec{R} , and of a function $\psi^{el}(\vec{r}, \vec{R})$, which is dependent upon the coordinates of the electrons \vec{r} as well as on parametric coordinates of the nuclei \vec{R} :

Solving the associated electronic Schrödinger equation

$$\hat{H}^{el}\psi_i^{el}(\vec{r}, \vec{R}) = \varepsilon_i^{el}\psi_i^{el}(\vec{r}, \vec{R}) \quad (3)$$

gives the i -th electronic eigenstate ψ_i^{el} and the corresponding eigenenergies ε_i^{el} for the i -th electronic state. Solving the electronic TISE (eq. 3) individually for k different nuclear coordinates (geometries) provides a set of k electronic eigenenergies $\varepsilon_{i,k}^{el}$, which can be

written as the function $\varepsilon^{el}(\bar{R})$ which is dependent parametrically upon the coordinates of the nuclei. Therefore, after adding the potential term for the nuclear-nuclear repulsion $\hat{V}^{nuc,nuc}(\bar{R})$, one obtains ε_i^{tot} , which is also a function of \bar{R} ,

$$\varepsilon_i^{tot}(\bar{R}) = \varepsilon_i^{el}(\bar{R}) + \hat{V}^{nuc,nuc}(\bar{R}). \quad (4)$$

$\varepsilon^{tot}(\bar{R})$ represents the resulting potential energy when moving along the nuclear coordinates \bar{R} . Thus, the function $\varepsilon_i^{tot}(\bar{R})$ is called the i -th electronic potential energy surface (PES) and represents the effective potential that N nuclei feel depending on their positions \bar{R} on the PESs.

3.1.2 Solution to the Electronic TISE

Limits of Hartree Fock In its simplest variant, the solution to the electronic TISE (eq. 3) is developed in terms of a single-determinant wavefunction. Within that Hartree-Fock (HaFo) framework (that is, one Slater determinant that follows the Pauli principle) [93, 94, 95] the electronic and structural properties of many stable molecules in the ground state can be described quite reasonably. However, the HaFo method generates solutions in which the real electron-electron interaction is replaced by an average potential; the Coulomb- and exchange terms describe the interaction of one electron with the effective potential generated by all other electrons. That means that the probability distribution for the electrons is independent upon one another. This is a rather rigid physical picture, since the motion of electrons is indeed correlated as they *move* through this field. With a sufficiently large basis set, the HaFo wavefunction accounts in the best case for approximately 99% of the total electronic energy of the system. The remaining 1%, though, is often very important for describing chemical phenomena [89]. In the case of e.g. biradical structures, however, a single HaFo determinant is by no means enough to describe the electronic problem even qualitatively. The difference between the HaFo energy E^{HaFo} and the lowest possible (exact) energy ε^{el} for a given basis set is called *correlation energy*:

$$E^{corr} = \varepsilon^{el} - E^{HaFo}. \quad (5)$$

Two types of electron correlation can be distinguished, the intra-orbital (or dynamic) correlation, describing the interaction of the two electrons in the same spatial orbital and the inter-orbital (or static) correlation, describing the interaction of two electrons in different spatial orbitals. A number of *ab initio* methods have been developed to add correlation to the HaFo-method, which are therefore called *post-Hartree-Fock-methods*.

Towards Multi-Configurational Methods: from CI to CASSCF Unlike the HaFo approach, in the configuration interaction method (CI) the wavefunction ψ^{el} will not be described only by one Slater determinant, in which the electrons occupy the energetic lowest orbitals, but by a number of determinants. Whereas the basis set functions describe the size of the *one-electron* basis (and are therefore the limiting factor for the description of the *one-electron* functions), the number of determinants determines the size of the *many-electron* basis and they are the limiting factor when accounting for electron correlation.

Within the HaFo framework, the solution of the Roothaan-Hall equations [94, 95] for closed-shell systems with n electrons and κ basis functions gives rise to $n/2$ occupied and $\kappa - n/2$ virtual molecular orbitals (MOs). By substituting occupied MOs from the restricted HaFo determinant with unoccupied virtual MOs, a whole new set of determinants can be built. Promoting one electron from the spatial orbital a to the orbital r constitutes a *single excitation* and it is denoted as ψ_a^r . Similarly, a *double excitation* involves exciting one electron from a to r and another one from b to s , which is written as ψ_{ab}^{rs} . Applying the same notation for all other multiple excitations, a trial wavefunction, Φ can be written as a linear combination of all possible excited determinants, relative to the HaFo reference determinant ψ_0 :

$$\Phi = c_0\psi_0 + \sum_{a,r} c_a^r \psi_a^r + \sum_{\substack{a<b \\ r<s}} c_{ab}^{rs} \psi_{ab}^{rs} + \sum_{\substack{a<b<c \\ r<s<t}} c_{abc}^{rst} \psi_{abc}^{rst} + \sum_{\substack{a<b<c<d \\ r<s<t<u}} c_{abcd}^{rstu} \psi_{abcd}^{rstu} + \dots \quad (6)$$

If all excitations in the one-electron basis are taken into account, the generated wavefunction is referred to as *full configuration interaction* (FCI) wavefunction. Because of the very large number of possible determinants FCI is connected with high computational costs, and hence, it is not practical except for small systems. Therefore, truncating the excitation series to the e.g. second term (CI singles doubles) and freezing very low lying orbitals (frozen core approach) is often used for bigger systems.

However, the situation is very different for the description of electronically excited states as well as for regions of the ground state PES far away from equilibrium structures, which often have more than one configuration of equal importance. Methods based on a single determinant especially fail to describe transition states or the dissociation of a homolytic bond and, in general, molecules with competing valence structures. For such cases, the wavefunction must have enough flexibility to include the required number of different configurations on an equal footing. This can be achieved by using the *multi-configurational self-consistent field* (MCSCF) approach [96]. The MCSCF method can be considered as a combination of a HaFo and a CI procedure, where the coefficients of the one-electron expansion (basis set) *and* the coefficients in the CI-expansion (eq. 6) are optimized simultaneously in a variational fashion. The lowering of the energy using multiple configurations, and therefore giving the wavefunction the flexibility to allow the

orbitals to become (partly) singly occupied (instead of forcing double occupation), covers mostly *static* correlation. It is for that reason that MCSCF methods are mainly used to generate qualitatively correct wavefunctions that cover the static part of the correlation. Nevertheless, increasing the number of configurations in the MCSCF wavefunction leads to further inclusion of *dynamic* correlation, until that of the full CI limit. This is, of course, at the expense of a computationally very demanding wavefunction.

Eventually, not all possible configurations are needed to describe a property of interest. Similar to the frozen core approximation in the CI methods, it is possible to decide which configurations must be included in the MCSCF procedure to describe a particularly feature. One of the most popular approaches is the *Complete Active Space Self-Consistent Field* method (CASSCF) [96, 97]. Here, the selection of configurations is done by partitioning the 2κ spin orbitals into subsets according on how they are intended to be used in the wavefunction. The MOs are divided into *inactive* orbitals, *active* orbitals and *external* or *virtual* orbitals. The inactive orbitals are fully, and the active orbitals are partially occupied in the final CASSCF wavefunction, while the external orbitals are unoccupied and span the rest of the orbital space, defined by the one-electron basis. The inactive orbitals always stay doubly occupied in all configurations that are used to build the CASSCF wavefunction. Thus, the number of electrons occupying these orbitals is twice the number of inactive orbitals defined. The remaining electrons are called the *active* electrons and fill the chosen active MOs. Consequently, the occupation number of the rest of the virtual orbitals is kept strictly 0 in all configurations. Within the active MOs, a full list of so-called *configurational state functions* (CSF), which have the required spin and space symmetry, is constructed. The CASSCF wavefunction is then expressed as a linear combination of all these CSFs, enclosing a complete expansion in the active orbital subspace. The most common notation for this method is $[n, m]$ -CASSCF, indicating that n electrons are distributed in all possible ways in m active orbitals [89].

As for any full CI expansion, the CASSCF wavefunction becomes very large even for small active spaces. The factorial increase in the number of CSFs effectively limits the active space for $[n, m]$ -CASSCF wavefunctions to $n = m = 16$ to 18 for small organic molecules. Selecting the relevant orbitals therefore becomes very important. MCSCF methods usually do not cover a large portion of the total correlation, but they rather recover all the changes that occur in the correlation energy for the given process [89]. Therefore, selecting the active space is the crucial step for obtaining sensible results, and good knowledge of the chemical process is required to ensure that the wavefunction has the correct flexibility. It should be noted that CASSCF methods tend to overestimate the importance of biradical structures when using small active spaces, due to the lack of dynamical correlation [89]. Therefore, selecting the proper number of configurations *and* the

correct orbitals, which give a balanced description of the problem, requires some experimentation and insight. In general, the active space has to represent the chemical situation of interest, and the result of the calculation will be very sensitive to this choice. This way, high-level ground state as well as excited state wavefunctions can be obtained, which give very good one-electron properties such as (transition) dipole moments or polarizabilities.

As mentioned above, the CASSCF method usually only recovers large portions of static correlation. If all valence electrons are included in the active space, the correlation energy would be complete in a sense of a full CI with the frozen core approximation. But this is only possible for very small systems. The electron correlation is covered completely within the active space, but *no* electron correlation energy is recovered from the inactive space, and between the inactive, the active space and virtual space, meaning that all the electron correlation energy recovered is *only* in the active space. The remaining electron correlation, associated with the instantaneous short-range electron-electron interaction (dynamic correlation), can be recovered by using the multi-configurational CASSCF wavefunction as a reference wavefunction for a configuration interaction (multi reference CI (MR-CI)), or for a Møller-Plesset perturbation calculation [98] (i.e. multi reference CASPT2 (MR-CASPT2) [96, 99]).

State Average CASSCF and Multi State CASPT2 When computing excited states it is very important to ensure the orthogonality of different excited wavefunctions. In the case of separately calculated excited states this is not necessarily given and can result in an unphysical picture. This artifact is not decisive in the case that the individual solutions are energetically far away from each other. In many photochemical problems, however, such as those describing degenerate electronic states and CoIns, the optimized state may be contaminated with the states lying close in energy. This problem can be overcome by using a *state average CASSCF* (SA-CASSCF). Here, a given number of electronic states (or roots) of the same symmetry are optimized simultaneously in the MCSCF approach. The resulting electronic states are described with the same set of molecular orbitals and differ only in the variationally optimized CI-coefficients.

When describing energetically close lying or mixed electronic states with the CASPT2 procedure one should rely on the multi-state version of CASPT2 (MS-CASPT2) [100]. Here, an effective Hamiltonian is set up, in which the different reference SA-CASSCF states are coupled at second order. Diagonalizing this Hamiltonian gives rise to a new set of wavefunctions and energies, where the new wavefunctions are composed of linear combinations of the original SA-CASSCF states.

In the following, ψ_i^{el} will represent the finally optimized wavefunction for the i -th electronic state, independently from the quantum chemistry method used.

3.2 Quantum Dynamics on Coupled Surfaces

The aim of this section is to give a brief insight into the development of solutions for the TDSE (eq. 1). In the present work wavepacket propagations have been performed on coupled electronic PESs. Hence, in the first part of this section (section 3.2.1) properties of these coupled surfaces shall be illustrated in a non Born-Oppenheimer framework. Consequently, in section 3.2.2 the solution to the nuclear TDSE will be presented and its numerical implementation, which will give rise to a nuclear wavefunction moving in time on coupled surfaces, will be explained.

3.2.1 Beyond Born-Oppenheimer: Coupled PESs

Non-adiabatic coupling terms (NACTs) The Born-Oppenheimer or adiabatic approximation is a good way to simplify the many-body problem of describing N nuclei and n electrons, as long as the PESs of different electronic states do not cross or get "close" within nuclear motion. In the latter case the Born-Oppenheimer approximation breaks down, and hence, the motion of the nuclei cannot be separated from the electronic motion. That means, that the character of one or several electronic states might change within the time scale of nuclear motion. In such cases, different electronic states or surfaces of the same multiplicity are coupled via the so-called non-adiabatic coupling terms (NACTs).

After solving the electronic TISE (eq. 3) the nuclear TISE can be written as:

$$\left[\hat{H}^{el} + \hat{T}^{nuc}(\vec{R}) + \hat{V}^{nuc,nuc}(\vec{R}) \right] \psi^{el}(\vec{r}, \vec{R}) \psi^{nuc}(\vec{R}) = \varepsilon^{nuc} \psi^{el}(\vec{r}, \vec{R}) \psi^{nuc}(\vec{R}), \quad (7)$$

giving rise to the nuclear eigenfunctions and eigenenergies, ψ^{nuc} and ε^{nuc} , respectively. Substituting the electronic TISE (eq. 3) and equation 4 into the nuclear TISE one gets

$$\hat{T}^{nuc}(\vec{R}) \psi^{el}(\vec{r}, \vec{R}) \psi^{nuc}(\vec{R}) + \varepsilon^{el} \psi^{el}(\vec{r}, \vec{R}) \psi^{nuc}(\vec{R}) = \varepsilon^{nuc} \psi^{el}(\vec{r}, \vec{R}) \psi^{nuc}(\vec{R}). \quad (8)$$

With $\hat{T}^{nuc}(\vec{R})$ being the kinetic energy of all N nuclei, the first term of the right hand side of equation 8 becomes (in atomic units)

$$\begin{aligned} \hat{T}^{nuc}(\vec{R}) \psi^{el}(\vec{r}, \vec{R}) \psi^{nuc}(\vec{R}) &= -\frac{1}{2} \sum_{\alpha}^N \frac{1}{M_{\alpha}} \nabla_{R_{\alpha}}^2 \left(\psi^{el}(\vec{r}, \vec{R}) \psi^{nuc}(\vec{R}) \right) \\ &= -\frac{1}{2} \sum_{\alpha}^N \frac{1}{M_{\alpha}} \left(\nabla_{R_{\alpha}}^2 \psi^{el}(\vec{r}, \vec{R}) \psi^{nuc}(\vec{R}) + 2 \nabla_{R_{\alpha}} \psi^{el}(\vec{r}, \vec{R}) \nabla_{R_{\alpha}} \psi^{nuc}(\vec{R}) \right. \\ &\quad \left. + \psi^{el}(\vec{r}, \vec{R}) \nabla_{R_{\alpha}}^2 \psi^{nuc}(\vec{R}) \right) \end{aligned} \quad (9)$$

This equation contains the NACTs of first and second order, $T^{(1)} = \nabla_{R_{\alpha}} \psi^{el}(\vec{r}, \vec{R})$ and $T^{(2)} = \nabla_{R_{\alpha}}^2 \psi^{el}(\vec{r}, \vec{R})$, respectively, describing the first and second derivatives of the electronic wavefunction with respect to the nuclear coordinates. These terms are often very

small and are thus neglected within the Born-Oppenheimer approximation [7].

Conical Intersections (CoIns) As mentioned above the Born-Oppenheimer approximation breaks down if two or more states come close in energy within the full-dimensional PES. In these cases the NACTs cannot be neglected anymore. Especially in the vicinity of CoIns they can become very large, even infinity at the CoIns itself.

A CoIn is the crossing point of two electronic states (e.g. state 1 and state 2) with the same spin multiplicity. In a N -atomic molecule with $3N - 6$ internal degrees of freedom two PESs are allowed to cross in $3N - 8$ coordinates fulfilling the condition of energetical degeneracy ($\varepsilon_2^{el} - \varepsilon_1^{el} = 0$). The two remaining nuclear coordinates make up the so-called branching space. Plotting the considered PESs in the branching space they form a double cone in the region around the degeneracy in which the CoIn is a single point - the apex of the cone. The coordinates of the branching space are the gradient difference (also called tuning mode) g_{12} and the derivative coupling vector h_{12} defined as [101]

$$g_{12} = \nabla_{R_\alpha}(\varepsilon_2^{el} - \varepsilon_1^{el}) \quad \text{and} \quad h_{12} = \langle \psi_1^{el} | \nabla_{R_\alpha} \hat{H}^{CoIn} | \psi_2^{el} \rangle. \quad (10)$$

with \hat{H}^{CoIn} being the conical intersection Hamiltonian [102]. Movement along these two vectors lifts the degeneracy, while the other $3N - 8$ coordinates constitute the intersection space that is a hyperline or seam of an infinite number of crossing points.

Adiabatic to Diabatic Transformation The description of nuclear dynamics in the presence of NACTs is often challenging. Near CoIns the NACTs between the two states undergo rapid changes – the sharper the crossing the more rapid the change. At the CoIn itself the kinetic coupling elements become a singularity. Numerically representing and treating such changes and even singularities is a challenging task; therefore, much effort has been devoted to find physically meaningful diabatic representations, see e.g. [103, 104, 105].

For simplicity, the transformation from an adiabatic to a diabatic representation shall be illustrated for a diatomic molecule with only one internal coordinate, R . Furthermore, only two electronic states will be considered.

For such a system, the total Hamiltonian in atomic units can be written as

$$\hat{H} = \hat{H}^{el} - \frac{1}{2\mu} \nabla_R^2, \quad (11)$$

with μ being the reduced mass between the two atoms. After integration with respect to the electronic coordinates one obtains the adiabatic Hamiltonian, \hat{H}^{ad} :

$$\hat{H}^{ad} = \mathbf{V}^{ad} - \frac{1}{2\mu} (\nabla_R^2 + 2\mathbf{T}^{(1)} \nabla_R + \mathbf{T}^{(2)}). \quad (12)$$

In the adiabatic representation the adiabatic potential energy matrix, \mathbf{V}^{ad} , is diagonal, with elements $V_i^{ad} = \varepsilon_i^{tot}(\bar{R})$ on its diagonal, which are solutions to the electronic TISE (recall eq. 4). The first order and second order non-adiabatic coupling matrices, $\mathbf{T}^{(1)}$ and $\mathbf{T}^{(2)}$ contain the NACT elements according to:

$$T_{ij}^{(1)} = \langle \psi_i^{el} | \nabla_R | \psi_j^{el} \rangle \quad \text{and} \quad T_{ij}^{(2)} = \langle \psi_i^{el} | \nabla_R^2 | \psi_j^{el} \rangle,$$

respectively. These matrices are not diagonal in the adiabatic representation and can contain fast changing off-diagonal terms. The diagonal terms are zero by definition [105].

In general, one can get rid of the NACTs, by switching to a diabatic representation through a unitary transformation matrix, \mathbf{U} , which diagonalizes the non-adiabatic coupling matrix, $\mathbf{T}^{(1)}$. Such a transformation matrix, therefore, needs to fulfill the following equation [105]:

$$-\mathbf{T}^{(1)}\mathbf{U} = \nabla_R \mathbf{U} \quad (13)$$

A suitable transformation matrix \mathbf{U} can be derived in different ways. The reader shall be hereby referred to details in the articles in sections 4.1 and 4.4 as well as to Ref. [105] and references within.

Once a transformation matrix is found, that fulfills equation 13, one can diabaticise the potential matrix, \mathbf{V}^{ad} , such that (for the two state case)

$$\mathbf{U}^\dagger \mathbf{V}^{ad} \mathbf{U} = \mathbf{U}^\dagger \begin{pmatrix} V_1^{ad} & 0 \\ 0 & V_2^{ad} \end{pmatrix} \mathbf{U} = \begin{pmatrix} V_1^d & V_{12}^d \\ V_{21}^d & V_2^d \end{pmatrix} = \mathbf{V}^d \quad (14)$$

Consequently, while the adiabatic representation yields equations in which the potential energy matrix is diagonal and the coupling enters through the kinetic-energy operator (NACTs), in the diabatic representation the coupling appears in the off-diagonal potential energy term (potential coupling), V_{ij}^d , whereas the kinetic energy operator is diagonal.

3.2.2 Solution to the Nuclear TDSE in the Presence of External Fields

Setting up the nuclear TDSE in the presence of a time-dependent electric field In order to investigate the nuclear dynamics on coupled surfaces one needs to solve the TDSE (eq. 1) for the nuclear wavefunction on each electronic state i , ψ_i^{nuc} . For a one-dimensional (one coordinate, R) two state system, consider the nuclear TDSE in the adiabatic representation given as:

$$i\hbar \frac{\partial}{\partial t} \begin{pmatrix} \psi_1^{nuc,ad}(t) \\ \psi_2^{nuc,ad}(t) \end{pmatrix} = \begin{pmatrix} H_{11}^{ad} & H_{12}^{ad} \\ H_{21}^{ad} & H_{22}^{ad} \end{pmatrix} \begin{pmatrix} \psi_1^{nuc,ad}(t) \\ \psi_2^{nuc,ad}(t) \end{pmatrix}. \quad (15)$$

with the matrix elements of the adiabatic Hamiltonian:

$$H_{ii}^{ad} = -\frac{1}{2\mu} \nabla_R^2 + V_i^{ad} \quad \text{and} \quad H_{ij}^{ad} = -\frac{1}{\mu} T_{ij}^{(1)} \nabla_R. \quad (16)$$

In the present work, the second order coupling matrix elements, $T_{ij}^{(2)}$, will be neglected in the solution of the nuclear TDSE, since they are usually considerably small.

For reasons mentioned in section 3.2.1, in the presence of NACTs, the nuclear TDSE will be solved in the diabatic representation. After applying the adiabatic-to-diabatic transformation via \mathbf{U} (eq. 13), the diabatic nuclear TDSE reads:

$$i\hbar \frac{\partial}{\partial t} \begin{pmatrix} \psi_1^{nuc,d}(t) \\ \psi_2^{nuc,d}(t) \end{pmatrix} = \begin{pmatrix} H_{11}^d & H_{12}^d \\ H_{21}^d & H_{22}^d \end{pmatrix} \begin{pmatrix} \psi_1^{nuc,d}(t) \\ \psi_2^{nuc,d}(t) \end{pmatrix}. \quad (17)$$

with the diabatic Hamilton matrix elements:

$$H_{ii}^d = -\frac{1}{2\mu} \nabla_R^2 + V_i^d \quad \text{and} \quad H_{ij}^d = V_{ij}^d. \quad (18)$$

In the presence of an external electric field $\epsilon(t)$, the diabatic potential matrix, \mathbf{V}^d is replaced by a matrix \mathbf{W} whose elements are given by the dipole field interaction Taylor series:

$$W_{ij} = V_{ij}^d - \mu_{ij}^d \epsilon(t) - \alpha_{ij}^d \epsilon(t)^2 - \beta_{ij}^d \epsilon(t)^3 - \dots, \quad (19)$$

where the elements μ_{ij}^d are the permanent ($i = j$) and the transition ($i \neq j$) dipoles, α_{ij}^d are the polarizability, and β_{ij}^d the hyperpolarizability elements. All these elements are one-electron properties and can be obtained by solving the electronic TISE (eq. 3), recall section 3.1.2.

Usually the strongest dipole field interaction arises from the first interaction term, namely the dipole moments, hence, in most of the cases one cuts the Taylor series in equation 19 after the first interaction term. The transition dipole moments are causing a dipole coupling such that in the presence of a field, $\epsilon(t)$, population transfer between electronic states i and j is induced by that very field, e.g. a UV pulse excitation from the ground state to an excited state. Additionally, the potential surfaces will be shifted due to the diagonal terms in the dipole matrices. This is of course more pronounced the higher the field strength or the value of the permanent dipole moments are, achieving Stark effects [23]. Diagonalization of \mathbf{W} gives the so-called dressed states or light-induced potentials, $\mathbf{V}^{dressed}$ [24].

In this thesis, the total dynamic electric field that interacts with the nuclear wavefunction is modeled as a sum of several resonant or non-resonant pulses:

$$\epsilon(t) = \sum_{pulse} (\vec{\epsilon}_{xyz} F_0 E(t) \cos(\omega t)) \quad (20)$$

with the polarization vectors $\vec{\epsilon}_{xyz}$, the field amplitudes F_0 , the frequencies $\omega = \frac{2\pi c}{\lambda}$ with c being the speed of light and λ being the wavelength, and envelope function $E(t)$, describing for example a Gaussian function.

Solutions to the nuclear TDSE Time-resolved information about the dynamics of a wavefunction on the electronic PESs will be available when solving the nuclear TDSE, here, starting in the diabatic representation (eq. 17). Assuming that the solution of the TDSE for several electronic states for the time-independent Hamiltonian matrix, $\mathbf{H}^d(\vec{R})$ (elements of \mathbf{H}^d see eq. 18), can be used to approximate the solution of the TDSE for the time-dependent Hamiltonian matrix, $\mathbf{H}^d(\vec{R}, t)$, the propagation of a nuclear wavefunction from time t_0 to time t can be described with a time-evolution operator or propagator [7], such that for a two state problem (in atomic units):

$$\begin{pmatrix} \psi_1^{nuc,d}(\vec{R}, t) \\ \psi_2^{nuc,d}(\vec{R}, t) \end{pmatrix} = e^{-i\mathbf{H}^d(\vec{R}, t-t_0)} \begin{pmatrix} \psi_1^{nuc,d}(\vec{R}, t_0) \\ \psi_2^{nuc,d}(\vec{R}, t_0) \end{pmatrix}. \quad (21)$$

The approximation in equation 21 requires a discrete time step short enough so that $\mathbf{H}^d(\vec{R}, t_1) \approx \mathbf{H}^d(\vec{R}, t_2)$. If this requirement is given equation 21 becomes discretized in time to give:

$$\begin{pmatrix} \psi_1^{nuc,d}(\vec{R}, t + \Delta t) \\ \psi_2^{nuc,d}(\vec{R}, t + \Delta t) \end{pmatrix} = e^{-i\mathbf{H}^d(\vec{R})\Delta t} \begin{pmatrix} \psi_1^{nuc,d}(\vec{R}, t) \\ \psi_2^{nuc,d}(\vec{R}, t) \end{pmatrix}. \quad (22)$$

Several techniques have been developed to solve equation 22 expressing the propagator, $e^{-i\mathbf{H}^d(\vec{R})\Delta t}$, in different ways, e.g. polynomial methods like Chebyshev [106] and short iterative Lanczos propagation [107] or the Split Operator method [108, 109, 110, 111]. The latter one was used in this thesis and shall be briefly introduced in the next paragraph.

The Split-Operator method If the total diabatic Hamilton matrix is expressed as (the dependency on \vec{R} will be dropped for simplicity):

$$\mathbf{H}^d = \mathbf{T} + \mathbf{W}, \quad (23)$$

whereas the kinetic energy matrix \mathbf{T} is in its diagonal form, then the time-evolution propagator in equation 22 could be approximated to:

$$e^{-i\mathbf{H}^d\Delta t} = e^{-i(\mathbf{T}+\mathbf{W})\Delta t} = e^{-i\mathbf{T}\Delta t}e^{-i\mathbf{W}\Delta t}. \quad (24)$$

Unfortunately this expression produces large errors since \mathbf{T} and \mathbf{W} do not commute. To reduce the error caused by the noncommuting operators, Feit and Fleck introduced the split operator [108, 109, 110] splitting the potential energy operator symmetrically, such that:

$$e^{-i\mathbf{H}^d\Delta t} = e^{-i\frac{\mathbf{W}}{2}\Delta t}e^{-i\mathbf{T}\Delta t}e^{-i\frac{\mathbf{W}}{2}\Delta t} + O(\Delta t^3), \quad (25)$$

giving an error of third-order in the time step Δt only.

The split of the Hamiltonian matrix \mathbf{H}^d works effectively when working on grids. Here, at every time step the nuclear wavefunction $\psi_i^{nuc}(\vec{R}, t)$ will be represented in position on a discrete grid of M grid points between R_0 and R_M . The potential, \mathbf{V} , acting on this wavefunction is best described on the position grid, while the acting of the kinetic term, \mathbf{T} , on $\psi_i^{nuc}(\vec{R}, t)$ will be described on a grid in momentum space. Hence, in the numerical evaluation of the whole propagation operator (eq. 25) acting on the wavefunction, one has to transform the $\psi_i^{nuc}(\vec{R}, t)$ from position to momentum space and back. This is done with a Fourier transform (FT). For further details on the discretation of the grids, both position and momentum, as well as on the FT procedure please see Ref. [7] and references within.

Furthermore, equation 25 involves the exponentiation of matrices in order to obtain the time-evolved wavefunction. However, this is only doable if the matrices, \mathbf{W} and \mathbf{T} , are diagonal. Thus, diagonalization of the time-dependent potential matrix \mathbf{W} is necessary at every time-step; \mathbf{T} is given diagonal at all times. In the beginning of each time step, diagonalization of \mathbf{W} gives a unitary matrix, that will be used to switch between the diabatic and adiabatic (or dressed state) representation during the evaluation of equation 22. The series of FTs and diagonalizations needed for propagating a wavefunction on coupled PESs for a single time step, $t \rightarrow t + \Delta t$ will be illustrated now, as they were implemented in an own Fortran90 program code.

- Evaluate the time-dependent potential matrix $\mathbf{W}(t)$ according to equation 19:

$$\mathbf{V}^d \xrightarrow{\epsilon(t)} \mathbf{W}(t)$$

- Diagonalize $\mathbf{W}(t)$, giving rise to a unitary matrix, $\mathbf{D}(t)$, that diagonalizes $\mathbf{W}(t)$, giving the time-dependent adiabatic (dressed) state potentials:

$$\mathbf{D}^\dagger(t) \mathbf{W}(t) \mathbf{D}(t) \longrightarrow \mathbf{V}^{dressed}(t)$$

- Transform $\psi^{nuc,d}$ into the adiabatic (dressed) representation:

$$\psi^{nuc,ad}(t) = \mathbf{D}(t) \psi^{nuc,d}(t)$$

- Multiply (half) potential operator with the adiabatic wavefunction on each state:

$$\tilde{\psi}_i^{nuc,ad}(t) = \psi_i^{nuc,ad}(t) e^{-i \mathbf{V}_i^{dressed} \Delta t/2}$$

- Transform $\tilde{\psi}^{nuc,ad}(t)$ into the diabatic representation:

$$\tilde{\psi}^{nuc,d}(t) = \mathbf{D}^\dagger(t) \tilde{\psi}^{nuc,ad}(t)$$

- Evaluate $\tilde{\psi}^{nuc,d}(t)$ in momentum space, via FT:

$$\tilde{\psi}^{nuc,d}(t) \xrightarrow{FT} \tilde{\psi}_p^{nuc,d}(t)$$

- Multiply kinetic operator with the diabatic wavefunction in momentum space on each state:

$$\tilde{\psi}_{p,i}^{nuc,d}(t) = \tilde{\psi}_{p,i}^{nuc,d}(t) e^{-i \mathbf{T}_i \Delta t}$$

- Backtransform $\tilde{\psi}_{p,i}^{nuc,d}(t)$ into position space via FT:

$$\tilde{\psi}_p^{nuc,d}(t) \xrightarrow{FT^{-1}} \tilde{\psi}^{nuc,d}(t)$$

- Transform $\tilde{\psi}^{nuc,d}$ into adiabatic (dressed) representation:

$$\tilde{\psi}^{nuc,ad}(t) = \mathbf{D}(t) \tilde{\psi}^{nuc,d}(t)$$

- Multiply (half) potential operator with the adiabatic wavefunction on each state:

$$\psi_i^{nuc,ad}(t + \Delta t) = \tilde{\psi}_i^{nuc,ad}(t) e^{-i \mathbf{V}_i^{dressed} \Delta t/2}$$

- Transform $\psi^{nuc,ad}(t + \Delta t)$ into diabatic representation:

$$\tilde{\psi}^{nuc,d}(t + \Delta t) = \mathbf{D}^\dagger(t) \psi^{nuc,ad}(t + \Delta t)$$

The initial nuclear wavefunction at time zero, $\psi^{nuc,d}(t = 0)$, is prepared in the diabatic electronic and vibrational ground state using the Fourier Grid Hamiltonian method (FGH) [112] or by propagating a guess function in imaginary time ($\Delta t = i\Delta t$) [113].

3.3 *Ab initio* Molecular Dynamics

Although propagating a wavepacket on coupled PESs leads to real quantum phenomena, such as constructive and destructive interferences of parts of the wavepacket or geometric phase effects, solving the nuclear TDSE on such grids (see section 3.2.2) bears a technical problem. The number of single point solutions to the electronic TISE to obtain the PESs (eq. 3) and electronic properties such as NACTs or dipole moments increases exponentially with the dimensionality of the problem, i.e. the number of nuclear degrees of freedom that are taken into consideration. Usually, one must choose among a few coordinates and ignore the other ones, bearing in mind, that this choice will be the boundary condition for the quantum dynamics simulation, and hence, hoping that the chosen coordinates describe the “real” motion of the system for a certain process. In cases where

too many degrees of freedom play a major role (complicated non-trivial PESs) or if major coordinates change due to a given process not yet known, it can be more useful to rely on full-dimensional *ab initio molecular dynamic* simulations (AIMD).

AIMD is a mixed quantum-classical method employing classical Newton's equations of motion describing the time-dependency of a particle feeling local electronic potentials and properties obtained by quantum chemistry solutions [114]. The effective force acting on that particle is the negative energy gradient of the full-dimensional potential surface at the position of the particle. The particle is then moved iteratively with a fixed time step Δt on the PES yielding a molecule trajectory, whereas the PESs and the corresponding properties (gradients, NACTs etc.) are calculated on-the-fly at each time step by means of quantum chemistry methods (see section 3.1). In this way, one trajectory moves in time on a single adiabatic surface. In this thesis, however, several surfaces are calculated which are coupled via the NACTs. Hence, a single trajectory must be able to jump between different electronic states. Due to the classical description of the nuclear movement, the regions where the Born-Oppenheimer approximation collapses have to be treated individually to describe the behavior of the system in a correct manner. One possibility is to use the *surface hopping method*, where the minimal amount of hoppings between potential surfaces is postulated as a requirement (fewest switches criterion) [115]. Herein, the probability, P_{ij} , of a trajectory to jump from state i to state j is calculated at every time step as:

$$P_{ij} = \frac{2\text{Re}(c_i^* c_j \mathbf{v})}{c_i^* c_j} \langle \psi_i^{el} | \nabla_R | \psi_j^{el} \rangle \Delta t, \quad (26)$$

where the coefficients c_i represent the expansion of the electronic wavefunction in the adiabatic states. The hopping probability depends strongly on the classical velocity of the trajectory, \mathbf{v} , and the NACT element, $\langle \psi_i^{el} | \nabla_R | \psi_j^{el} \rangle$. At each time step during the propagation of the trajectory, P_{ij} between each state is compared to a random number given by the program code, in order to decide if the trajectory is switching to the other state or not.

Because of this, an ensemble of independent trajectories needs to be propagated in order to achieve statistically converged results on the time-dependent behaviour of the system in full-dimensionality. If the number of trajectories in the ensemble is large enough one can assume a statistically validated wavepacket-like behaviour. In order to simulate an initial wavepacket incorporating the ensemble of trajectories, usually a Breit-Wigner distribution of initial geometries along the $3N - 6$ normal modes of a system in its electronic and vibrational ground state is calculated as:

$$f(R) = \frac{1}{\pi} \frac{\gamma}{(R - R_0)^2 + \gamma^2} \quad (27)$$

Here, the coordinate R , represents any of the normal mode coordinates of the system. The

maximum of the distribution is at R_0 , and the width of distribution is given by γ , which is directly related to the frequency of the normal mode in its vibronic ground state.

Due to the classical motion and independency of the trajectories, quantum effects as described above cannot be revealed using AIMD. In the present work, AIMD is used to identify the major coordinate changes during the relaxation process in 4MCF (section 4.3). With this information at hand, reduced-dimensional quantum dynamics in the presence of an external time-dependent field could be performed.

4 Results

This section presents the results of this thesis in form of the articles published in peer-reviewed international journals.

Based upon the previous research on 4MCF (recall section 2) the first paper, presented in section 4.1, shows the results of the two-dimensional dynamics investigating the competing relaxation paths involving the torsion around the olefinic double bond and the dissociation of hydrogen fluoride after instantaneous excitation into the bright $\pi\pi^*$ state. The second publication (section 4.2) investigates the presence of a $\pi\sigma^*$ state in the vicinity of the Franck-Condon region and along the HF-dissociation path in 4MCF by means of high level quantum chemistry methods. This investigation is giving rise to a new picture of the possible dissociation paths in 4MCF upon excitation. Hence, a full-dimensional *ab initio* molecular dynamics study has been performed in order to extract the most important and relevant coordinates that change during the relaxation process; coordinates that may have been overlooked in the previous studies. As a result of the full-dimensional dynamics, presented in section 4.3, it is found that the main deactivation path upon excitation of 4MCF into the $\pi\pi^*$ state is hydrogen abstraction, and that the torsion, that should drive a possible rotor, is rarely taking place. Towards a functioning rotor, thus, the H-dissociation has to be suppressed. In the paper presented in section 4.4, a one-dimensional quantum dynamics study finally shows that it is possible to use the Stark effect (by means of non-resonant strong laser fields that shift the potentials) so that the H-abstraction is slowed down significantly and torsion can take place.

Each section will give a short summary of the results given in their respective articles. The published articles themselves will be presented as facsimiles¹ after each summary.

¹The permission of the respective copyright owners has been granted.

4.1 *Cis-Trans* Photoisomerization vs. HF-Photodissociation in 4MCF

The quantum chemical and dynamical study in the paper “*Non-adiabatic photoisomerization versus photodissociation dynamics of the chiral fluoroethylene derivative (4-methylcyclohexylidene) fluoromethane*” is motivated by the newly found CoIn described by Zilberg *et. al.* [80]. In general, UV excitation into the $\pi\pi^*$ electronic excited state reduces the bond order of the C-C double bond, so that the HF moiety in 4MCF can rotate around the bond axis, leading to a *cis-trans* isomerization, illustrated in path (i) in Figure 7. During the isomerization process, the excited molecules can deactivate back to the ground state via the twisted and/or pyramidalized CoIns presented in the study of Schreiber *et al.* [85] (recall section 2). The CoIn found by Zilberg *et. al.*, however, represents another possible ultrafast funnel between the bright $\pi\pi^*$ and the ground state and connects the torsional motion of the HF-fragment with its concerted dissociation, illustrated in Figure 7 path (ii). This CoIn then leads to elimination of hydrogen fluoride, and competes with the isomerization processes.

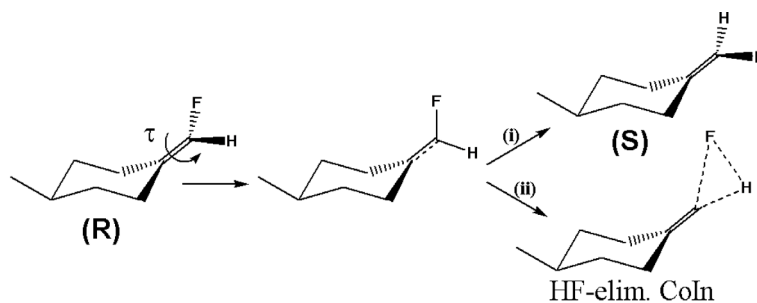


Figure 7: Scheme of the two competing paths, (i) *cis-trans* isomerization and (ii) dissociation of hydrogen fluoride via the HF-elimination CoIn.

Until the present study has been performed, the formation of HF in fluoroethylenes has been studied theoretically only as a ground state reaction via various transition states [74, 75]. After excitation, the energy to overcome these barriers is assumed to be the kinetic excess energy that arises when the system is deactivated through the e.g. twisted CoIn (recall section 2). Here, the newly found HF-elimination CoIn makes it possible to achieve HF dissociation on the excited state, while the deactivation to the ground state happens at a time where the HF fragment is already “on the way” to dissociate. The question that needs to be answered, using e.g. quantum dynamics, is, whether the HF-elimination CoIn can be accessed and how it competes with the other CoIns found in 4MCF (see section 2). In particular, in this study the competition between the twisted and the HF-elimination CoIns, and hence the competition between the *cis-trans* isomerization

and the HF-elimination relaxation paths, is of interest.

To this aim, one- and two-dimensional PESs for 4MCF have been calculated using the multiconfigurational method CASSCF, along the torsion around the C-C bond, denominated with τ , and the distance between the center of masses of the hydrocarbon moiety and the HF fragment, denoted R (for details see the following article). Other coordinates, such as the HF distance, are kept frozen at the equilibrium geometry. Furthermore, for simplicity, only the electronic ground state and the bright $\pi\pi^*$ excited states have been considered, while Rydberg or other states are excluded. Although only the $\pi\pi^*$ state is calculated, the active space requires to include more than just the π and the π^* orbitals. Due to the homolytic cleavage of both the C-H and the C-F bond, the corresponding σ and σ^* orbitals need to be added. Hence, an active space including eight electrons in eight orbitals was used. The obtained two electronic PESs are non-adiabatically coupled mainly by the presence of the CoIn leading to HF elimination. The optimized twisted CoIn (see section 2) is not part of the PESs, yet there is some coupling between the excited and ground state at a geometry twisted by $\tau = 90$. Using ab initio CASSCF kinetic couplings elements (NACTs), the PESs are diabaticized and wavepacket propagations in the diabatic representation have been carried out. The initial nuclear wavefunction has been excited to the $\pi\pi^*$ state using a δ -pulse, i.e. instantaneously.

The resulting non-adiabatic dynamics shows, that there is no transfer of population to the ground state in a sub ps time scale although the system starts with enough kinetic energy to arrive to the HF-elimination CoIn. Up to 1 ps the momentum of the initial wavepacket remains localized in the torsion with a negligible transfer to the HF-elimination coordinate. Hence, during the first hundreds of fs, our model indicates that isomerization dominates over HF dissociation, while most of the population stays in the adiabatic excited $\pi\pi^*$ state. The torsional half cycle (torsion of the HF-fragment about $\tau = 180$) is found to be in a time scale of 150 fs. As a final conclusion, we state that, within the limitations of the reduced-dimensional model, the HF-elimination CoIn is not competitive to the isomerization process upon excitation of 4MCF, simply because the region around the HF-elimination CoIn, showing substantial coupling to the ground state, is not reached during the dynamics calculation.

Interestingly, a closer investigation of the electronic configurations near the HF-elimination CoIn reveals a spurious mixing of the $\pi\pi^*$ transition with a $\pi\sigma^*$ one. That means, that not only the reduced dimensionality of the used model is limiting the outcome of the dynamics, but also the number of included electronic PESs. Hence, as a next step (section 4.2), the role of these $\pi\sigma^*$ states in the overall dissociation process has been investigated.

Next, the original article “*Non-adiabatic photoisomerization versus photodissociation dynamics of the chiral fluoroethylene derivative (4-methylcyclohexylidene) fluoro-methane*” published in *Chemical Physics*, volume 369, in 2010 will be reprinted.

(S. A. contributed to the following investigation by calculating the one- and two-dimensional PESs and by performing preliminary quantum dynamical simulations.

D. K. contributed to the following study by performing the one- and two-dimensional quantum dynamics simulations and evaluating the population dynamics in the basis of one-dimensional torsional levels. Moreover, D. K. prepared the manuscript.

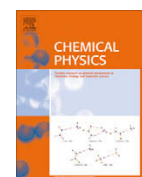
J. G.-V. provided the quantum dynamical code necessary for performing the quantum dynamical simulations. Additionally, J. G.-V. supervised the investigations and prepared and revised the manuscript.

L. G. supervised the whole research and revised the manuscript.)



Contents lists available at ScienceDirect

Chemical Physics

journal homepage: www.elsevier.com/locate/chemphys

Non-adiabatic photoisomerization versus photodissociation dynamics of the chiral fluoroethylene derivative (4-methylcyclohexylidene) fluoromethane

Sherin Alfalah, Daniel Kinzel, Jesús González-Vázquez¹, Leticia González*

Institut für Physikalische Chemie, Friedrich-Schiller-Universität Jena, Helmholtzweg 4, 07743 Jena, Germany

ARTICLE INFO

Article history:

Received 8 December 2009
In final form 12 March 2010
Available online 17 March 2010

Keywords:

Wavepacket dynamics
Excited states
Conical intersections
Photodissociation
Photoisomerization

ABSTRACT

The photoisomerization around the C=C double bond and the competing elimination of hydrogen fluoride (HF) are studied in (4-methylcyclohexylidene) fluoromethane. Both reactions are mediated by twisted conical intersections (CI) around the C=C bond. Potential energy surfaces (PES) for the electronic ground state and first bright excited state of $\pi\pi^*$ character are calculated using the CASSCF method along two reaction coordinates: the torsion around the C=C bond and the distance between the center of masses of the hydrocarbon moiety and the HF fragment. Non-adiabatic couplings between both PES are obtained at the same level of theory. Wavepacket dynamics on the coupled surfaces show that after light irradiation torsion in the $\pi\pi^*$ state dominates over HF dissociation, although the system starts with enough kinetic energy to reach the CI leading to HF-elimination.

© 2010 Elsevier B.V. All rights reserved.

1. Introduction

Photoinduced *cis/trans* isomerization around a double bond in olefins is a fundamental phenomenon in organic photochemistry [1] and photobiology [2,3]. Also, it is playing an increasing role in the field of molecular engineering, since it represents one of the simplest mechanisms to convert energy into motion on a molecular scale [4]. Often, the simplest molecule chosen to study this issue is ethylene. In ethylene, several conical intersections (CI) involving the torsion around the double bond allow for a very fast relaxation from the lowest bright electronic excited state (of $\pi\pi^*$ character) to the ground state [4–6]. In particular, a CI between the S_1 (V state) and S_0 (N state) exist at a twisted geometry with pyramidalization at one of the carbon atoms. It has been pointed out that this twisted–pyramidalized geometry is the main channel for deactivation to the ground state [7–9]. However, more recent six-dimensional quantum dynamical simulations have identified the pyramidalization as the bottleneck for the radiationless decay [10]. Instead, the C–C stretching mode is found strongly coupled with the torsional mode [10].

Despite it is tempting to use ethylene as a model for any olefinic system, caution should be exercised when different substituents are added to the molecule. For instance, quantum chemical calculations on fluoroethylene show that the torsion alone (without pyramidalization) is enough to drive the system from the V to

the N state [11]. Therefore, the dynamics of ethylene derivatives can change very much depending on the specific substituent and its position (see e.g. Ref. [12]).

Interestingly, besides isomerization, ethylene, as well as ethylene derivatives, can undergo photoinduced dissociation. Experimentally, it has been observed that both atomic and molecular hydrogen are eliminated in ethylene after irradiation [13,14]. Similarly, elimination of halogen derivatives has been detected in difluoroethylenes [15–17] and vinyl chloride [18,19]. The photodissociation dynamics of ethylene [20], fluoroethylene [21,22], difluoroethylenes [12,23–25] and vinyl chloride [26,27] have also been investigated from the theoretical point of view.

The chiral (4-methylcyclohexylidene) fluoromethane molecule (4MCF) is a fluoroethylene derivative with two R/S enantiomers connected by a torsion around the C=C double bond. Similar to the degeneracy points found for fluoroethylene [11], different CIs have been reported for 4MCF involving torsion, pyramidalization, and H-atom migration [28]. Additionally, a new CI associated with the elimination of hydrogen fluoride (HF) at a twisted geometry has been recently located [29]. Based on these optimized CIs it has been predicted that upon irradiation, the chiral isomers of 4MCF should be obtained after C=C rotation in the presence of polar solvents, while in gas phase dissociation of the HF fragment should dominate [29].

In a series of papers, 4MCF has been proposed as a model system for a light-induced chiral molecular switch or a molecular rotor [30–32]. These devices are all based on the ability of 4MCF to switch between the R/S enantiomers in an efficient way, triggered by a specific laser or sequence of laser pulses especially designed for this purpose. In order to eventually control any of these

* Corresponding author.

E-mail address: leticia.gonzalez@uni-jena.de (L. González).

¹ Present address: Department of Physical Chemistry, Universidad Complutense de Madrid, Av. Complutense s/n, 28040 Madrid, Spain.

molecular devices, the dissociation of any fragment (say HF) is obviously a non-desired competing mechanism that should be avoided.

Inspired by the prototypical twisted–pyramidalized CI found in ethylene [7–9], previous dynamical studies on 4MCF have been done considering the torsion and pyramidalization coordinates [30–32]. In this paper, we focus on the HF-elimination process suggested in Ref. [29]. We consider an approximate model which only includes the torsion around the C=C double bond and the HF-dissociation as reaction coordinates. The competing dynamics are carried out on coupled potential energy surfaces (PES) calculated with *ab initio* methods. Non-adiabatic wavepacket propagations in this reduced model show that, although the system has enough energy to access the HF-elimination CI, isomerization dominates after light irradiation. Even if this conclusion could be modified upon inclusion of further degrees of freedom, the use of reduced dimensionality is expected to accelerate dissociation in most cases. Therefore, our results are encouraging towards the final aim of using 4MCF as a molecular device.

2. Theoretical background

2.1. Quantum chemistry

Fig. 1 shows the two competing reactions studied here: the photoisomerization around the double bond leading to R/S enantiomers versus the photodissociation of the HF moiety. The photoisomerization is mediated by a CI twisted by 90°. The derivative coupling (*h*) and gradient difference (*g*) vectors of this CI are mainly composed of the torsional coordinate of the CHF-group and the stretching of the double bond [28]. The CI mediating the HF-elimination is also twisted around the C=C by 90° [29], but it possesses stretched C–F, C–H and H–F bond distances, as specified in Fig. 2. Its *h* and *g* vectors involve the H–F stretching vibration and some pyramidalization at the terminal carbon atom.

From the *h* and *g* vectors of the two CIs considered here, a proper dynamical study should at least include torsion, pyramidalization, C=C stretching, HF-elimination and H–F vibration, or simply the four mixed reaction coordinates defined by the *h* and *g* vectors. In this paper we aim at a preliminary study restricting ourselves only to two explicit coordinates. Since both CIs are twisted by 90° and the final goal of our device is R/S isomerization, one degree of freedom is necessarily the torsion around C=C bond. This is denoted by φ . In order to have a first glance at the competing HF-dissociation process, the second relevant degree of freedom is dissociation along *R*. For simplicity in defining the kinetic energy operator (see Section 2.2) *R* is defined as the distance between

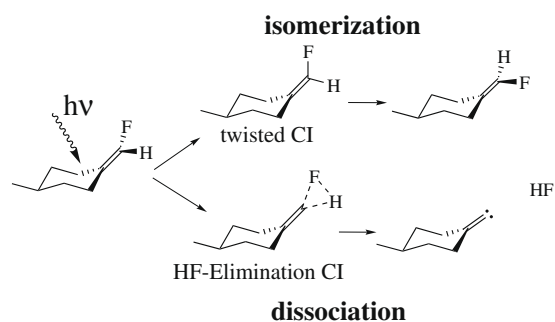


Fig. 1. Competing isomerization and dissociation reactions in 4MCF after light irradiation. The figure shows a scheme of 4MCF in its equilibrium structure. After being excited by light, two different conical intersections (CI) could be accessed: the twisted CI, responsible for isomerization around the double bond and leading to the opposite enantiomer, or the HF-elimination CI, which leads to HF abstraction.

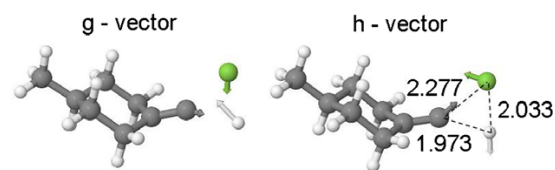


Fig. 2. The gradient difference *g* and derivative coupling *h* vectors of the HF-elimination CI. Distances between the CHF atoms in Angstroms.

the center of masses of the hydrocarbon moiety and the HF fragment. Other degrees of freedom could be added *a posteriori*, e.g. with the help of the Multi-Configurational Time-Dependent Hartree (MCTDH) method [33].

In order to construct the PES, the molecule is assumed to be pre-oriented as shown in Fig. 3, with the *z*-axis lying along the C=C double bond. Starting from the twisted structure of 4MCF (with the HF fragment rotated by 90° around the C=C double bond), a grid of points is calculated along the two coordinates of interest: φ and *R*. That is, the HF fragment is rotated around the C=C double bond and translated in the *R* direction. The HF distance and other coordinates of the molecular scaffolding are kept frozen at the equilibrium geometry (see Fig. 3) obtained at B3LYP/cc-pVTZ level of theory using the Gaussian 03 suite of programs [34]. In this twisted orientation the molecule has local C_s symmetry in the *x,z*-plane, whereas in the rest of the grid the molecule has C_1 symmetry. The two two-dimensional (2D) PESs are each constructed from 22 single point calculations ranging from $\varphi = -90^\circ$ to $\varphi = 90^\circ$, and 13 points between *R* = 2.5 and 6.0 Å. The spacing between the points is inhomogeneous to allow more points around the CIs and the equilibrium structure. An additional point at *R* = 50 Å has been added to the grid to guarantee the correct asymptotic behavior at the dissociation limit. A total of $22 \times 14 = 308$ single point calculations were carried out. Since the PESs are cyclic in φ and possess an inversion center at $\varphi = 90^\circ$, after mirroring with respect to the inversion center, a total of $43 \times 14 = 602$ *ab initio* points were obtained. The PESs were then cubic splined to a grid of $1024 \times 512 = 524\,288$ points, retrieving the final PESs ranging from $\varphi = -90^\circ$ to $\varphi = 270^\circ$, and from *R* = 2.5 to 6.0 Å.

For simplicity, our model is restricted to the first electronic excited state of $\pi\pi^*$ character and the ground state. The single point calculations aimed at obtaining the electronic wavefunctions (which we will denote χ_1 and χ_2 for the ground and first excited state, respectively) were performed using the state-averaged complete active space self-consistent field (SA-CASSCF) method [35] with equal weights for both states. The employed basis set is the double zeta basis set cc-pVDZ [36]. The active space includes eight electrons in eight orbitals, namely the π_{CC} , σ_{CH} , σ_{CF} , σ_{CC} and their

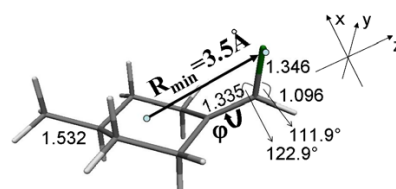


Fig. 3. Equilibrium structure of 4MCF in the electronic ground state rotated by 90° around the double bond. The most relevant bond distances and angles (in Å and degrees, respectively) optimized at B3LYP/cc-pVTZ level of theory are indicated. The coordinate system adopted in the calculation of the potential energy surfaces along the torsional angle φ and the vector *R*, defined from the center of mass of the hydrocarbon moiety to the center of mass of the HF fragment (indicated by dots) is also plotted.

corresponding antibonding ones. The two PESs are coupled and the corresponding non-adiabatic coupling terms (NACTs) (or kinetic couplings) with respect to R and φ , defined as

$$T_{12}^R = \left\langle \chi_1 \left| \frac{\partial}{\partial R} \chi_2 \right. \right\rangle, \quad (1)$$

$$T_{12}^\varphi = \left\langle \chi_1 \left| \frac{\partial}{\partial \varphi} \chi_2 \right. \right\rangle, \quad (2)$$

are calculated at the same level of theory using a finite difference method with the 3-point formula in each dimension. These calculations were performed with the MOLPRO program package [37].

2.2. Diabatization and quantum dynamics

In order to investigate the photodissociation and -isomerization dynamics of 4MCF, we solve the time-dependent Schrödinger equation (TDSE) for the nuclei, which in the adiabatic picture is written as

$$i\hbar \frac{\partial}{\partial t} \begin{pmatrix} \psi_1^{ad}(t) \\ \psi_2^{ad}(t) \end{pmatrix} = \begin{pmatrix} H_{11}^{ad} & H_{12}^{ad} \\ H_{21}^{ad} & H_{22}^{ad} \end{pmatrix} \begin{pmatrix} \psi_1^{ad}(t) \\ \psi_2^{ad}(t) \end{pmatrix}. \quad (3)$$

In our 2D model, an approximate adiabatic Hamiltonian considering part of the coupling between the coordinates φ and R in the kinetic part is given by the terms

$$H_{ii}^{ad} = -\frac{\hbar^2}{2\mu} \left(\frac{\partial^2}{\partial R^2} + T_{ij}^{RR} \right) - \frac{\hbar^2}{2I_r} \left(\frac{\partial^2}{\partial \varphi^2} + T_{ij}^{\varphi\varphi} \right) + V_i^{ad} \quad (4)$$

and

$$H_{ij}^{ad} = -\frac{\hbar^2}{2\mu} \left(2T_{ij}^R \frac{\partial}{\partial R} + T_{ij}^{RR} \right) - \frac{\hbar^2}{2I_r} \left(2T_{ij}^\varphi \frac{\partial}{\partial \varphi} + T_{ij}^{\varphi\varphi} \right), \quad (5)$$

where μ is the reduced mass between the HF fragment and the rest of the molecule, and I_r is the rotational moment of inertia of HF with respect to the C=C axis. V_i^{ad} are the adiabatic PESs for the electronic ground and first excited state computed as described in Section 2.1. $T_{ij}^{R/\varphi}$ are the kinetic couplings terms given in Eqs. (1) and (2); the diagonal elements $T_{ii}^{R/\varphi}$ are zero by definition. The terms $T_{ij}^{RR/\varphi\varphi}$ contain the second derivatives of the electronic wavefunction χ_i with respect to the nuclear coordinates R and φ , respectively, and they are defined by:

$$T_{ij}^{RR} = \left\langle \chi_i \left| \frac{\partial^2}{\partial R^2} \chi_j \right. \right\rangle, \quad (6)$$

$$T_{ij}^{\varphi\varphi} = \left\langle \chi_i \left| \frac{\partial^2}{\partial \varphi^2} \chi_j \right. \right\rangle. \quad (7)$$

The second order kinetic coupling can be ignored since it is much smaller than the first-order one.

The description of nuclear dynamics in the presence of NACTs is often challenging. Near CIs the NACTs between the two states undergo rapid changes; the sharper the crossing the more rapid the change. At the CI itself the kinetic coupling elements become a singularity. Numerically representing and treating such changes and even singularities is a challenging task; therefore, much effort has been devoted to find physically meaningful diabatic representations, see e.g. [38–42]. In this paper, the diabatic potentials V^d are derived directly by transforming the adiabatic ones V^{ad} as

$$V^d = U^i V^{ad} U, \quad (8)$$

where U is a unitary transformation matrix, which for a two state problem has the form

$$U = \begin{pmatrix} \cos \alpha & -\sin \alpha \\ \sin \alpha & \cos \alpha \end{pmatrix}. \quad (9)$$

V_i^d are then the diabatic potentials for the two states of interest and $V_{ij} = V_{ji}$ is the potential coupling. The mixing angle α for each point, defined by R_i and φ_i , is the integral over the corresponding first-order kinetic couplings. To evaluate the mixing angle one has to ensure that the diabatic wavefunctions at 0° and 360° are the same. As a consequence, the path along a given contour Γ must be well-defined, such that [42]

$$\oint_\Gamma T_{12}^\varphi d\varphi = n\pi, \quad (10)$$

where in our case, we choose Γ to be the contour defined by the torsional angle φ . To fulfil such condition we define α_R in 4MCF as

$$\alpha_R(R_i, \varphi_i) = \int_{\varphi_0}^{\varphi_i} T_{12}^\varphi(R_i, \varphi) d\varphi, \quad (11)$$

which for symmetry reasons must be equal between 0° and 180° and between 180° and 360° . Then, the total mixing angle is evaluated as

$$\alpha(R_i, \varphi_i) = \alpha_R(R_i, \varphi_i) + \int_{R_0}^{R_i} T_{12}^R(R, \varphi_0) dR, \quad (12)$$

where R_0 and φ_0 are the points where the adiabatic and diabatic PES are forced to be identical; in our case, these points are defined at the equilibrium coordinates ($R_0 = 3.5 \text{ \AA}$ and $\varphi_0 = 0^\circ$). The path defined in Eq. (12) (first integrating along R and then along φ) is motivated by the fact that T_{12}^R hardly changes along φ (see later Section 3.1). As long as Eq. (10) is fulfilled, many other paths can also be conceived, for instance, using Eq. (11) but with different φ values in Eq. (12), or integrating first along φ and then along R . Different paths could give different diabatic models but ideally they should all lead to similar qualitative dynamics.

In the diabatic representation, the TDSE is written as

$$i\hbar \frac{\partial}{\partial t} \begin{pmatrix} \psi_1^d(t) \\ \psi_2^d(t) \end{pmatrix} = \begin{pmatrix} H_{11}^d & H_{12}^d \\ H_{21}^d & H_{22}^d \end{pmatrix} \begin{pmatrix} \psi_1^d(t) \\ \psi_2^d(t) \end{pmatrix}, \quad (13)$$

where

$$H_{ii}^d = -\frac{\hbar^2}{2\mu} \frac{\partial^2}{\partial R^2} - \frac{\hbar^2}{2I_r} \frac{\partial^2}{\partial \varphi^2} + V_i^d \quad (14)$$

and

$$H_{ij}^d = V_{ij}. \quad (15)$$

The diabatic wavefunctions ψ_i^d are obtained from the adiabatic ones as

$$\psi^d = U^i \psi^{ad}. \quad (16)$$

Therefore, while the adiabatic representation yields equations in which the potential energy matrix is diagonal and the coupling enters through the kinetic energy operator (NACTs), see Eqs. (4) and (5), in the diabatic representation the coupling appears in the potential energy term, whereas the kinetic energy operator is diagonal, see Eqs. (14) and (15).

Using the diabatic PESs of 4MCF, V_1^d and V_2^d , quantum dynamical calculations in 1D (along φ) and 2D (along φ and R) were performed in a grid of 2048 and 1024×512 points, respectively, using the split-operator method [43–46] with a time discretization of 0.01 fs.

The system is initially prepared in the torsional ground state of V_1^d that is localized in the left minimum. Then, it is instantaneously promoted to V_2^d employing a δ -pulse. Torsional eigenfunctions and eigenenergies in 1D were computed with the Fourier-Grid-Hamiltonian method [47] (FGH) using a grid of 2048 points. In 2D the ground state torsional eigenfunction is obtained in the following way. First, two ground state 1D eigenfunctions are calculated with

the FGH method in a grid of 512 points along R for $\varphi = 0^\circ$ and in a grid of 1024 points along φ for $R = 3.5 \text{ \AA}$. Then, an initial 2D guess is prepared as the product of both 1D eigenfunctions. Finally, this guess is relaxed to a minimum by propagating it in imaginary time [48].

3. Results and discussion

3.1. Quantum chemistry

In Fig. 4 we show 1D cuts along φ and R of the adiabatic V_i^{ad} and diabatic V_i^d PESs and their corresponding kinetic and potential couplings, respectively. The ground state potential V_1^{ad} is symmetric and cyclic, and as such, it possesses two equivalent minima at $\varphi = 0^\circ$ and 180° , which correspond to the R and S enantiomers (Fig. 4a). The minima are well separated by two potential barriers at $\varphi = \pm 90^\circ$ of ca. 3.4 eV, guaranteeing that a single enantiomer is stable at room temperature without racemizing. At $\varphi = \pm 90^\circ$ the electronic excited state shows minima, indicating the presence of avoided crossings, as it is typical for olefinic systems at a twisted geometry. However, the gap between V_1^{ad} and V_2^{ad} at these geometries amounts to 2 eV. As it can be seen in Fig. 4b, which shows a 1D cut along R for $\varphi = 90^\circ$, this gap diminishes with R , until $R = 4.6 \text{ \AA}$ where a clear crossing between both states takes place. This point corresponds to the position of the HF-elimination CI within this unrelaxed grid.

Despite the large gap between the maximum of V_1^{ad} and the minimum of V_2^{ad} at $\varphi = 90^\circ$ and $R = 3.5 \text{ \AA}$, a non-zero kinetic coupling of -1.7 a.u. (see T_{12}^φ in Fig. 4c) indicates that this point is

an avoided crossing belonging to the twisted CI [28]. The large kinetic coupling of -10.7 a.u. at $R = 4.6 \text{ \AA}$ (see T_{12}^R in Fig. 4d) confirms that this point is part of the HF-elimination CI. Note that the coupling elements T_{12}^R are negligible along both coordinates, a fact that substantiates the diabaticization path chosen in Eq. (12). Since the adiabatic V_1^{ad} and V_2^{ad} potentials are symmetric and cyclic along the torsion coordinate, one expects the corresponding diabatic ones V_1^d and V_2^d to be symmetric and cyclic, too. The diabatic potentials and associated potential couplings are shown in Fig. 4e–h. To perform the 1D diabaticization, the unitary transformation matrix U was chosen to be the identity at $\varphi = 0^\circ$. The cyclic condition was achieved by forcing the mixing angle α (see Eq. (12)) in U to be zero after the integration over 360° . We note that whereas the cyclic condition for the diabatic potentials is mandatory for the subsequent wavepacket propagations the symmetric condition is not. The two diabatic states are symmetric only if the mixing angle reaches a multiple of π or $\pi/2$ at its maximum [42]. In practice, this ideal condition is not necessarily sustained. Fig. 5 shows the corresponding adiabatic and diabatic 2D PES along φ and R , as well as the potential coupling V_{12} in 2D. As can be seen, the adiabatic and diabatic PESs are cyclic in φ , but while the adiabatic PESs are symmetric (by construction), the diabatic ones are not. The origin of this asymmetry can be found in Fig. 6. Panel (a) shows the mixing angle along both coordinates, and already it can be acknowledged that the topology is not behaving ideally everywhere. In Fig. 6b and c, two exemplary 1D cuts of the mixing angle α are shown at $R = 3.5 \text{ \AA}$ and 4.8 \AA and at $\varphi = 0^\circ$ and 180° , respectively. The trend of the mixing angle along φ is as to be expected; however, while for $R = 3.5 \text{ \AA}$ the difference between α at $\varphi = 0^\circ$ and 180° is close to $\pi/2$, for $R = 4.8 \text{ \AA}$ it is less than that (see Fig. 6b). More noticeable is that the difference between the mixing angle in R for $\varphi = 0^\circ$ and 180° is neither constant, nor is it equal to $\pi/2$ (Fig. 6c). An analysis of the electronic wavefunction reveals that the deviations of the mixing angle α are due to some spurious configuration mixing of the $\pi\pi^*$ transition with the $\pi\sigma^*$ one.

3.2. Quantum dynamics

For didactic purposes, first we analyze the non-adiabatic isomerization dynamics alone. This is done using the 1D diabatic potential energy profiles along torsion at the minimum $R = 3.5 \text{ \AA}$

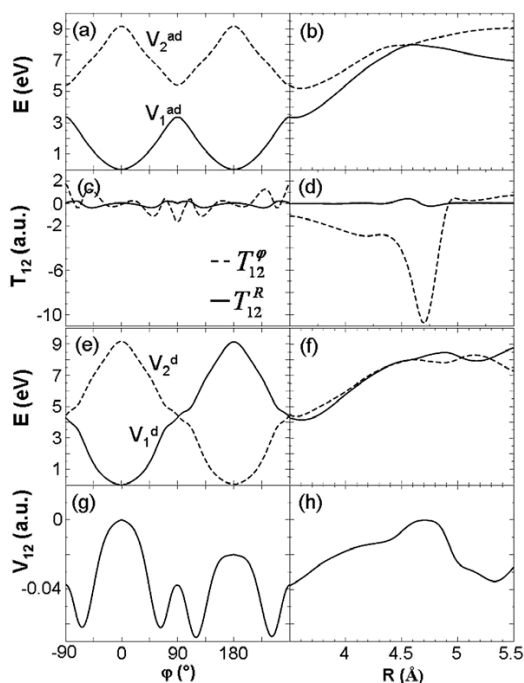


Fig. 4. One-dimensional (1D) potential energy curves and corresponding couplings calculated at the CASSCF(8,8)/cc-pVDZ level of theory. (a) Unrelaxed adiabatic electronic ground (V_1^{ad} in solid) and first singlet excited (V_2^{ad} in dotted) states along φ for $R = 3.5 \text{ \AA}$. (b) Dito along R for $\varphi = 90^\circ$. (c and d) Non-adiabatic (or kinetic) couplings along φ and R , respectively, for the 1D cuts shown in (a) and (b), respectively. (e and f) Diabatic electronic V_1^d (solid) and V_2^d (dotted) states along φ for $R = 3.5 \text{ \AA}$, and R for $\varphi = 90^\circ$, respectively. (g and h) Potential couplings along φ and R , respectively, for the 1D cuts shown in panels (e) and (f), respectively.

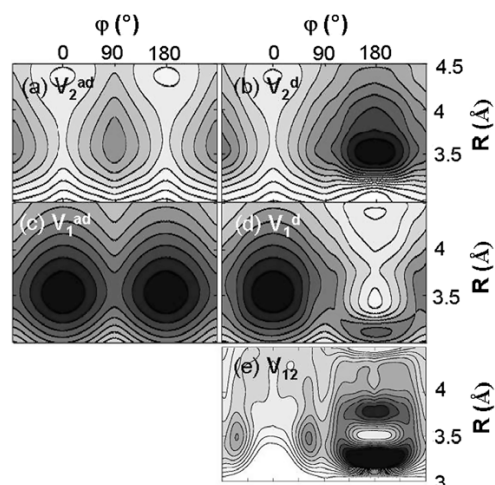


Fig. 5. Adiabatic and diabatic two-dimensional potentials, as well as potential coupling, in a.u. calculated at the CASSCF(8,8)/cc-pVDZ level of theory. Contour lines drawn every 0.05 hartrees. (a) V_2^{ad} , (b) V_2^d , (c) V_1^{ad} , (d) V_1^d , (e) V_{12} .

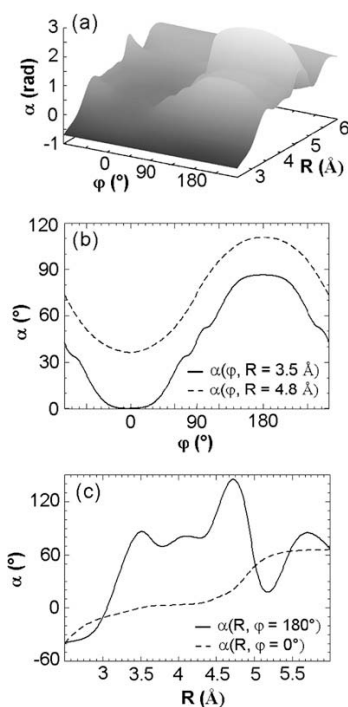


Fig. 6. Mixing angle α calculated with Eq. (12). (a) 2D surface along ϕ and R . (b) 1D cuts for $R = 3.5 \text{ \AA}$ (solid) and 4.8 \AA (dashed). (c) 1D cuts for $\phi = 180^\circ$ (solid) and 0° (dashed).

(Fig. 4e). We assume all molecules to be in the configuration of the *S* enantiomer ($\phi = 0^\circ$), and therefore to be located in the minimum of the V_1^d state. After a δ -pulse the complete population is vertically excited to V_2^d . Snapshots of the wavepacket in 1D for selected times are shown in Fig. 7 in the diabatic picture (Fig. 7a–d) as well as transformed back to the adiabatic representation (Fig. 7e–h). The adiabatic wavefunctions are obtained from the diabatic ones using Eq. (16). As it can be seen in Fig. 7b or f, the wavepacket spreads very quickly in both directions along the torsion coordinate. Since the potential is cyclic, both wavepacket portions interfere constructively after ca. 150 fs recovering a localized wavepacket at $\phi = 180^\circ$ (*R*-enantiomer) (Fig. 7c or g). The last snapshot after 700 fs shows the wavepacket completely delocalized between the

R and *S* enantiomers (Fig. 7d and h). As it can be expected, both adiabatic and diabatic simulations provide the same result. The population transfer to the electronic ground state is less than 10^{-5} , even at 700 fs. The fact that the non-adiabatic population transfer to the ground state is negligibly small is not surprising since the NACT at $\phi = 90^\circ$ is small and the gap between the PESs is still large (recall Figs. 4a and c), indicating that other coordinates are necessary to deactivate to the ground state.

In the following, we show the results of the quantum dynamic simulations in 2D, which allow us to investigate the branching of the wavepacket along the torsional coordinate (which would preserve a potential molecular rotor or switch) and along the dissociation coordinate (HF fragment elimination) after excitation to the bright $\pi\pi^*$ excited state. Due to the presence of the CI, we assume that HF dissociation takes place only on the ground state, while a rotor can be preserved in the excited as well as in the ground state. Therefore, it is interesting to investigate the efficiency of the non-adiabatic population transfer to the ground state at or near the CI.

Snapshots of the wavepacket propagation on the 2D diabatic surfaces at selected times are shown in Fig. 8. As in the 1D case, the initial wavepacket in the *S* enantiomer is excited to the V_2^d with a δ -pulse. After 70 fs (Fig. 8b), we can see that the wavepacket moves along both R and ϕ coordinates following the gradient of the corresponding V_2^d PES (superimposed in Fig. 8a). We also see that a portion of the wavepacket is already transferred to V_1^d (Fig. 8f), as it occurs in the 1D case (see solid line in Fig. 7b). Also, after 150 fs a recombination of the wavepacket in the *R*-enantiomer is observed (Fig. 8c and g). After 700 fs the wavepacket has not moved beyond ca. $R = 4 \text{ \AA}$. This indicates, that up to 700 fs no dissociation is observed within our reduced model. Torsion dominates, although the wavepacket starts with an excess of energy of ca. 2 eV with respect to the HF-elimination CI (compare the Franck–Condon energy at Fig. 4a and the energy of the HF-elimination CI in Fig. 4b). The absence of dissociation during these early times is related to insufficient momentum transfer from ϕ to R . This can be observed in the momentum representation of the diabatic wavepacket distributions ψ_2^d and ψ_1^d , shown in Fig. 8i and j, respectively, after 700 fs.

In photodissociation dynamical studies it is very typical to explore the quantum distributions of the products (see e.g., Refs. [14,49]). Similarly, to evaluate the efficiency of a possible rotor within our 2D model, we can follow the population dynamics in the basis of the 1D torsional levels ϕ_v^i calculated at the equilibrium geometry for the potential i . The population $P_v^i(t)$ in each torsional state v for the potential i is then defined by:

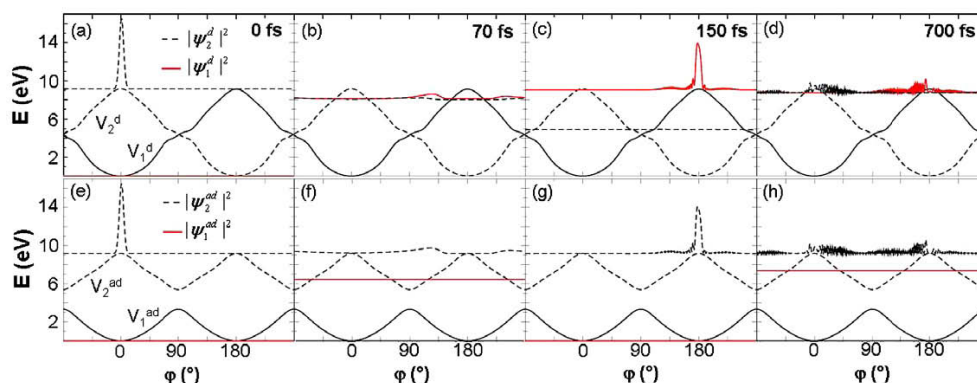


Fig. 7. Snapshots of the diabatic (a–d) and adiabatic (e and h) wavefunctions in their corresponding potential energy curves at selected times, as indicated. The baselines of the wavefunctions $\psi_1^{d/ad}$ (solid) and $\psi_2^{d/ad}$ (dotted) indicate their energy.

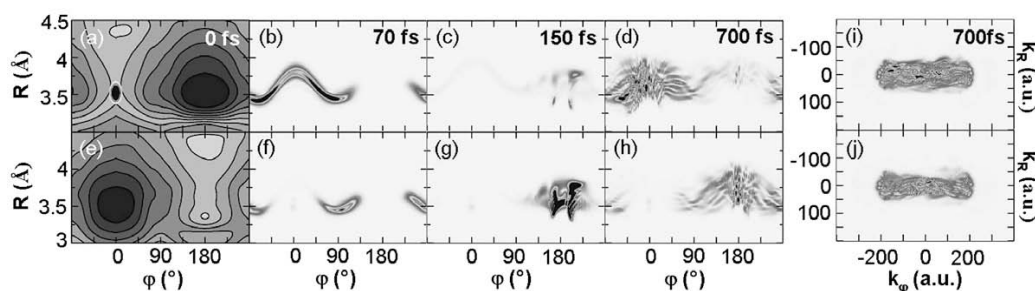


Fig. 8. Snapshots of wavepacket distributions in the two-dimensional diabatic potentials V_2^d (panels a–d) and V_1^d (panels e–h) along R and φ for selected times. The corresponding PESs are superimposed in panels (a) and (e). At $t = 0$ fs the wavepacket is assumed to be excited instantaneously with a δ -pulse from the left well of the ground state to the excited state. (i) ψ_2^d wavepacket probability distribution in the momentum representation along R and φ -grid for $t = 700$ fs. (j) Dito for ψ_1^d .

$$P_v^i(t) = \int_R \left| \int_{\varphi} \phi_v^{is}(\varphi) \psi_i^d(R, \varphi, t) d\varphi \right|^2 dR. \quad (17)$$

If the sum of the populations in both potentials $P_v = \sum_i P_v^i$ is constant in time, the 2D dynamics is equivalent to the 1D one. This would imply that the energy of the system remains in the torsion, and therefore a molecular rotor can be achieved. However, if P_v varies strongly with time the rotor is destroyed due to dissociation. Fig. 9a and b show the out-of-phase P_v^1 and P_v^2 populations until 1 ps, indicating population exchange between the two diabatic potentials. From the out-of-phase period, one can estimate that the required time to pass from the R to the S enantiomer is ca. 150 fs, in gratifying agreement with the time inferred from the 1D and 2D snapshots (see Figs. 7 and 8, respectively). The time evolution of the sum of both populations is plotted in Fig. 9c. We observe that lower torsional levels are slowly populated over time. This slight decrease can be also seen in the inset (Fig. 9d), where the average torsional level $\langle v \rangle = v P_v$ until 1 ps is plotted. At the end of the propagation time, the expectation value of v has merely dropped from ca. 440 to 400. The dissociation energy of 4MCF is ca. 7.5 eV (see Fig. 4b) and this is equivalent to a torsional level of

around 350; hence, we see that, at least in a sub-ps time scale, torsion dominates.

4. Conclusions

In this paper a simple model is set up to investigate the chiral interconversion between R and S enantiomers of the (4-methylcyclohexylidene) fluoromethane molecule (4MCF), obtained upon rotation around the olefinic double bond, versus the competing reaction of eliminating HF. The study of these competing reactions is motivated by the experimental observation that ethylene or halogenated ethylene derivatives show molecular hydrogen or hydrogen hydride fragmentation, and by the HF-elimination CI located for 4MCF. To this aim, PESs for 4MCF have been calculated using the multiconfigurational method CASSCF, along the torsion around the C=C bond and the distance between the center of masses of the hydrocarbon moiety and the HF fragment. For simplicity, only the electronic ground state and the bright $\pi\pi^*$ excited states have been considered, while Rydberg [28] or other states are excluded. The PESs are non-adiabatically coupled by the presence of a CI leading to HF elimination. Using *ab initio* CASSCF kinetic couplings, the PESs are diabitized and wavepacket propagations have been carried out.

Interestingly, our calculations show that despite the system starts with enough kinetic energy to arrive to the HF-elimination CI, there is no transfer of population to the ground state in a sub-ps time scale. Up to 1 ps the momentum of the initial wavepacket remains localized in the torsion with a negligible transfer to the HF-elimination coordinate. At longer time scales, intramolecular vibrational redistribution of the energy is expected and our model cannot be considered reliable anymore. During the first hundreds of fs, our model indicates that isomerization dominates over dissociation. This conclusion can result striking at first glance, since it is experimentally well known that difluoroethylenes show different dissociation channels after light irradiation [15–17], and HF-elimination is one of them. No time-resolved experiments are available for 4MCF allowing for a direct comparison; however, by analogy with fluoroethylene derivatives one would expect HF photodissociation taking place in 4MCF. Of course, it is possible that this reaction channel operates in a much longer time scale than the one investigated here. Our calculations indicate a clear trend of slowly populating lower torsional levels with time (recall Fig. 9d), which, extrapolated to longer time scales, could ultimately result in HF-elimination.

At this point it is also worth to think about the theoretical approximations which are behind the model employed here. The most important limitation of our calculations is the use of a reduced 2D system. It is tempting to assume, that – in principle – the lack of other coordinates calls for caution of the interpretation

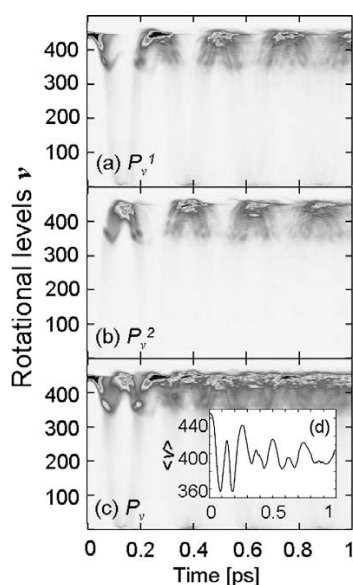


Fig. 9. Population dynamics in the basis of the torsional eigenstates for V_1^d (a), V_2^d (b) and the sum of both (c). The inset (d) shows the average torsional level v .

of the results. However, because after vertical excitation 4MCF does have enough excess kinetic energy to reach the HF-elimination CI, we think that photodissociation should have manifested already within this 2D model, but it has not. Other coordinates, like the H–F distance or pyramidalization, will certainly move the position of the CI, lowering it, and thus adding more excess of kinetic energy to the initial wavepacket. Even though this could accelerate the transfer of momentum from the torsion to the HF-dissociation coordinate, it is not plausible that the time scale of the photolysis changes from ns to fs.

Based on these considerations, we are therefore left to conclude that the HF-dissociation dynamics from the $\pi\pi^*$ state is not competitive to isomerization in 4MCF, at least on a sub-ps time scale.

Acknowledgement

This work is supported by the Deutsche Forschungsgemeinschaft in the framework of a trilateral cooperation between Israel, Palestine, and Germany with the project GO 1059/5-2.

References

- [1] M. Klessinger, J. Michl, *Excited States and Photochemistry of Organic Molecules*, VCH, New York, 1995.
- [2] R.W. Schoenlein, L.A. Peteanu, R.A. Mathies, C.V. Shank, *Science* 254 (1991) 412.
- [3] S. Olsen, A. Toniolo, C. Ko, L. Manohar, K. Lamothe, T.J. Martínez, *Computational Photochemistry, Computational Reaction Mechanisms and Dynamics in Photobiology*, Elsevier, Amsterdam, 2005, p. 225.
- [4] B.G. Levine, T.J. Martínez, *Ann. Rev. Phys. Chem.* 58 (2007) 613.
- [5] R.P. Krawczyk, A. Viel, U. Manthe, W. Domcke, *J. Chem. Phys.* 119 (2003) 1397.
- [6] M. Barbatti, J. Paier, H. Lischka, *J. Chem. Phys.* 121 (2004) 11614.
- [7] M. Ben-Nun, T.J. Martínez, *Chem. Phys. Lett.* 298 (1998) 57.
- [8] M. Ben-Nun, T.J. Martínez, *J. Phys. Chem. A* 103 (1999) 10517.
- [9] M. Ben-Nun, T.J. Martínez, *Chem. Phys.* 259 (2000) 237.
- [10] A. Viel, R.P. Krawczyk, U. Manthe, W. Domcke, *J. Chem. Phys.* 120 (2004) 11000.
- [11] M. Barbatti, A.J.A. Aquino, H. Lischka, *J. Phys. Chem. A* 109 (2005) 5168.
- [12] J. González-Vázquez, L. González, *Chem. Phys.* 349 (2008) 287.
- [13] B.A. Balko, J. Zhang, Y.T. Lee, *J. Chem. Phys.* 97 (1992) 935.
- [14] E.F. Cromwell, A. Stolow, M.J.J. Vrakking, Y.T. Lee, *J. Chem. Phys.* 97 (1992) 4029.
- [15] G.E. Hall, J.T. Muckerman, J.M. Preses, J. Ralph, E. Weston, G.W. Flynn, A. Persky, *J. Chem. Phys.* 101 (1994) 3679.
- [16] B.A. Balko, J. Zhang, Y.T. Lee, *J. Phys. Chem. A* 101 (1997) 6611.
- [17] J.J. Lin, S.M. Wu, D.W. Hwang, Y.T. Lee, X. Yang, *J. Chem. Phys.* 109 (1998) 10838.
- [18] D.A. Blank, W. Sun, A.G. Suits, Y.T. Lee, S.W. North, G.E. Hall, *J. Chem. Phys.* 108 (1998) 5414.
- [19] K. Sato, S. Tsunashima, T. Takayanagi, G. Fijisawa, A. Yokoyama, *Chem. Phys. Lett.* 242 (1995) 401.
- [20] A. Peña-Gallego, E. Martínez-Núñez, S.A. Vázquez, *Chem. Phys. Lett.* 353 (2002) 418.
- [21] E.M. Núñez, S.A. Vázquez, *Struct. Chem.* 12 (2001) 95.
- [22] E. Martínez-Núñez, C.M. Estévez, J.R. Flores, S.A. Vázquez, *Chem. Phys. Lett.* 348 (2001) 81.
- [23] J. González-Vázquez, A. Fernández-Ramos, E. Martínez-Núñez, S.A. Vázquez, *J. Phys. Chem. A* 107 (2003) 1389.
- [24] J. González-Vázquez, A. Fernández-Ramos, E. Martínez-Núñez, S.A. Vázquez, *J. Phys. Chem. A* 107 (2003) 1398.
- [25] S.A. Vázquez, F.J. Aoi, L. Bañares, J. Santamaría, E. Martínez-Núñez, A. Fernández-Ramos, *J. Chem. Phys.* 118 (2003) 9641.
- [26] E.M. Núñez, A. Fernández-Ramos, S.A. Vázquez, F.J. Aoi, L. Bañares, *J. Phys. Chem. A* 107 (2003) 7611.
- [27] J. González-Vázquez, E. Martínez-Núñez, S.A. Vázquez, J. Santamaría, L. Bañares, *Chem. Phys. Lett.* 396 (2004) 442.
- [28] M. Schreiber, M. Barbatti, S. Zilberg, H. Lischka, L. González, *J. Phys. Chem. A* 111 (2007) 238.
- [29] S. Zilberg, S. Cogan, Y. Haas, O. Deeb, L. González, *Chem. Phys. Lett.* 443 (2007) 43.
- [30] D. Kröner, L. González, *Phys. Chem. Chem. Phys.* 5 (2003) 3933.
- [31] D. Kröner, L. González, *Chem. Phys.* 298 (2004) 55.
- [32] Y. Fujimura, L. González, D. Kröner, J. Manz, I. Mehdaoui, B. Schmidt, *Chem. Phys. Lett.* 386 (2004) 248.
- [33] H.-D. Meyer, F. Gatti, G.A. Worth, *Multidimensional Quantum Dynamics: MCTDH Theory and Applications*, Wiley VCH, 2009.
- [34] M.J. Frisch, G.W. Trucks, H.B. Schlegel, G.E. Scuseria, M.A. Robb, J.R. Cheeseman, J.A. Montgomery, Jr., T. Vreven, K.N. Kudin, J.C. Burant, J.M. Millam, S.S. Iyengar, J. Tomasi, V. Barone, B. Mennucci, M. Cossi, G. Scalmani, N. Rega, G.A. Petersson, H. Nakatsuji, M. Hada, M. Ehara, K. Toyota, R. Fukuda, J. Hasegawa, M. Ishida, T. Nakajima, Y. Honda, O. Kitao, H. Nakai, M. Klene, X. Li, J.E. Knox, H.P. Hratchian, J.B. Cross, V. Bakken, C. Adamo, J. Jaramillo, R. Gomperts, R.E. Stratmann, O. Yazyev, A.J. Austin, R. Cammi, C. Pomelli, J.W. Ochterski, P.Y. Ayala, K. Morokuma, G.A. Voth, P. Salvador, J.J. Dannenberg, V.G. Zakrzewski, S. Dapprich, A.D. Daniels, M.C. Strain, O. Farkas, D.K. Malick, A.D. Rabuck, K. Raghavachari, J.B. Foresman, J.V. Ortiz, Q. Cui, A.G. Baboul, S. Clifford, J. Cioslowski, B.B. Stefanov, G. Liu, A. Liashenko, P. Piskorz, I. Komaromi, R.L. Martin, D.J. Fox, T. Keith, M.A. Al-Laham, C.Y. Peng, A. Nanayakkara, M. Challacombe, P.M.W. Gill, B. Johnson, W. Chen, M. W. Wong, C. Gonzalez, J.A. Pople, Gaussian 03, Revision D.01 Gaussian, Inc., Wallingford, CT, 2004.
- [35] B.O. Roos, *Adv. Chem. Phys.* 69 (1987) 399.
- [36] T.H. Dunning Jr., *J. Chem. Phys.* 90 (1989) 1007.
- [37] H.-J. Werner, P.J. Knowles, R. Lindh, F.R. Manby, M. Schütz, P. Celani, T. Korona, A. Mitrushenkov, G. Rauhut, T.B. Adler, R.D. Amos, A. Bernhardsson, A. Berning, D.L. Cooper, M.J.O. Deegan, A.J. Dobbyn, F. Eckert, E. Goll, C. Hampel, G. Hetzer, T. Hrenar, G. Knizia, C. Köppl, Y. Liu, A.W. Lloyd, R.A. Mata, A.J. May, S.J. McNicholas, W. Meyer, M.E. Mura, A. Nicklass, P. Palmieri, K. Pflüger, R. Pitzer, M. Reiher, U. Schumann, H. Stoll, A.J. Stone, R. Tarroni, T. Thorsteinsson, M. Wang, A. Wolf, Molpro, version 2006.1, a package of ab initio programs, 2006.
- [38] H. Köppl, W. Domcke, L.S. Cederbaum, *Adv. Chem. Phys.* 57 (1984) 59.
- [39] B.H. Lengsfeld III, D.R. Yarkony, *Adv. Chem. Phys.* 82 (1992) 1.
- [40] T. Pachter, L.S. Cederbaum, H. Köppl, *Adv. Chem. Phys.* 84 (1993) 293.
- [41] W. Domcke, D.R. Yarkony, H. Köppl (Eds.), *Conical Intersections: Electronic Structure, Dynamics and Spectroscopy*, World Scientific, Singapore, 2004.
- [42] M. Baer, *Beyond Born–Oppenheimer: Electronic Nonadiabatic Coupling Terms and Conical Intersections*, John Wiley & Sons, Hoboken, 2006.
- [43] M.D. Feit, J.A. Fleck Jr., A. Steiger, *J. Comput. Phys.* 47 (1982) 412.
- [44] M.D. Feit, J.A. Fleck Jr., *J. Chem. Phys.* 78 (1983) 301.
- [45] M.D. Feit, J.A. Fleck Jr., *J. Chem. Phys.* 80 (1984) 2578.
- [46] R. Kosloff, *Annu. Rev. Phys. Chem.* 45 (1994) 145.
- [47] C.C. Martson, G.G. Balint-Kurti, *J. Chem. Phys.* 91 (1989) 3571.
- [48] R. Kosloff, *Dynamics of Molecules and Chemical Reactions*, Marcel Dekker, New York, 1996, p. 185.
- [49] M. Oppel, G.K. Paramonov, *Phys. Rev. A* 60 (1999) 3663.

4.2 The Role of $\pi\sigma^*$ States in 4MCF

The following article “*The Role of $\pi\sigma^*$ States in the Photochemistry of the Chiral Fluoroethylene Derivative (4-methylcyclohexylidene) fluoromethane*” is motivated by the previous investigation of the competing relaxation paths, torsion versus HF-elimination, described in section 4.1. There, only the ground and the bright $\pi\pi^*$ electronic excited state were taken into consideration. Along the dissociation coordinate, however, a configuration state mixing of the $\pi\pi^*$ with a $\pi\sigma^*$ state has been found. Hence, in the following paper a careful study of the role of $\pi\sigma^*$ states during the dissociation process in 4MCF is presented.

Actually, in very many cases, bond cleavage after light irradiation involves $\pi\sigma^*$ states [116, 117, 118]. The simplest hydrogen halide, HF, water, or ammonia are textbook examples. A review of the ubiquitous nature of $\pi\sigma^*$ states in many molecules and their importance in photochemistry has been recently published by Ashfold et al. [119]. These states correspond to an excitation from a π occupied bonding orbital to an empty antibonding σ^* orbital and can be populated either directly (although oscillator strengths are typically small) or nonradiatively via CoIns. The PESs associated with these $\pi\sigma^*$ excited states are directly repulsive and correlate asymptotically with the electronic state energy depending on the radical products. In Figure 8 an excited state dissociation of an A-B system is exemplary illustrated. First, an excitation to a bright bound state $[A-B]^*$ takes place. Along the dissociation coordinate, R (distance between the fragments A and B), the wavepacket can cross a CoIn between the bound (e.g. $\pi\pi^*$) and a repulsive state (e.g. $\pi\sigma^*$) and diabatically move on the repulsive state to form the radical products $A\bullet^* + \bullet B$.

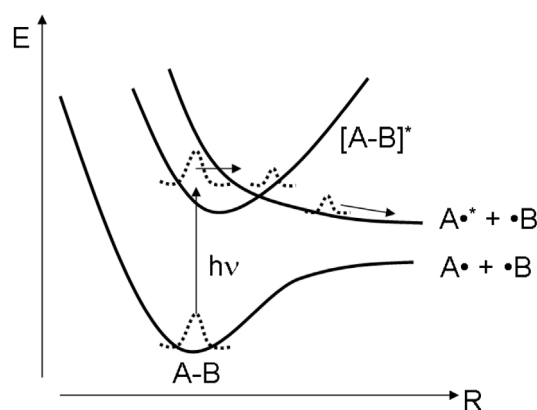


Figure 8: Schematic illustration of an excited state photodissociation in an exemplary A-B system: A wavepacket excited to a bound state $[A-B]^*$ experiences a coupling to a repulsive state, which leads to a partial dissociation to $A\bullet^* + \bullet B$.

The dynamics in such systems, that show N-H dissociation [120, 121, 122, 123, 124], for example small aromatic N-heterocycles, like pyrrole, indole, imidazole, or nucleobases [123, 125], very much depends on the location of the $\pi\pi^*/\pi\sigma^*$ CoIn near the Franck-Condon (FC) geometries as well as on the stability of the resulting excited radical products, i.e. another CoIn between the repulsive and the ground state at extended R exists in cases where the energy of $A\bullet^* + \bullet B$ is actually lower than $A\bullet + \bullet B$ at very large distances.

Until now, there are no ethene like systems demonstrated, in which a scheme like in Figure 8 was found or studied. Here, in 4MCF, we study the concerted dissociation of the HF-fragment, which involves a cleavage of two σ -bonds (see Figure 7). Hence, the description of a possible repulsive state along the dissociation coordinate could be quite complicated. In the following publication, two questions are of interest. (i) If $\pi\sigma^*$ states exist in the vicinity of the bright $\pi\pi^*$ state, does a CoIn exist similar to the crossing depicted in Figure 8 such that the $\pi\sigma^*$ state can be populated after photoexcitation to the $\pi\pi^*$ state? (ii) How do possible $\pi\sigma^*$ states evolve along the HF-dissociation coordinate and how stable are the excited state dissociation products compared to a ground state reaction?

To the aim of answering these questions, several calculations of the vertical excitation energies of 4MCF have been carried out at CASSCF and CASPT2 level of theory taking into account large active spaces which, while excluding Rydberg orbitals, are able to describe $\pi\sigma^*$ and $\pi\pi^*$ valence states simultaneously. The results show that the relative position of the bright $\pi\pi^*$ and lowest $\pi\sigma^*$ state is very sensitive to the choice of active space, basis set, and level of theory. This is actually due to the fact that both states are very close in energy, and belong to a seam of CoIns between the $\pi\pi^*$ and the $\pi\sigma^*$ states. Moreover, a spectrum has been simulated by calculating the vertical excitation energies for several geometries near the equilibrium one, that were created by a Wigner distribution around the normal modes (recall section 3.3). Investigation of the spectrum reveals that the bright $\pi\pi^*$ state is distributed in the adiabatic first and second electronic excited states, an indication that small geometric changes in 4MCF are sufficient to change the outcome of the dissociation dynamics.

Within the two-state relaxation model (section 4.1), that considers only the ground and the bright $\pi\pi^*$ states, dissociation of HF in 4MCF is discussed to take place in the electronic ground state. However, as described above, HF dissociation involves the presence of $\pi\sigma^*$ states that cross the bright $\pi\pi^*$ state already at the FC geometry. Calculating the two-dimensional PESs along both torsional and HF-dissociation coordinates using six roots, we show that the $\pi\sigma^*$ states are repulsive along the dissociation coordinate. As a consequence, it is also plausible that HF fragmentation takes place in these electronic

excited states. Hence, with the resulting potentials, it is evident that the ultrafast radiationless relaxation dynamics in 4MCF might be different from the one suggested until now. The “old” versus the “new” picture of HF-dissociation in 4MCF is schematically illustrated in Figure 9a) and b), respectively.

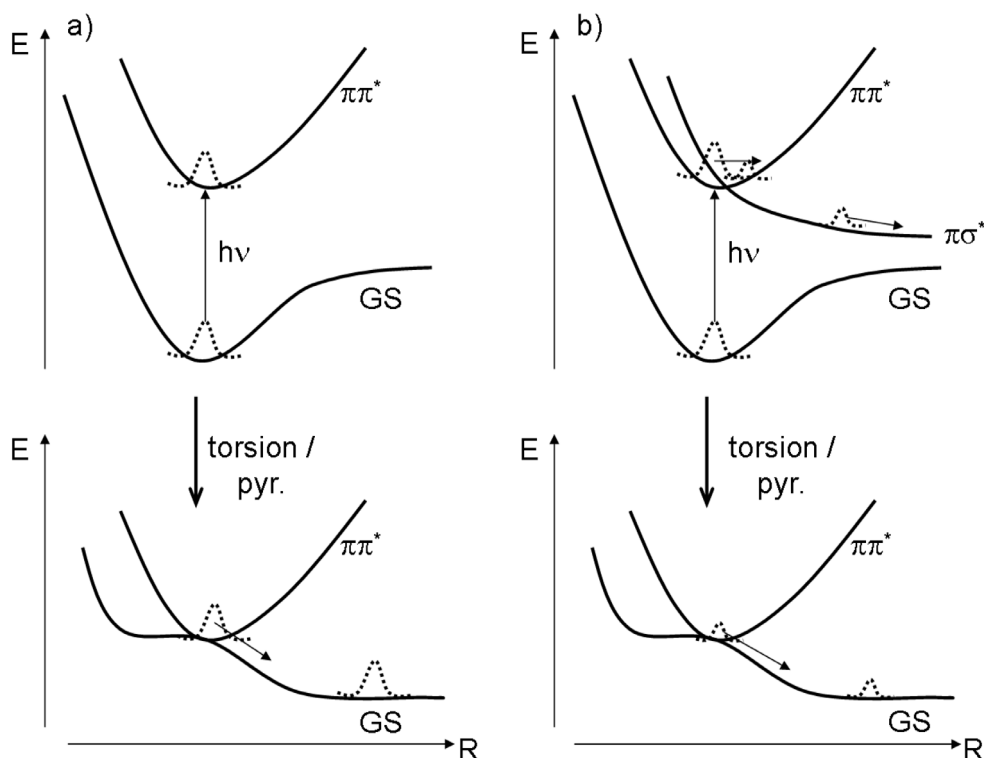


Figure 9: Deactivation paths in the HF photodissociation of 4MCF along dissociation coordinates R in a): two-state model ground state path and b): competing paths in the many-states model including $\pi\sigma^*$ states, i.e. excited state path vs. ground state path after torsion. Time evolution and branching of a wavepacket is indicated.

While population can still be transferred to the ground state via a torsion of the HF fragment like in the two-state system (Figure 9a)), the molecule can also dissociate through the dissociative $\pi\sigma^*$ states without preliminary torsion (Figure 9b)). The possible dissociation path can be even more complicated since the $\pi\sigma^*$ states described are distinct for the two bonds broken during the dissociation, i.e. there are two repulsive states that can individually cause a situation described in Figure 8. One of them is describing the promotion of an electron into the σ^* of the C-H bond, while the other state describes the promotion into the antibonding C-F σ orbital. Hence, in order to achieve a concerted HF-elimination these two states need to be populated equally during the excited state process.

Furthermore, it is shown that in order to describe photodissociation dynamics in

4MCF it will be necessary to include at least three electronic states from the energetic point of view, i.e. the lowest three electronic states for the dissociation products are located below the excitation energy to the bright $\pi\pi^*$ state at the Franck-Condon geometry. Higher excited states lie above the initial potential energy after excitation and, thus, will be not accessible in terms of energy conservation.

The main result of the study presented in the following article, is that, as in other organic molecules, $\pi\sigma^*$ states are also of great importance in the description of the photodissociation in the ethylene derivative 4MCF. Hence, inclusion and description of at least one $\pi\sigma^*$ state besides the mandatory ground and $\pi\pi^*$ state is necessary to investigate the whole deactivation dynamics of 4MCF upon excitation into the $\pi\pi^*$ state. Concluding, full-dimensional dynamics are necessary in order to extract the most important deactivation path in 4MCF and to answer the question of the efficiency of an excited state dissociation process versus a ground state one. In the following paper, it is found that for such dynamics the flexibility of the quantum chemistry description is of great importance in order not to be limited by it *a priori*, i.e. any dynamic simulation for 4MCF will not show excited state dissociation, unless the quantum chemistry is able to describe dissociative $\pi\sigma^*$ states (recall Figure 9).

Next, the article “*The Role of $\pi\sigma^*$ States in the Photochemistry of the Chiral Fluoroethylene Derivative (4-methylcyclohexylidene)fluoromethane*”, originally published in the *International Journal of Quantum Chemistry*, Volume 111, in 2011, will be reprinted.

(D. K. contributed to the following study by investigating the vertical excitation spectrum of 4MCF using different levels of quantum chemistry approaches (i.e. varying size of active space, basis set and inclusion of dynamic correlation (CASSCF vs. CASPT2)), by calculating the PESs along the HF-elimination and torsional degrees of freedom, identifying the $\pi\pi^*/\pi\sigma^*$ CoIn at the Franck-Condon region and by calculating the UV spectrum from a Wigner distribution of geometries in the vibrational ground state around the equilibrium structure of 4MCF. D. K. also prepared the manuscript.

J. G.-V. and L. G. supervised the research and revised the manuscript.)

The Role of $\pi\sigma^*$ States in the Photochemistry of the Chiral Fluoroethylene Derivative (4-methylcyclohexylidene)fluoromethane

DANIEL KINZEL, JESÚS GONZÁLEZ-VÁZQUEZ, LETICIA GONZÁLEZ

Institut für Physikalische Chemie, Friedrich-Schiller-Universität Jena, Helmholtzweg 4, 07743 Jena, Germany

Received 25 October 2010; accepted 30 November 2010

Published online 29 March 2011 in Wiley Online Library (wileyonlinelibrary.com).

DOI 10.1002/qua.23026

ABSTRACT: Multiconfigurational ab initio calculations of the excited states and potential energy curves of the chiral fluoroethylene derivative (4-methylcyclohexylidene)fluoromethane provide evidence that $\pi\sigma^*$ states play an important role in the abstraction of HF. We show that more than the ground and valence $\pi\pi^*$ states are necessary to correctly describe the relaxation of the title molecule upon excitation to the bright valence $\pi\pi^*$ state. A conical intersection between the $\pi\sigma^*$ and $\pi\pi^*$ states has been identified at the FC geometry which makes dissociation of HF in the electronic excited state possible. This conclusion is different from all the previous studies on ethylenic systems where dissociation is postulated as a ground state reaction.

© 2011 Wiley Periodicals, Inc. *Int J Quantum Chem* 111: 3394–3404, 2011

Key words: photochemistry; excited states; conical intersections; photodissociation

Correspondence to: L. González; e-mail: leticia.gonzalez@uni-jena.de

In memoriam of Prof. Björn Roos, for his fundamental contributions to quantum chemistry.

Jesús González-Vázquez is currently at: Departamento de Química Física I, Universidad Complutense, 28040 Madrid, Spain.

Contract grant sponsor: Deutsche Forschungsgemeinschaft.

Contract grant number: GO 1059/7-3.

Additional Supporting Information may be found in the online version of this article.

1. Introduction

The ubiquitous nature of $\pi\sigma^*$ states in many molecules and their importance in photochemistry has been recently reviewed by Ashfold et al. [1]. These states correspond to an excitation from a π occupied bonding orbital to an empty antibonding σ^* orbital and can be populated either directly (although oscillator strengths are typically small) or nonradiatively via conical intersections (CI).

In very many cases, bond fission after light irradiation involves $\pi\sigma^*$ states. The simplest hydrogen halide, HF, water, or ammonia are textbook examples. For instance in HF, the first excited state is obtained by promoting an electron from the occupied $2p_x$ or $2p_y$ orbital of the F atom to the antibonding σ^* orbital. The potential energy curves (PECs) associated with the resulting $\pi\sigma^*$ excited states are directly repulsive and asymptotically degenerated with the electronic ground state (see e.g., Ref. [1]). In H_2O or NH_3 the respective first excited state is also of $\pi\sigma^*$ character and correlates asymptotically with an H atom and a radical product. However, since the ground and excited states are of different symmetries, both ground and excited states cross at an extended O–H (or N–H) geometry forming a CI [2, 3]. As a consequence of the CIs, dissociation of H can take place in diabatic excited or ground state PE surfaces. In general, the presence of CIs leads to a product branching which depends on the initial energy and momentum of the excited wavefunction. In many other less trivial and less studied cases than water and ammonia, ab initio calculations have shown that bright $\pi\pi^*$ states can cross with $\pi\sigma^*$ states associated with OH or NH bond extension. This is the case of small aromatic N-heterocycles [4–8], like pyrrole, indole, imidazole, or nucleobases [7, 9]. A different class of molecules from the ones described above are those where dissociation takes place directly in $\pi\sigma^*$ excited states which evolve diabatically to the excited products. This is for example the case in nitriles, where the $\pi\sigma^*$ excited state is associated with the elongation of C–H bonds [1, 10].

The presence of $\pi\sigma^*$ states in hydrocarbons have not been directly demonstrated. Ethenes present Rydberg states [11] which severely complicate the description of their electronic excited states. The C–H bond rupture of e.g., ethylene is an endothermic process [12], which takes place in a state so-called $\pi 3s\sigma^*$ since at the equilibrium geometry the acceptor orbital has $3s$ Rydberg character, but after a small stretch of the C–H bond changes to σ^* character. This

is a case of the so-called Rydbergization—change of character from Rydberg to valence upon bond extension. A similar situation has been found in ethyne [13].

In this article, we investigate in detail the $\pi\sigma^*$ states of an ethylene derivative, (4-methylcyclohexylidene)fluoromethane (4MCF). We purposely leave the Rydberg states aside; therefore, avoiding Rydbergization. In this way, and up to our knowledge, this is the first case where direct $\pi\sigma^*$ states have been identified in olefins. With the help of high-level ab initio calculations the role of $\pi\sigma^*$ states in the photochemistry of this system can be assessed for the first time.

4MCF is a chiral fluoroethylene derivative with R and S enantiomers connected by a torsion around the C=C double bond. In a series of papers, we have proposed 4MCF as a model for a light-induced molecular rotor [14–16]. Such a device is based on the potential ability of 4MCF to rotate around the C=C bond after light irradiation in a unidirectional manner. Similar to fluoroethylene [17] or ethylene itself (see e.g., [18–20]), a series of CIs between the ground state S_0 and the S_1 excited state have been recently reported for 4MCF [21, 22]. The CIs optimized until now involve torsion, pyramidalization, H-atom migration, and HF elimination. Based on them, it has been predicted that irradiation of 4MCF should yield the chiral isomer upon C=C rotation via a twisted CI in the presence of polar solvents, while in gas phase dissociation of the HF fragment via a HF-elimination CI should be observed [22]. Figure 1 shows schematically the two reactions mediated by the corresponding CIs. Both CIs are twisted around the C=C double bond at 90° , but the HF-elimination CI possesses stretched C–F and C–H bonds. Yet, a preliminary quantum dynamical study in gas phase including only the ground and $\pi\pi^*$ states along the torsion and the HF elimination coordinates showed that torsion in the $\pi\pi^*$ state dominates for about 1 ps [23]. Here we revisit the quantum chemistry of 4MCF involving explicitly $\pi\sigma^*$ states, since, as we will show, they are explicitly involved in the abstraction of the HF fragment after light irradiation.

2. Computational Details

The equilibrium structure of 4MCF has been optimized at MP2/6-311+G(d,p) level of theory as in Ref. [21] using the GAUSSIAN03 package [24]. The most relevant geometrical parameters are depicted in

KINZEL, GONZÁLEZ-VÁZQUEZ, AND GONZÁLEZ

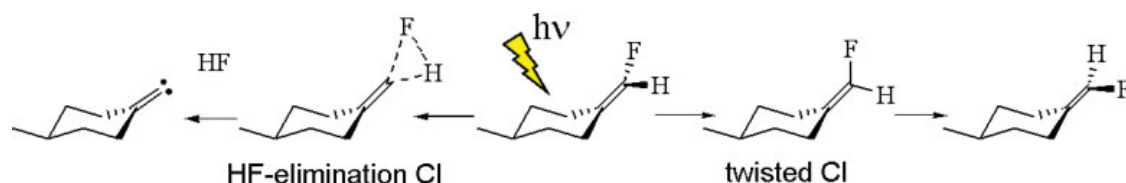


FIGURE 1. Competing isomerization and dissociation reactions in 4MCF after light irradiation. After irradiation, at least two different conical intersections (CI) can be potentially accessed: a twisted CI, responsible for isomerization around the double bond and leading to the opposite enantiomer, or a HF-elimination CI, which leads to HF abstraction. [Color figure can be viewed in the online issue, which is available at wileyonlinelibrary.com.]

Figure 2. Using this geometry, the ionization potential is calculated 9.17 eV. Vertical excitations energies have been calculated using the state-averaged complete active space self-consistent field (SA-CASSCF) method [25] with different active spaces (as detailed below) and two different basis sets: the Pople [26] 6-31G* double-zeta (DZ) quality basis set and the atomic natural orbital ANO-L large basis set [27] contracted for DZ quality: a set of (14s9p4d3f) was contracted to [3s2p1d] for C and F atoms and (8s4p3d) to [2s1p] for H atom. Both basis sets cannot properly describe Rydberg states (in contrast to Ref. [21]) so that here we purposely focus only on the description of valence states.

Due to the complicated spectroscopy, different active spaces needed to be employed until a consistent picture of the electronic structure of 4MCF was obtained. To illustrate the behavior of the system, only the results of three different active spaces will be discussed: CAS(4,4), CAS(10,8) and CAS(12,10) (the results of other active spaces are shown in the Supporting Information). The orbitals included in each active space are depicted in Figure 3. The largest

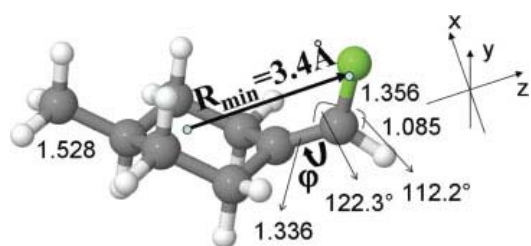


FIGURE 2. MP2/6-311+G(d,p) equilibrium structure of 4MCF in the electronic ground state with the C=C bond twisted by 90°. Also shown is the coordinate system as well as the torsional angle φ and the vector R , the latter defined from the center of mass of the hydrocarbon moiety to the center of mass of the HF fragment (indicated by dots). [Color figure can be viewed in the online issue, which is available at wileyonlinelibrary.com.]

CAS(12,10) contains twelve electrons in ten orbitals comprising the π , σ_{CH} , σ_{CF} , σ_{CC} , their corresponding antibonding orbitals, and two lone pairs of the F atom, n . The σ_{CC} and σ_{CC}^* orbitals are located in the olefinic double bond. The intermediate active spaces (4,4) and (10,8) skip the $\sigma_{CC}, \sigma_{CC}^*$ pair, while including the lone pairs and/or different σ orbitals (see Fig. 3).

Depending on the active space, three or six states are averaged with equal weights in the CASSCF procedure. Then, all the energies have been corrected with second-order perturbation theory in its multi-state version (MS-CASPT2) [28] using the same number of states. To avoid intruder states, the level-shift technique [29] with a parameter of 0.3 a.u. has been employed. This parameter was chosen after a careful examination of the stability of the excitation energies and the comparison of the excited state reference weights with that of the ground state. The MS-CASPT2/SA-CASSCF single point calculations were performed with the MOLCAS7.4 program package [30].

From the series of calculations described above and discussed in Section 3.1, the protocol SA3-CAS(12,10) has been chosen to calculate the two lowest electronic excited states of a set of 271 geometries defined by a Wigner harmonic distribution, a procedure implemented in the NEWTON-X package [31, 32]. This distribution reflects the quantum

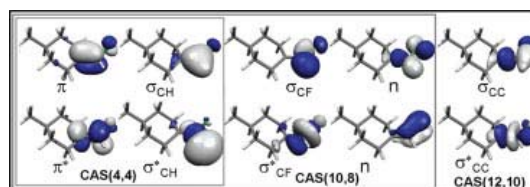


FIGURE 3. Active spaces employed in SA-CASSCF and subsequent MS-CASPT2 calculations. [Color figure can be viewed in the online issue, which is available at wileyonlinelibrary.com.]

ROLE OF $\pi\sigma^*$ STATES IN A CHIRAL FLUOROETHYLENE DERIVATIVE

vibrational ground state probability of the electronic ground state potential and was obtained using the corresponding harmonic frequencies for the optimized geometry at the B3LYP/SV(P) level of theory calculated with the TURBOMOLE [33, 34] package. The B3LYP functional includes the Becke's three parameter nonlocal hybrid exchange potential [35] and the correlation functional of Lee et al. [36]. The final single point CASSCF calculations for each geometry were performed under C_1 symmetry with the COLUMBUS [37–40] package and the DALTON module [41].

The role of $\pi\sigma^*$ states in 4MCF is further illustrated by computing PE curves along the HF dissociation coordinate. In general, we label the torsion around the double bond by φ and the HF dissociation coordinate by R , defined as the distance between the center of masses of the hydrocarbon moiety and the HF fragment. The molecule is assumed to be preoriented as shown in Figure 2, with the z -axis lying along the C=C double bond. Starting from the planar ($\varphi = 0^\circ$) and twisted ($\varphi = 90^\circ$) structure of 4MCF, respectively, two grids of each 32 points are calculated along R . The HF bond distance and other coordinates of the molecular scaffolding are kept frozen at the equilibrium geometry of 4MCF (see Fig. 2). In the twisted orientation the molecule has local C_s symmetry along the x,z -plane, otherwise has C_1 symmetry.

Due to the presence of nearby CIs, the PECs are nonadiabatically coupled. The corresponding nonadiabatic coupling terms (NACTs) (or kinetic couplings) with respect to R and φ defined as

$$T_R^{ij} = \left\langle \chi_i \left| \frac{\partial}{\partial R} \chi_j \right. \right\rangle, \quad (2.1)$$

$$T_\varphi^{ij} = \left\langle \chi_i \left| \frac{\partial}{\partial \varphi} \chi_j \right. \right\rangle, \quad (2.2)$$

are calculated at the same level of theory using a finite difference method with the 3-point formula in each dimension. The PECs and corresponding NACTs calculations were performed with the MOLPRO program package [42] at the SA6-CAS(12,10) level of theory.

3. Results and Discussion

3.1. $\pi\pi^*$ AND $\pi\sigma^*$ EXCITED STATES: ACTIVE SPACE, BASIS SET AND GEOMETRY EFFECTS

Tables I and II collect relative energies, oscillator strengths and state configurations of the

low-lying valence excited states of 4MCF using different active spaces and the 6-31G* and ANO-L basis sets, respectively.

When neglecting Rydberg states, one is tempted to use a small (2,2) active space to study isomerization around C=C. As Table S1 of the Supporting Information shows, the first $\pi\pi^*$ state of 4MCF using SA2-CAS(2,2)/6-31G* is predicted at 9.65 and 7.92 eV before and after inclusion of dynamical correlation, respectively. The more accurate MS-CASPT2 value is still largely overestimated with respect to both, the experimental value of 6.5 eV measured by Gedanken et al. [43] and the more accurate calculations presented in Ref. [21]. Since this article investigates not only C=C isomerization but also bond dissociation, state configurations including σ^* orbitals might play a role in describing the breaking of each the CH and CF bond. Moreover, we expect that more than one excited state should be involved in this process. Due to the rigidity of the HF coordinate (fixed at 2.03 Å in the equilibrium structure), a H · · F biradical is found at long R distances. Thus, since at the HF-dissociation limit the unpaired electron at the fluorine atom can be in any of the three 2p-orbitals ($2p^5$ configuration), three electronic states correlate with the same asymptote: the S_0 , S_1 and S_2 states have ground state configuration and correspond to the singlet carbene ground state; S_3 , S_4 and S_5 have the excited state configuration of the carbene; S_6 , S_7 , S_8 have $n_C\pi^*$ configuration; and S_9 , S_{10} , S_{11} have $\pi\pi^*$ configuration. Hence, the description of HF-dissociation in 4MCF requires to include $3n$ states (where n is an integer) at the dissociation limit. For consistency, we also investigate $3n$ states at the Franck-Condon (FC) equilibrium geometry.

Table I shows the result of including σ_{CH} and σ_{CH}^* orbitals in the active space. At SA3-CAS(4,4) level of theory, the lowest-lying excited state is a weak $\pi\sigma^*$ located at 9.64 eV (oscillator strength 0.056), very close to the bright $\pi\pi^*$ state at 9.70 eV (oscillator strength 0.758). Inclusion of σ_{CF} and n_F orbitals results in a similar picture: At SA6-CAS(10,8) level of theory, the lowest valence state has $\pi\sigma^*$ character, but the $\pi\pi^*$ state follows close in energy. A further increase of the active space adding the σ_{CC} and σ_{CC}^* orbitals (CAS(12,10)) does not change the excitation energies significantly, but it alters the order of states: The bright $\pi\pi^*$ state is found to be the first excited state, energetically below the dark $\pi\sigma_{CH}^*$ and $\pi\sigma_{CF}^*$ states, which appear to be strongly mixed (see the wavefunctions of S_2 and S_3). Upon inclusion of dynamical correlation, the $\pi\pi^*$ state is strongly stabilized and it is always the lowest excited state.

KINZEL, GONZÁLEZ-VÁZQUEZ, AND GONZÁLEZ

TABLE I

Vertical excitation energies (in eV) of 4MCF calculated at CASSCF and MS-CASPT2 level of theory using the 6-31G* basis set.

	SA3 - CAS(4,4)			SA6 - CAS(10,8)			SA6 - CAS(12,10)		
	E_{rel}	coeff ²	f	E_{rel}	coeff ²	f	E_{rel}	coeff ²	f
CASSCF									
S ₀	0.00			0.00			0.00		
S ₁	9.64	0.89 $\pi\sigma_{CH}^*$	0.056	9.85	0.86 $\pi\sigma_{CH}^*$	0.002	9.63	0.91 $\pi\pi^*$	0.514
S ₂	9.70	0.91 $\pi\pi^*$	0.758	9.96	0.94 $\pi\pi^*$	0.727	9.91	0.60 $\pi\sigma_{CH}^*$	0.004
S ₃				10.55	0.79 $\pi\sigma_{CF}^*$	0.011	10.30	0.30 $\pi\sigma_{CF}^*$	0.007
S ₄				10.99	0.83 $n\pi^*$	0.004	10.86	0.52 $\pi\sigma_{CF}^*$	0.007
S ₅				13.31	0.74 $n\pi^*$	0.098	13.13	0.22 $\pi\sigma_{CH}^*$	0.007
								0.76 $n\pi^*$	0.007
								0.86 $n\sigma_{CF}^*$	0.000
MS-CASPT2									
S ₀	0.00			0.00			0.00		
S ₁	8.08	0.97 $\pi\pi^*$	0.677	7.82	0.94 $\pi\pi^*$	0.606	8.07	0.91 $\pi\pi^*$	0.433
S ₂	9.58	0.95 $\pi\sigma_{CH}^*$	0.000	9.44	0.48 $\pi\sigma_{CH}^*$	0.007	9.33	0.70 $\pi\sigma_{CF}^*$	0.008
S ₃				9.71	0.39 $\pi\sigma_{CF}^*$	0.001	9.64	0.20 $\pi\sigma_{CH}^*$	0.000
					0.23 $\pi\sigma_{CF}^*$			0.47 $\pi\sigma_{CH}^*$	0.000
					0.13 $\pi\sigma_{CH}^*$			0.30 $n\pi^*$	
S ₄				9.94	0.39 $n\pi^*$	0.006	9.92	0.59 $n\pi^*$	0.007
					0.27 $\pi\sigma_{CH}^*$			0.24 $\pi\sigma_{CH}^*$	
					0.21 $\pi\sigma_{CF}^*$				
S ₅				12.43	0.74 $n\pi^*$	0.040	12.73	0.86 $n\sigma_{CF}^*$	0.000

To summarize Table I, we observe that the order between the $\pi\pi^*$ and $\pi\sigma^*$ excited states is rather sensible to the choice of active space and the inclusion of dynamical correlation. The problem to decide which state is lower in energy is accentuated by the fact that both states appear to be rather close in energy, at least at CASSCF level of theory, although they split with MS-CASPT2. Moreover, we see that regardless of the size and composition of the active space, the vertical excitation energy of the spectroscopic $\pi\pi^*$ state is about 3 eV higher than the one reported experimentally by Gedanken et al. [43]. The CASSCF excitation energies can be lowered by subsequent MS-CASPT2 single point calculations by ca. 1 to 2 eV, but excitation to the $\pi\pi^*$ is still quantitatively overestimated by at least 1.3 eV. The inclusion of dynamical correlation often results in a state switching of the $\pi\pi^*$ state, which is then the first excited state about 1 eV below the $\pi\sigma^*$ states. In general, both, the CASSCF and MS-CASPT2 excitation energies do not substantially change when increasing the active space.

Next, we consider basis set effects in Table II. Although the contraction chosen for ANO-L has a similar DZ quality as the 6-31G* basis set, it is

interesting to observe that the obtained energies are different. At SA3-CAS(4,4)/ANO-L level of theory the bright $\pi\pi^*$ state is predicted at 8.76 eV with CASSCF and 7.15 eV at MS-CASPT2 – that is, 1 eV lower than with the 6-31G* basis set, compare Tables I and II. The order of the $\pi\pi^*$ and $\pi\sigma^*$ states is reversed from CASSCF to CASPT2, as it occurred when using the 6-31G* basis set.

The increase of the active space to CAS(10,8) and CAS(12,10) does not change the energies qualitatively. Yet, in all cases the $\pi\sigma^*$ state is predicted much lower in energy than the $\pi\pi^*$ state, around 1.5 eV, whereas the energy gap when using the 6-31G* basis set only amounts up to 0.4 eV. As mentioned before, MS-CASPT2 heavily stabilizes the $\pi\pi^*$ state while keeping the $\pi\sigma^*$ nearly unchanged in energy. Therefore, the lowest valence state is the $\pi\sigma^*$ state, both at CASSCF and CASPT2 levels of theory when employing the ANO-L basis set, opposite to the situation found with the 6-31G* basis set (recall Table I). Moreover, it should be noted that the wavefunctions describing the $\pi\pi^*$ and $\pi\sigma^*$ states are strongly mixed at MS-CASPT2 level of theory with ANO-L; see also the conspicuous relatively high

ROLE OF $\pi\sigma^*$ STATES IN A CHIRAL FLUOROETHYLENE DERIVATIVE

TABLE II

Vertical excitation energies (in eV) of 4MCF calculated at CASSCF and MS-CASPT2 level of theory using the ANO-L basis set.

State	SA3 - CAS(4,4)			SA6 - CAS(10,8)			SA6 - CAS(12,10)		
	E_{rel}	coeff ²	f	E_{rel}	coeff ²	f	E_{rel}	coeff ²	f
CASSCF									
S ₀	0.00			0.00			0.00		
S ₁	7.29	0.94 $\pi\sigma_{CH}^*$	0.058	7.73	0.96 $\pi\sigma_{CH}^*$	0.052	7.30	0.95 $\pi\sigma_{CH}^*$	0.050
S ₂	8.76	0.91 $\pi\pi^*$	0.613	9.41	0.87 $\pi\pi^*$	0.574	9.39	0.86 $\pi\pi^*$	0.581
S ₃				9.91	0.93 $\sigma_{\text{ring}}\pi^*$	0.003	9.95	0.92 $\sigma_{\text{ring}}\pi^*$	0.003
S ₄				10.19	0.91 $\pi\sigma_{CF}^*$	0.007	10.64	0.86 $\pi\sigma_{CH}^*$	0.009
S ₅				10.66	0.92 $\sigma_{\text{ring}}\sigma_{CH}^*$	0.109	10.66	0.86 $\sigma_{\text{ring}}\sigma_{CH}^*$	0.106
MS-CASPT2									
S ₀	0.00			0.00			0.00		
S ₁	7.15	0.53 $\pi\pi^*$	0.234	7.15	0.79 $\pi\sigma_{CH}^*$	0.128	7.17	0.76 $\pi\sigma_{CH}^*$	0.139
S ₂	7.39	0.45 $\pi\sigma_{CH}^*$	0.332	7.39	0.16 $\pi\pi^*$	0.387	7.39	0.18 $\pi\pi^*$	0.384
		0.55 $\pi\pi^*$			0.74 $\pi\pi^*$			0.71 $\pi\pi^*$	
S ₃		0.44 $\pi\sigma_{CH}^*$		8.83	0.17 $\pi\sigma_{CH}^*$	0.003	8.82	0.19 $\pi\sigma_{CH}^*$	0.004
					0.92 $\sigma_{\text{ring}}\pi^*$			0.65 $\sigma_{\text{ring}}\pi^*$	
S ₄				8.87	0.88 $\pi\sigma_{CF}^*$	0.003	8.86	0.28 $\pi\sigma_{CF}^*$	0.001
					0.60 $\pi\sigma_{CF}^*$			0.28 $\sigma_{\text{ring}}\pi^*$	
S ₅				9.93	0.94 $\sigma_{\text{ring}}\sigma_{CH}^*$	0.073	9.89	0.90 $\sigma_{\text{ring}}\sigma_{CH}^*$	0.072

oscillator strength of ca 0.1 for the usually dark $\pi\sigma_{CH}^*$ state at the expense of the $\pi\pi^*$ intensity. This is again an indication that both states are very close in energy and MS-CASPT2 mixed them strongly. Indeed, in the cases of CAS(10,8) and CAS(12,10), the energy difference between S₂ and S₃ states is only ca. 0.25 eV. We also note in Table II that when using the ANO-L basis set a σ_{CC} orbital which is connected to the cyclohexane ring σ_{ring} seems to become important and thus replaces one of the lone pair orbitals of the fluorine. However, despite the change of the active space composition the order of the important $\pi\pi^*$ and $\pi\sigma^*$ states remain unchanged: The lowest valence state is the $\pi\sigma^*$ state, both at CASSCF and CASPT2 levels of theory, followed by the $\pi\pi^*$ state and higher $\pi\sigma^*$ states. We note that MS-CASPT2/SA6-CAS(12,10)/ANO-L energies for the $\pi\pi^*$ state (7.39 eV) is only 1 eV off the experimentally reported excitation energy (6.5 eV) [43].

Interestingly, in the paper of Alfalah et al. [23] a vertical excitation energy of 9.16 eV is reported for the first excited state of $\pi\pi^*$ character at SA2-CASSCF(8,8)/cc-pVDZ level of theory using an equilibrium geometry optimized with B3LYP/cc-pVDZ. This active space includes eight electrons in the π , σ_{CC} , σ_{CH} , σ_{CF} and their corresponding antibonding orbitals. The equilibrium geometries of 4MCF show little geometrical differences, however,

the lowest excited state is of $\pi\pi^*$ character, and not $\pi\sigma^*$ as found here using large active spaces. This instability made us suspect that $\pi\pi^*$ and $\pi\sigma^*$ excited states are very close not only energetically but also geometrically around the FC region.

To assess whether small geometrical changes in the equilibrium geometry also have an impact on the order of the $\pi\pi^*$ and $\pi\sigma^*$ states, we generated a distribution of geometries by a Wigner distribution in the vibrational ground state of the electronic ground state. For each of these geometries the ground and lowest $\pi\pi^*$ and $\pi\sigma^*$ states were calculated, i.e., a SA3-CASSCF calculation was performed. To allow the maximum flexibility in the active space, the largest active space was selected. In general, the wavefunctions of the S₁ and S₂ states show mixed configurations of $\pi\pi^*$ and $\pi\sigma^*$ character, therefore, an histogram for the ratio \mathfrak{R}_π between the CASSCF coefficients (c) for the $\pi\pi^*$ configuration and the sum of $\pi\pi^*$ and $\pi\sigma^*$ coefficients has been plotted. The ratio \mathfrak{R}_π is defined as

$$\mathfrak{R}_\pi = \frac{c_{\pi\pi^*}^2}{(c_{\pi\pi^*}^2 + c_{\pi\sigma^*}^2)} \quad (3.1)$$

The results at SA3-CAS(12,10)/6-31G* level of theory for each of the S₁ and S₂ states are shown in Figures 4(a) and (b), respectively. Counts represents

KINZEL, GONZÁLEZ-VÁZQUEZ, AND GONZÁLEZ

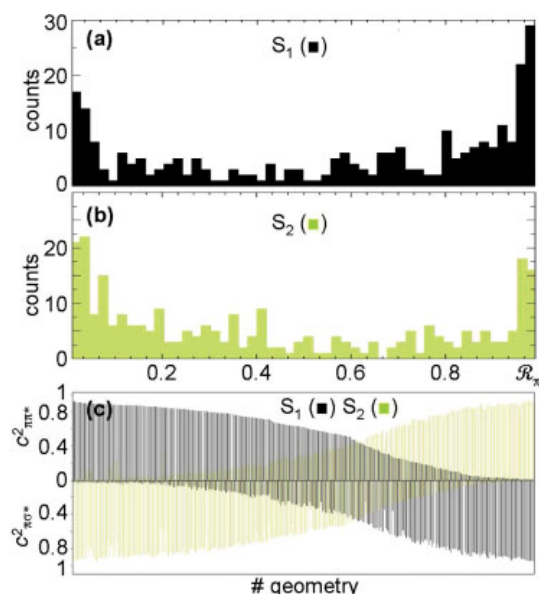


FIGURE 4. Histogram of individual geometries around a Wigner distribution with the ratio \mathfrak{R}_π (defined in text) in the state S_1 (a) and S_2 (b); (c) squared coefficients for $\pi\pi^*$ and $\pi\sigma^*$ state configurations in S_1 (black, dark) as well as in S_2 (green, light). [Color figure can be viewed in the online issue, which is available at wileyonlinelibrary.com.]

the number of geometries with a particular ratio \mathfrak{R}_π . As we can see in Figure 4(a), there is a large amount of geometries with a pure (i.e., $\mathfrak{R}_\pi = 1.0$) $\pi\pi^*$ character in the S_1 . This is of course correlated with a large number of geometries –albeit not the same amount—which in the S_2 have pure $\pi\sigma^*$ character ($\mathfrak{R}_\pi = 0.0$), see Figure 4(b). Surprisingly, there is also a large amount of geometries showing pure $\pi\sigma^*$ character in the S_1 and accordingly, a $\pi\pi^*$ character in the S_2 . However, between both extremes, most of the geometries show a mixed character. This mixing can be best appreciated in Figure 4(c), where the actual CASSCF coefficients for $\pi\pi^*$ and $\pi\sigma^*$ states are plotted for each individual geometry in S_1 and S_2 sorted by descending $\pi\pi^*$ coefficients in the S_1 state. As we can see, most of the geometries show a more or less pronounced mixing of the $\pi\pi^*$ and $\pi\sigma^*$ configurations. This confirms that small geometrical modifications, as those induced by the vibrational modes with zero point energy, are enough to alter the order of the states at the FC geometry. In other words, it seems that the equilibrium geometry is located close to a seam of CIs between the $\pi\pi^*$ and

$\pi\sigma^*$ states, and therefore it is specially sensitive to any change of the geometry, as well as to fine details when optimizing the CASSCF wavefunction (see Tables I and II).

A closer look to Table I, e.g., at SA3-CAS(4,4) level of theory, already points to a possible degeneracy of the S_1 and S_2 states at the FC geometry. Although this is not the minimum energy crossing point between the S_1 and S_2 states, the equilibrium geometry already has a large nonadiabatic coupling and it can be considered as an efficient crossing location. Figure 5 shows the gradient difference (GD) and derivative coupling (DC) vectors between the S_1 and S_2 states calculated at the equilibrium geometry with the COLUMBUS program package [37–40]. Both vectors show strong C-H and C-C stretching modes and the GD vector is also composed of pyramidalization at the C atoms located in the olefinic bond. We then conclude that this geometry is part of the seam of CIs between the S_2 and S_1 leading to H-dissociation. Because pyramidalization is also involved, this new CI is probably leading to the S_1/S_0 pyramidalized CI reported in Ref. [21].

3.2. POTENTIAL ENERGY CURVES ALONG HF DISSOCIATION

To further investigate the role of the $\pi\sigma^*$ states in the C-F and C-H bond fission of 4MCF, PECs along the HF dissociation coordinate R and the corresponding nonadiabatic coupling elements have been computed. Following the previous section, a SA6-CASSCF(12,10)/6-31G* level of theory has been chosen.

We recall [23] that the ground state potential S_0 along φ is symmetric and cyclic, and as such, it possesses two equivalent minima at $\varphi = 0^\circ$ and 180° ,

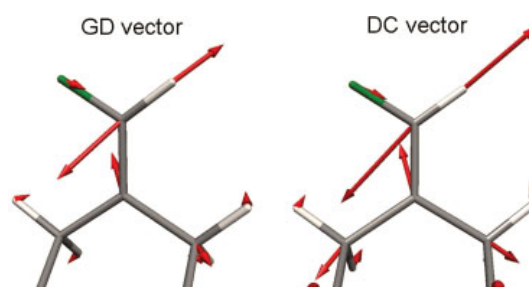


FIGURE 5. Gradient difference (GD) and derivative coupling (DC) vectors at the Franck-Condon geometry. [Color figure can be viewed in the online issue, which is available at wileyonlinelibrary.com.]

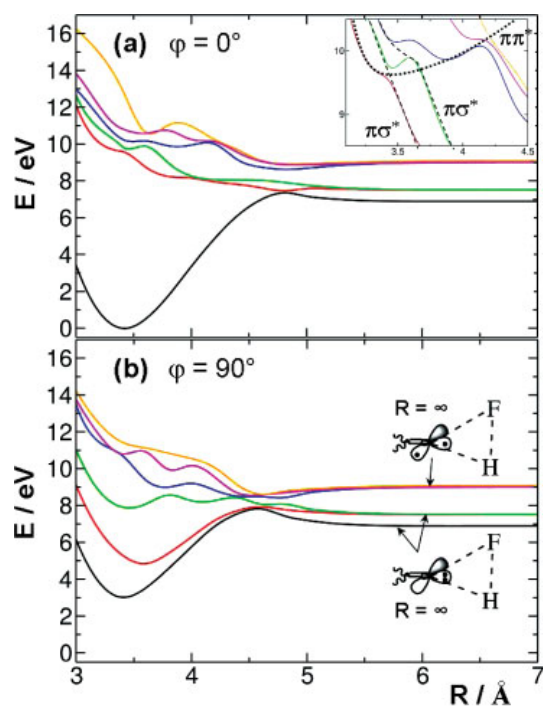
ROLE OF $\pi\sigma^*$ STATES IN A CHIRAL FLUOROETHYLENE DERIVATIVE

FIGURE 6. Adiabatic potential energy curves for states S_0 to S_5 for $\varphi = 0^\circ$ (a) and $\varphi = 90^\circ$ (b) calculated at SA6-CAS(12,10) / 6-31G* level of theory; inset in (a) shows schematic diabatic curves around the FC region; inset schemes of ground and excited state of carbene at asymptotic R values are valid for both PECs (a) and (b). [Color figure can be viewed in the online issue, which is available at wileyonlinelibrary.com.]

which correspond to the R and S enantiomers. The minima are well separated by a potential barrier at $\varphi = \pm 90^\circ$ of ca. 3 eV. In Figures 6(a) and (b), we plot the adiabatic PECs along R for $\varphi = 0^\circ$ and $\varphi = 90^\circ$, respectively.

At the FC point at $\varphi = 0^\circ$, S_1 and S_2 states are of $\pi\pi^*$ and $\pi\sigma^*$ character, respectively (recall Table I). As it can be seen in Figure 6(a) around the FC window, both states show an avoided crossing and indeed the nonadiabatic coupling T_R^{12} amounts to 7.2 a.u. Assuming that the system is spectroscopically excited to the bright S_1 state, the character of the potential will change from $\pi\pi^*$ to $\pi\sigma^*$ after a small bond elongation. Due to the topology of the lowest excited state, the system will remain in the adiabatic S_1 state, but as long as the distance R is increasing, it experiences further avoided crossings with S_2 at ca. 4 Å and with S_0 at ca. 4.8 Å. Although the nonadiabatic coupling of T_R^{01} at $R = 4.8$ is only

0.1 a.u. the coupling element with respect to the torsional coordinate φ , T_φ^{01} , amounts to 5.8 a.u., pointing to the strong mixing along this coordinate. Following the character of wavefunction along the potentials, one can see that the $\pi\pi^*$ character is completely lost after few Angstroms elongation. This is indicated in the schematic diabats in the inset of Figure 6(a). A important consequence is that the diabatic $\pi\pi^*$ state is bound and that HF dissociation takes place in a repulsive $\pi\sigma^*$ excited state.

At $\varphi = \pm 90^\circ$, [Fig. 6(b)] the S_1 is also of $\pi\pi^*$ character and it shows a minimum much below the FC energy of 9.6 eV. This behavior is reminiscent of the typical avoided crossing with the ground state in olefinic systems [19, 21, 44, 45], which at twisted (and pyramidalized) geometries show a S_1/S_0 CI. Despite the initial gap between the S_0 and S_1 states at the twisted geometry is quite large (ca 2 eV), it diminishes until at ca $R = 4.6$ Å, where an avoided crossing between the S_0 and the S_1 , but also with the S_2 , takes place. At this distance, which corresponds to the S_1/S_0 HF-elimination CI [22], the kinetic coupling elements T_R^{01} and T_R^{12} are 0.7 and 5.1 a.u., respectively, while the corresponding NACTs with respect to φ amount to 6.0 and 0.1 a.u., respectively.

Both $\varphi = 0^\circ$ and $\varphi = 90^\circ$ PECs illustrate the triple degeneracy of the states in the asymptotic limit. As mentioned above, this is due to the three possible arrangements of the unpaired electron of the F atom when at infinite R values the HF bond length is kept fixed at the distance optimized in 4MCF. The lowest S_0 , S_1 , and S_2 potential curves at infinite correlate with the ground state of the carbene. The following S_3 , S_4 , and S_5 correlate with an excited carbene, see inset in Figure 6(b). Figure 7 shows the configuration, relative energies and corresponding squared CAS coefficients at $R = 7$ Å- a distance, at which we consider dissociation to be complete. As we can see, besides the biradical occupations, the wavefunction of the S_0 also shows the participation of a zwitterionic configuration in the HF fragment (s_H orbital is empty). See that the S_0 has only 70% biradical character, while in the rest of the states this reaches ca. 90%. The extra stabilization of the zwitterion configuration is the reason why the electronic ground state is not completely degenerated with the S_1 and S_2 states.

Finally, we note that the asymptotic energy of the degenerated S_3 , S_4 , and S_5 states (9.1 eV) is close to, yet below the excitation energy to the bright S_1 state (9.6 eV). Therefore, higher-lying electronic states are not accessible from irradiation to the valence $\pi\pi^*$ state and have not been further considered.

KINZEL, GONZÁLEZ-VÁZQUEZ, AND GONZÁLEZ

3.3. RELAXATION MECHANISM OF 4MCF

Previous work dealing with the photodissociation products in ethylene [46] or ethylene derivatives [23, 47–49] always assumed that bond fission takes place in the ground state. Typically, only two states, the electronic S_0 and the bright $\pi\pi^*$ S_1 state are considered and the first step in the relaxation of these compounds is an ultrafast decay via a twisted and pyramidalized CI (similar to that shown in Fig. 1). The energy excess after passing the CI is responsible for the bond fission, creating hot products in the electronic ground state. This situation is illustrated in Figure 8(a): after light irradiation the system twists making the $\pi\pi^*/S_0$ CI accessible and then photodissociation takes place in the ground state.

However, when taking $\pi\sigma^*$ states into account (this requires at least three or more states) a new picture of the relaxation paths of 4MCF upon excitation to the bright $\pi\pi^*$ state emerges. Now two competing paths can lead to photodissociation. The existence of a S_2/S_1 CI at the FC geometry implies that after exciting to the $\pi\pi^*$ state, part of the population can leak to the repulsive $\pi\sigma^*$ state, where dissociation can take place. This is what we denote as path I in Figure 8(b). Alternative, if torsion operates faster than the

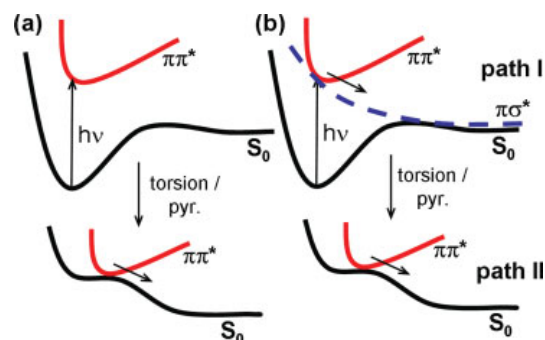


FIGURE 8. Deactivation paths in the photodissociation of 4MCF in the two-state model (a) and competing paths (I or II) in the three-state model (b), respectively. [Color figure can be viewed in the online issue, which is available at wileyonlinelibrary.com.]

crossing takes place, the system can return to the ground state via the twisted-CI and then dissociate [path II in Fig. 8(b)]. In the first case, carbene and HF products are created in the electronic excited state; in the second, 4MCF undergoes torsion around C=C before relaxing to the ground state, creating hot products in the S_0 .

	S_0	S_1	S_2	S_3	S_4	S_5
$E_{\text{rel}} / \text{eV}$:	6.89	7.51	7.52	9.01	9.01	9.10
coeff ² :	0.21 0.70	0.92	0.92	0.91	0.91	0.91
s_H	—	↑	↑	↑	↑	↑
p_x	↑↑	↑↑	↑↓	↑↑	↑↓	↑↑
p_y	↑↑	↑	↑↑	↑↑	↑↑	↑
p_z	↑↑ + ↑↑	↑↓	↑↑	↑↓	↑↑	↑↑
n_C	↑↑	↑↑	↑↑	↑	↑	↑
n_C^*	—	—	—	↑↓	↑↓	↑↓

FIGURE 7. Configurations of the states at asymptotic R; occupations in the relevant p_F , s_H and n_C orbitals reveal triple state degeneracy at large distances due to degenerate p orbitals at the fluorine atom; CASSCF coefficients and energies relative to the equilibrium energy calculated at the SA6-CAS(12,10) level of theory are shown. [Color figure can be viewed in the online issue, which is available at wileyonlinelibrary.com.]

4. Conclusions

The role of the $\pi\sigma^*$ states in the photochemistry of 4MCF has been studied. In particular, the dissociation of HF versus isomerization around the C=C bond after light irradiation has been investigated.

Isomerization, or the chiral interconversion between the R and S enantiomers of 4MCF, should be promoted in a $\pi\pi^*$ state, which after being populated relaxes to a CI between the S_1 and the S_0 along the torsion (and pyramidalization at one of the olefinic carbons) coordinates [22]. The experimental observation that ethylene or halogenated ethylene derivatives show molecular hydrogen or hydrogen hydride fragmentation [50–56], suggests that dissociation could also be relevant in 4MCF and competitive to isomerization. Yet, within a two-state relaxation model considering only the ground and the bright $\pi\pi^*$ states, dissociation of e.g. HF in 4MCF, should take place in the electronic ground state. In this article, however, we have shown that the HF dissociation involves the presence of $\pi\sigma^*$ states that cross the bright $\pi\pi^*$ state already at the FC geometry. As a consequence, it is also plausible that HF

ROLE OF $\pi\sigma^*$ STATES IN A CHIRAL FLUOROETHYLENE DERIVATIVE

fragmentation takes place in the electronic excited state.

Calculations of the vertical excitation energies of 4MCF have been carried out at CASSCF and CASPT2 level of theory taking into account large active spaces which, while excluding Rydberg orbitals, are able to describe $\pi\sigma^*$ and $\pi\pi^*$ valence states simultaneously. The results show that the relative position of the bright $\pi\pi^*$ and lowest $\pi\sigma^*$ state is in this particular case very sensitive to the active space, basis set, and level of theory. This is due to the fact that both states are very close in energy, and belong to a seam of CIs between the $\pi\pi^*$ and the $\pi\sigma^*$ states. By calculating the lowest two excited states in a Wigner distribution of geometries, we have seen that the zero point energy alone suffices to induce small geometrical changes at which the order of the states is different.

By constructing PECs along HF dissociation in 4MCF, we have shown that Rydbergization is not a necessary condition for bond fission in 4MCF. Possibly, this is also the case in other olefins, as well as in the fragmentation of only H or a halogen atom. With the resulting potentials, it is evident that the ultrafast radiationless relaxation of 4MCF is different from the one suggested until now. While population can still be transferred to the ground state via a torsion of the HF fragment like in the two-state system, the molecule can also dissociate through the dissociative $\pi\sigma^*$ states without preliminary torsion. Which of these paths is operating in 4MCF and whether they are accessible in other fluorinated ethylenes is currently under investigation.

References

- Ashfold, M. N. R.; King, G. A.; Murdock, D.; Nix, M. G. D.; Oliver, T. A. A.; Sage, A. G. *Phys Chem Chem Phys* 2010, 12, 1218.
- Ashfold, M. N. R.; Mordaunt, D. H.; Wilson, S. H. S. *Advances in Photochemistry*, vol. 21; Wiley: New York, 1996.
- Robin, M. B. *Higher Excited States in Polyatomic Molecules*, vols. 1 and 2; Academic Press: New York, 1974.
- Sobolewski, A. L.; Domcke, W. *Chem Phys Lett* 1999, 315, 293.
- Sobolewski, A. L.; Domcke, W. *Chem Phys Lett* 2000, 321, 479.
- Sobolewski, A. L.; Domcke, W. *Chem Phys* 2000, 259, 181.
- Perun, S.; Sobolewski, A.; Domcke, W. *Chem Phys* 2005, 313, 107.
- Vallet, V.; Lan, Z.; Mahapatra, S.; Sobolewski, A. L.; Domcke, W. *Faraday Discuss* 2004, 127, 283.
- Sobolewski, A. L.; Domcke, W.; Dedonder-Lardeux, C.; Jouvet, C. *Phys Chem Chem Phys* 2002, 4, 1093.
- Peric, M.; Dohmann, H.; Pyerimhoff, S.; Buenker, R. J. *Z Phys D At Mol Clusters* 1987, 5, 65.
- Serrano-Andrés, L.; Merchán, M.; Ignacio Nebot-Gil; Lindh, R.; Roos, B. O. *J Chem Phys* 1992, 98, 3151.
- Evleth, E. M.; Sevin, A. *J Am Chem Soc* 1981, 103, 7414.
- Laruelle, F.; Boyé-Péronne, S.; Gauyacq, D.; Liévin, J. *J Phys Chem A* 2009, 113, 13210.
- Kröner, D.; González, L. *Phys Chem Chem Phys* 2003, 5, 3933.
- Kröner, D.; González, L. *Chem Phys* 2004, 298, 55.
- Fujimura, Y.; González, L.; Kröner, D.; Manz, J.; Mehdaoui, I.; Schmidt, B. *Chem Phys Lett* 2004, 386, 248.
- Barbatti, M.; Aquino, A. J. A.; Lischka, H. *J Phys Chem A* 2005, 109, 5168.
- Krawczyk, R. P.; Viel, A.; Manthe, U.; Domcke, W. *J Chem Phys* 2003, 119, 1397.
- Barbatti, M.; Paier, J.; Lischka, H. *J Chem Phys* 2004, 121, 11614.
- Levine, B. G.; Martínez, T. J. *Ann Rev Phys Chem* 2007, 58, 613.
- Schreiber, M.; Barbatti, M.; Zilberg, S.; Lischka, H.; González, L. *J Phys Chem A* 2007, 111, 238.
- Zilberg, S.; Cogan, S.; Haas, Y.; Deeb, O.; González, L. *Chem Phys Lett* 2007, 443, 43.
- Alfalalah, S.; Kinzel, D.; González-Vázquez, J.; González, L. *Chem Phys* 2010, 369, 138.
- Frisch, M. J.; Trucks, G. W.; Schlegel, H. B.; Scuseria, G. E.; Robb, M. A.; Cheeseman, J. R.; Montgomery, J. A., Jr.; Vreven, T.; Kudin, K. N.; Burant, J. C.; Millam, J. M.; Iyengar, S. S.; Tomasi, J.; Barone, V.; Mennucci, B.; Cossi, M.; Scalmani, G.; Rega, N.; Petersson, G. A.; Nakatsuji, H.; Hada, M.; Ehara, M.; Toyota, K.; Fukuda, R.; Hasegawa, J.; Ishida, M.; Nakajima, T.; Honda, Y.; Kitao, O.; Nakai, H.; Klene, M.; Li, X.; Knox, J. E.; Hratchian, H. P.; Cross, J. B.; Bakken, V.; Adamo, C.; Jaramillo, J.; Gomperts, R.; Stratmann, R. E.; Yazyev, O.; Austin, A. J.; Cammi, R.; Pomelli, C.; Ochterski, J. W.; Ayala, P. Y.; Morokuma, K.; Voth, G. A.; Salvador, P.; Dannenberg, J. J.; Zakrzewski, V. G.; Dapprich, S.; Daniels, A. D.; Strain, M. C.; Farkas, O.; Malick, D. K.; Rabuck, A. D.; Raghavachari, K.; Foresman, J. B.; Ortiz, J. V.; Cui, Q.; Baboul, A. G.; Clifford, S.; Cioslowski, J.; Stefanov, B. B.; Liu, G.; Liashenko, A.; Piskorz, P.; Komaromi, I.; Martin, R. L.; Fox, D. J.; Keit Gaussian 03, Revision D.01 2004. Gaussian, Inc., Wallingford, CT, 2004.
- Roos, B. O.; Widmark, P. In *European Summerschool in Quantum Chemistry*, vol. 2, 2005; p. 287.
- Hehre, W. J.; Radom, L.; Schleyer, P. v. R.; Pople, J. A. *Ab Initio Molecular Orbital Theory*; Wiley: New York, 1986.
- Widmark, P.-O.; Malmqvist, P.-A.; Roos, B. O. *Theor Chim Acta* 1990, 77, 291.
- Finley, J.; Malmqvist, P.-A.; Roos, B. O.; Serrano-Andrés, L. *Chem Phys Lett* 1998, 288, 299.
- Roos, B. O.; Andersson, K. *Chem Phys Lett* 1995, 245, 215.
- Karlsröm, G.; Lindh, R.; Malmqvist, P.-A.; Roos, B. O.; Ryde, U.; Veryazov, V.; Widmark, P.-O.; Cossi, M.; Schimmelpennig, B.; Neogrady, P.; Seijo, L. *Comput Mater Sci* 2003, 28, 222.
- Barbatti, M.; Granucci, G.; Persico, M.; Ruckebauer, M.; Vazdar, M.; Eckert-Maksic, M.; Lischka, H. *J Photochem Photobiol A* 2007, 190, 228.
- Barbatti, M.; Granucci, G.; M. Ruckebauer, J. P.; Persico, M.; Lischka, H. *Newton-x: a package for newtonian dynamics*

KINZEL, GONZÁLEZ-VÁZQUEZ, AND GONZÁLEZ

- close to the crossing seam, Available at: www.newtonx.org 2007.
33. Ahlrichs, R.; Bar, M.; Haser, M.; Horn, H.; Kolmel, C. *Chem Phys Lett* 1989, 162, 165.
 34. Treutler, O.; Ahlrichs, R. *J Chem Phys* 1995, 102, 346.
 35. Becke, A. D. *J Chem Phys* 1993, 98, 5648.
 36. Lee, C.; Yang, W.; Parr, R. G. *Phys Rev B* 1988, 37, 785.
 37. Lischka, H.; Shepard, R.; Brown, F. B.; Shavitt, I. *Int J Quantum Chem Quantum Chem Symp* 1981, 15, 91.
 38. Shepard, R.; Shavitt, I.; Pitzer, R. M.; Comeau, D. C.; Peppera, M.; Lischka, H.; P. G. Szalay, R. A.; Brown, F. B.; Zhao, J. *Int J Quantum Chem Quantum Chem Symp* 1988, 22, 149.
 39. Shepard, H. L. R.; Pitzer, R. M.; Shavitt, I.; Dallos, M.; Müller, T.; Szalay, P. G.; Seth, M.; Kedziora, G. S.; Yabushita, S.; Zhang, Z. *Phys Chem Chem Phys* 2001, 3, 664.
 40. Lischka, H.; Shepard, R.; Shavitt, I.; Pitzer, R. M.; Dallos, M.; Müller, T.; Szalay, P. G.; Brown, F. B.; Ahlrichs, R.; Böhm, H. J.; Chang, A.; Comeau, D. C.; Gdanitz, R.; Dachsel, H.; Ehrhardt, C.; Ernzerhof, M.; Höchtel, P.; Irle, S.; Kedziora, G.; Kovar, T.; Parasuk, V.; Pepper, M. J. M.; Scharf, P.; Schiffrer, H.; Schindler, M.; Schüler, M.; Seth, M.; Stahlberg, E. A.; Zhao, J.-G.; Yabushita, S.; Zhang, Z.; Barbatti, M.; Matsika, S.; Schuurmann, M.; Yarkony, D. R.; Brozell, S. R.; Beck, E. V.; Blaudeau, J.-P. Columbus, an ab initio electronic structure program, release 5.9.1 2006.
 41. Helgaker, T.; Jensen, H. J. A.; Jørgensen, P.; Olsen, J.; Ruud, K.; Ågren, H.; Andersen, T.; Bak, K. L.; Bakken, V.; Christiansen, O.; Dahle, P.; Dalskov, E. K.; Enevoldsen, T.; Heiberg, H.; Hetttema, H.; Jonsson, D.; Kirpekar, S.; Kobayashi, R.; Koch, H.; Mikkelsen, K. V.; Norman, P.; Packer, M. J.; Saue, T.; Taylor, P. R.; Vahtras, O. Dalton, an ab initio electronic structure program, release 1.0 1997.
 42. Werner, H.-J.; Knowles, P. J.; Lindh, R.; Manby, F. R.; Schütz, M.; Celani, P.; Korona, T.; Mitrushenkov, A.; Rauhut, G.; Adler, T. B.; Amos, R. D.; Bernhardsson, A.; Berning, A.; Cooper, D. L.; Deegan, M. J. O.; Dobbyn, A. J.; Eckert, F.; Goll, E.; Hampel, C.; Hetzer, G.; Hrenar, T.; Knizia, G.; Köppl, C.; Liu, Y.; Lloyd, A. W.; Mata, R. A.; May, A. J.; McNicholas, S. J.; Meyer, W.; Mura, M. E.; Nicklass, A.; Palmieri, P.; Pflüger, K.; Pitzer, R.; Reiher, M.; Schumann, U.; Stoll, H.; Stone, A. J.; Tarroni, R.; Thorsteinsson, T.; Wang, M.; Wolf, A. Molpro, version 2006.1, a package of ab initio programs 2006. Available at: <http://www.molpro.net>.
 43. Gedanken, A.; Duraisamy, M.; Huang, J.; Rachon, J.; Walborsky, H. M. *J Am Chem Soc* 1988, 110, 4593.
 44. Ben-Nun, M.; Martínez, T. J. *Chem Phys* 2000, 259, 237.
 45. Ben-Nun, M.; Molnar, F.; Schulten, K.; Martínez, T. J. *PNAS* 2002, 99, 1769.
 46. Peña-Gallego, A.; Martínez-Núñez, E.; Vázquez, S. A. *Chem Phys Lett* 2002, 353, 418.
 47. González-Vázquez, J.; Fernández-Ramos, A.; Martínez-Núñez, E.; Vázquez, S. A. *J Phys Chem A* 2003, 107, 1389.
 48. González-Vázquez, J.; Fernández-Ramos, A.; Martínez-Núñez, E.; Vázquez, S. A. *J Phys Chem A* 2003, 107, 1398.
 49. González-Vázquez, J.; Martínez-Núñez, E.; Vázquez, S. A.; Santamaria, J.; Banares, L. *Chem Phys Lett* 2004, 396, 442.
 50. Balko, B. A.; Zhang, J.; Lee, Y. T. *J Chem Phys* 1992, 97, 935.
 51. Cromwell, E. F.; Stolor, A.; Vrakking, M. J. J.; Lee, Y. T. *J Chem Phys* 1992, 97, 4029.
 52. Hall, G. E.; Muckerman, J. T.; Preses, J. M.; Ralph E. Weston, J.; Flynn, G. W.; Persky, A. *J Chem Phys* 1994, 101, 3679.
 53. Balko, B. A.; Zhang, J.; Lee, Y. T. *J Phys Chem A* 1997, 101, 6611.
 54. Lin, J. J.; Wu, S. M.; Hwang, D. W.; Lee, Y. T.; Yang, X. *J Chem Phys* 1998, 109, 10838.
 55. Blank, D. A.; Sun, W.; Suits, A. G.; Lee, Y. T.; North, S. W.; Hall, G. E. *J Chem Phys* 1998, 108, 5414.
 56. Sato, K.; Tsunashima, S.; Takayanagi, T.; Fijisawa, G.; Yokoyama, A. *Chem Phys Lett* 1995, 242, 401.

4.3 Non-adiabatic Full-dimensional *ab initio* Molecular Dynamics for 4MCF

Motivated by the previous findings, in the subsequent study 4MCF has been investigated using *ab initio* molecular dynamics (AIMD). In this fashion all the degrees of freedom can be considered simultaneously due to the fact that the PESs are determined on-the-fly by accurate quantum chemistry calculations (recall section 3.3). It was found in section 4.2 that the quantum chemistry in 4MCF requires to describe at least one repulsive $\pi\sigma^*$ state besides electronic ground and the bright $\pi\pi^*$ state. In the following article “*H-abstraction is more efficient than cis-trans isomerization in (4-methylcyclo-hexylidene) fluoromethane. An ab initio molecular dynamics study*” results of 4MCF’s global stationary points, i.e. all possible dissociation products, and *ab initio* molecular dynamics on coupled electronic states is presented. In this study at least three electronic states have been considered at the same time using a large, and thus flexible active space including twelve electrons in ten orbitals. Such an active space is able to describe different dissociation products in 4MCF. As stated in section 4.2 the flexibility of the quantum chemistry is very important here, in order to allow different relaxation paths in 4MCF.

Previous to the AIMD calculations, dissociation products of 4MCF, such as the above studied HF-elimination, but also atomic H and F abstraction as well as rupture of the C-C double bond, have been optimized on the global ground state PES. It is found that upon excitation to the bright $\pi\pi^*$ state all dissociation products are thermodynamically accessible, both from the CASSCF and CASPT2 energy point of view. Furthermore, unrelaxed one-dimensional PESs along the atomic H as well as F dissociation coordinate have been calculated and compared to the previous found HF-elimination process. As concluded in section 4.2 indeed the topology of the PESs for the different dissociation possibilities (HF and atomic H/F) are found to be similar.

Hence, AIMD calculations for 4MCF have been done to unveil which of the elimination pathways (or any other) is competitive with *cis-trans* isomerization. To this aim a total of 400 trajectories have been prepared in the ground state of the R-enantiomer of 4MCF. In order to keep the calculation time on an affordable scale, only the first three electronic PESs have been considered, yet using a large flexible active space. Due to the $\pi\pi^*/\pi\sigma^*$ crossing at the Franck-Condon region, the state configurations for the adiabatic first and second excited states around the equilibrium geometry are mixed, i.e. depending on the initial geometry, the bright $\pi\pi^*$ is located either on the first or second adiabatic state (recall section 4.2). To achieve a realistic behaviour for excitation to the diabatic $\pi\pi^*$ state only, trajectories have been started from the adiabatic state, that shows a high oscillator strength to the ground state. As a result, 92 independent trajectories on the first excited adiabatic state, S_1 , and 105 independent trajectories on the second excited adia-

batic state, S_2 , have been started. Each trajectory has been analysed during the relaxation back to the ground state, and then categorized into different paths according to the individual outcome. Figure 10 shows trajectories exemplifying each of the most important deactivation pathways observed in 4MCF. To each trajectory the overlap of the geometries at every time step before hopping to the ground state, as well as the geometry at the time of the crossing is displayed. The percentage of trajectories following these paths is also given.

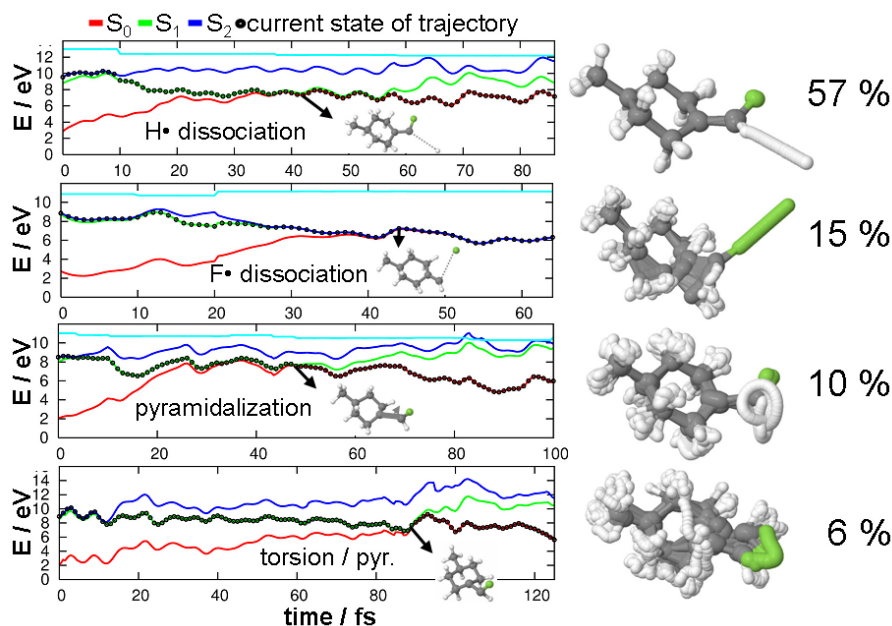


Figure 10: Selected trajectories and percentages of trajectories following main deactivation paths. Left panel: time evolution of the adiabatic potentials, momentary state indicated by rings; right panel: overlap of geometries before the crossing to the ground state.

It can be seen that the crossing between the $\pi\pi^*$ and $\pi\sigma^*$ states at the Franck-Condon region allows for ultrafast direct dissociation in the electronic excited $\pi\sigma^*$ state before the system decays to the ground state. The time scale for the first crossing process is found to be around 12 fs, showing that the CoIn between these states is very close to the Franck-Condon region and, more important, easily accessible. The time connected to the ground state decay on the other hand is ca. 60 fs after launching the trajectory. Interestingly, among all of the processes observed in 4MCF, torsion, and hence isomerization is found one of the most rare. The preferred reaction after irradiation to the bright $\pi\pi^*$ state is atomic H-dissociation (57%). A minor amount of molecules undergoes F-dissociation (15%), followed by pyramidalization showing no isomerization (10%). As discussed in

the previous studies for the HF-elimination (sections 4.1 and 4.2) dissociation of both H and F takes place on an excited state, not in the ground state. Concerted HF-elimination on the other hand has not been observed at all. Furthermore, the calculations show that the sparsely observed torsion motion giving rise to both enantiomers is strongly coupled to pyramidalization at both carbons connected to the olefinic double bond. Taking only the trajectories into account that perform the pyramidalization/torsion motion, a new CoIn responsible for the ultrafast deactivation to the electronic ground state could be identified, that has not been found in previous studies for 4MCF [80, 85].

Concluding, the following study shows that atomic H-dissociation is the main deactivation channel upon exciting 4MCF into the bright $\pi\pi^*$ state. The trajectories undergoing this process resemble very nicely a one-dimensional unrelaxed PESs along the C-H dissociation coordinate, i.e. during the whole process hydrogen is moving along the C-H bond vector and the rest of the molecule keeps nearly unchanged. The excited state H-dissociation in 4MCF then follows the mechanism proposed for other organic molecules, see Figure 8.

In order to enable 4MCF to be an effective R/S molecular switch (e.g. IR+UV pulse schemes [79]), it is therefore necessary to eliminate the possibilities of destroying the molecule, mainly breaking of the olefinic C-H bond, and therefore favour the torsional process around the double bond. One possibility is to reduce the efficiency of the CoIn between the $\pi\pi^*$ and $\pi\sigma^*$ states at the Franck-Condon region. Hence, in the next study a control scheme is presented that is able to slow down atomic H-dissociation significantly using laser pulses, such that torsion and/or pyramidalization can take place.

Next, the original article "*H-abstraction is more efficient than cis-trans isomerization in (4-methylcyclo-hexylidene) fluoromethane. An ab initio molecular dynamics study*" published in the Journal *Physical Chemistry Chemical Physics*, Vol. 14, in 2012 is reprinted.

(D. K. contributed to the following study by identifying and optimizing stationary points on the global 4MCF ground state PES using CASSCF and CASPT2 level of theory, by calculating one-dimensional PESs along H-, F-, and HF-dissociation coordinates, respectively, as well as by setting up, running and analysing the AIMD calculations. Additionally, D. K. prepared the manuscript.

J. G.-V. contributed to the investigation by preparing the AIMD simulations.

J. G.-V. and L. G. supervised the research and revised the manuscript.)

Cite this: *Phys. Chem. Chem. Phys.*, 2012, **14**, 6241–6249

www.rsc.org/pccp

PAPER

H-abstraction is more efficient than *cis*–*trans* isomerization in (4-methylcyclohexylidene) fluoromethane. An *ab initio* molecular dynamics study

Daniel Kinzel, Jesús González-Vázquez† and Leticia González*‡

Received 17th August 2011, Accepted 28th September 2011

DOI: 10.1039/c1cp22646k

Non-adiabatic molecular dynamics simulations have been performed in the fluoro-olefin (4-methylcyclohexylidene) fluoromethane (4MCF) using multiconfigurational CASSCF (complete active space self-consistent field) on-the-fly calculations. As an olefin containing a C=C double bond, 4MCF is expected to undergo *cis*–*trans* isomerization after light irradiation. However, *ab initio* molecular dynamics shows that a preferential dissociation of atomic hydrogen is taking place after population transfer to the bright $\pi\pi^*$ state. This state is strongly mixed with $\pi\sigma^*$ states allowing dissociation in the electronic excited state before deactivation to the ground state occurs. A minor amount of trajectories experiences F-dissociation, followed by pyramidalization at the sp^2 carbons and CHF dissociation. In contrast, the amount of trajectories undergoing torsion around the double bond, and therefore *cis*–*trans* isomerization, is marginal. The H-abstraction reaction is ultrafast, taking place in less than 60 fs.

1 Introduction

One of the fundamental processes in organic photochemistry is the light-driven torsional dynamics around a C=C double bond.¹ It can convert energy into functional motion, as *e.g.* in the biologically relevant retinal^{2,3} (the chromophore involved in vision) or in sterically overcrowded alkenes that serve as molecular rotatory machines.^{4–8} In olefins this torsion is triggered by irradiation to a $\pi\pi^*$ state from which the system rapidly decays, typically, *via* a conical intersection (CI) between the valence state (denoted by V , following Mulliken's notation⁹) and the electronic ground state, N .^{10,11} Ethylene, as a prototype where *cis*–*trans* isomerization can take place after light irradiation, has been intensively studied. Despite its apparent simplicity, the characterization of the electronic states involved upon excitation and during the deactivation is rather challenging due to valence-Rydberg mixing.^{12–16} Also important in the photochemistry of ethylene and systems alike is to characterize the surface crossing points or CIs involved in the corresponding relaxation pathways.^{10,11,14,17–23}

Internal conversion between the V and N states of ethylene involves first a C=C stretching and then a twist around the double bond. Then, possible relaxation paths include the

pyramidalization at one of the methylene units²⁰ or hydrogen migration.¹¹ In fluoroethylene the torsion over the double bond directly leads to a CI between the V and N states.¹⁵ Besides *cis*–*trans* isomerization, it is well-known that after photoexcitation ethylene and ethylene derivatives can undergo dissociation reactions. The elimination of atomic and molecular hydrogen or halogen hydrides is well documented in different experimental papers.^{24–30} The reported experiments are consistent with the idea that simple olefins first deactivate to the electronic ground state *via* a CI and then dissociate, justifying that classical trajectories in the electronic ground state only have been used to model photodissociation dynamics.^{31–38}

The title molecule, (4-methylcyclohexylidene) fluoromethane (4MCF), is a larger fluoro-olefin that possesses *R*- and *S*-enantiomers connected by a torsion around the C=C double bond, see Fig. 1a. In a series of papers, we have considered 4MCF as a simple model for a chiral light-induced molecular rotor.^{39–41} After excitation to the bright $\pi\pi^*$ state, 4MCF is expected to undergo torsion of the CHF group around the double bond, giving rise to the two chiral stable isomers. Similar to the CIs optimized for ethylene^{13,14,16} and fluoroethylene,¹⁵ a number of degeneracies have been located in 4MCF.^{42–44} The CIs shown in Fig. 1b involve torsion, pyramidalization at the ring carbon and H-atom migration and allow for deactivation from the spectroscopic $\pi\pi^*$ (S_1) state to the ground state (S_0). An additional CI associated with the elimination of HF at a twisted geometry (Fig. 1b) has been located between the S_1 and S_0 states.⁴³ Based on these CIs, it has been postulated that *cis*–*trans* isomerization should take place in the presence of

Institute of Physical Chemistry, Friedrich-Schiller-University Jena, Helmholtzweg 4, 07743 Jena, Germany

† Present address: Departamento de Química Física I, Universidad Complutense, 28040 Madrid, Spain.

‡ Present address: Institute of Theoretical Chemistry, University of Vienna, Währinger Str. 17, 1090 Vienna, Austria.

E-mail: leticia.gonzalez@univie.ac.at

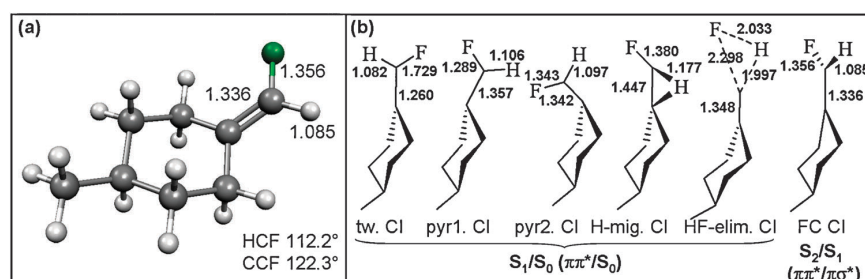


Fig. 1 (a) Structure of (*R*)-(4-methylcyclohexylidene)fluoromethane (4MCF) in the electronic ground state. Parameters obtained at the MP2/6-31G* level of theory.⁴² (b) Conical intersections (CIs) of 4MCF: twisted CI,⁴² two pyramidalized CIs,⁴² H-migration CI,⁴² HF-elimination CI,⁴³ and Franck-Condon degeneracy.⁴⁴

polar solvents mediated by the twisted CI while in the gas phase the HF-elimination CI should be operative leading to HF dissociation.⁴³ Gas phase quantum dynamical simulations considering only the ground state and the $\pi\pi^*$ state in two dimensions (the torsion and the HF elimination coordinates) showed that torsion in the $\pi\pi^*$ state dominates for about 1 ps.⁴⁵ Moreover, although the system possessed enough kinetic energy to arrive at the HF-elimination CI, the quantum dynamical simulations showed hardly no population transfer to the electronic ground state during the propagation time (1 ps).⁴⁵ These results thus indicated that HF-dissociation is not competitive with *cis-trans* isomerization in 4MCF. However, neglecting other degrees of freedom might prevent the system from decaying to the ground state *via* different mechanisms, see *e.g.* ref. 46.

Noteworthy, we have recently discovered that $\pi\sigma^*$ states are directly involved in the photochemistry of 4MCF.⁴⁴ Experiment and theory have demonstrated that $\pi\sigma^*$ states can have a prominent role in the photochemistry of plenty of organic systems,⁴⁷ including DNA bases.^{48–50} However, their role in alkenes is in general not well studied. In 4MCF, such states are responsible for homolytic dissociation of the HF fragment, but certainly could also be responsible for the abstraction of the single H or F atom, respectively. An exhaustive study at CASSCF and CASPT2 levels of theory using active spaces large enough to describe simultaneously the $\pi\pi^*$ and $\pi\sigma^*$ excited states of 4MCF showed that both states are very close in energy at the Franck-Condon (FC) equilibrium geometry, and that this point actually belongs to a seam of CIs between both states (Fig. 1b). In ref. 44, it was therefore proposed that the ultrafast radiationless relaxation of 4MCF could be different from the one suggested until now. While population can still be transferred to the ground state *via* a torsion of the CHF fragment, the molecule can also dissociate through $\pi\sigma^*$ states without preliminary torsion.⁴⁴ Motivated by these recent findings, in this paper we investigate 4MCF using mixed quantum-classical dynamics. In this fashion all the degrees of freedom are considered simultaneously since the full-dimensional potential energy surfaces are determined on-the-fly by accurate *ab initio* calculations. The present work allows then for the first time to obtain a complete insight into the deactivation mechanism of 4MCF and to investigate all the processes that are competitive with *cis-trans* isomerization on an equal footing.

2 Computational details

The calculations of the electronic excited states have been done using the state-averaged version of the complete active space self-consistent field (SA-CASSCF)⁵¹ method with an active space including twelve electrons in ten orbitals, namely the σ_{CC} , σ_{CH} , σ_{CF} , π_{CC} , their corresponding antibonding ones and two lone pair orbitals centered at the fluorine atom, as discussed in ref. 44. The basis set chosen for all the calculations is the double zeta Pople basis set 6-31G*.⁵²

Local ground state minima optimizations for possible dissociation products on the CASSCF(12,10) global potential energy surface (PES) were performed with the MOLPRO program package.⁵³ Subsequent single point calculations were done on the optimized minima at the SA-CASSCF level of theory using 6 roots (SA6). More accurate energy values were obtained with the multi-state CAS perturbation theory 2nd order (MS-CASPT2)⁵⁴ and a level-shift of 0.3 a.u.⁵⁵ The level-shift is employed in order to avoid intruder states and to achieve reasonable reference weights of at least 80%. The single point calculations have been performed with the MOLCAS program package.⁵⁶

The mixed quantum-classical dynamics,⁵⁷ starting from the *R*-enantiomer of 4MCF, are carried out by integrating Newton's equations for the nuclear motion with a time step of 0.5 fs using the Velocity-Verlet algorithm⁵⁸ and the time-dependent electronic Schrödinger equation with the fifth-order Butcher algorithm.⁵⁹ Surface hopping probabilities for nonadiabatic transitions were computed at each time step with the fewest-switches algorithm^{57,60} in the version developed by Hammes-Schiffer and Tully.⁶¹ In the event of hopping, the excess of momentum was adjusted in the direction of the non-adiabatic coupling vectors as justified in ref. 62 and 63. In the case of frustrated hoppings the momentum was kept constant. According to Alfalah *et al.*,⁴⁵ who propose a full torsional cycle in about 300 fs for 4MCF, trajectories are run for at least 500 fs.

A total of 400 initial geometries and velocities were generated by a Wigner distribution treating each nuclear coordinate as a harmonic oscillator in the ground state. Normal modes used for the Wigner distribution were calculated at the B3LYP/SV(P) level of theory with the Turbomole program package.^{64,65} A characterization of the distribution has been done by calculating an absorption spectrum by means of the

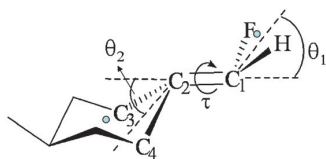


Fig. 2 The most important internal coordinates involved in the photo-deactivation of (R)-4MCF.

Gaussian broadening method described in ref. 66. A total of 197 trajectories with an oscillator strength greater than 0.1 a.u. have been chosen as a result of this characterization. Out of these 197 trajectories, a subset of 92 and a subset of 105 trajectories were started in the first excited state S_1 and the second excited state S_2 , respectively.

The spectrum and trajectories were calculated at the SA3-CASSCF(12,10)/6-31G* level of theory with the Newton-X program package^{66,67} interfaced with Columbus.^{68–71} Furthermore, as shown by Olivucci and coworkers,⁷² the CASSCF energies and energy gradients were scaled by a factor of 0.7, which has been implemented in Newton-X. This scaling is necessary to compensate for the difference between the CASPT2 and CASSCF energy values.⁷² In particular, our scaling factor is estimated to meet the experimental excitation energy of 6.5 eV.⁷³ By removing the energy excess, artificial dynamical processes can be avoided.

The analysis of the trajectories was done using the internal coordinates that are directly related with the decay of (R)-4MCF from the $\pi\pi^*$ state to the ground state (see Fig. 2). These are: (i) the distances $d(\text{C-H})$, $d(\text{C-F})$ and $d(\text{C-C})$, defined as the bond length between the $\text{C}_1\text{-H}$, $\text{C}_1\text{-F}$ and $\text{C}_1\text{-C}_2$ atoms; (ii) the distance R , defined as the distance between the center of mass of the cyclohexylidene moiety and the center of mass of the HF fragment (indicated by dots in Fig. 2); (iii) the pyramidalization angles θ_1 and θ_2 , which describe the angle between the $\text{C}_1\text{-C}_2$ double bond and the planes constructed by the bonds $\text{C}_1\text{-H}$, $\text{C}_1\text{-F}$ and the bonds $\text{C}_2\text{-C}_3$, $\text{C}_2\text{-C}_4$, respectively; and (iv) the torsional angle τ , which is the dihedral angle $\text{C}_3\text{-C}_2\text{-C}_1\text{-F}$ defined as the angle between the plane constructed by the bonds $\text{C}_2\text{-C}_3$, $\text{C}_2\text{-C}_1$ at the equilibrium structure (and thus at time $t = 0$) and the plane constructed by the bonds $\text{C}_1\text{-C}_2$, $\text{C}_1\text{-F}$.

3 Results and discussion

3.1 Potential energy surfaces of 4MCF

The absorption spectrum of 4MCF measured by Gedanken *et al.*⁷³ is characterized by a bright $\pi\pi^*$ excitation following a dark $3s$ Rydberg transition. The role of Rydberg states in 4MCF has been studied previously by our group⁴² and it will not be considered here. Instead, we focus on the role of $\pi\sigma^*$ states since, although dark, they shall play a decisive role in the deactivation of 4MCF after irradiation into the $\pi\pi^*$ state. The use of the 6-31G* basis set intentionally neglects the description of Rydberg orbitals and because at the Franck–Condon region Rydberg and $\pi\sigma^*$ states do not mix, it is justified to use this basis set for treating $\pi\sigma^*$ states. With this basis set the bright $\pi\pi^*$ state is the first excited state located at 9.28 eV at the SA6-CASSCF level of theory and 7.92 eV when CASPT2

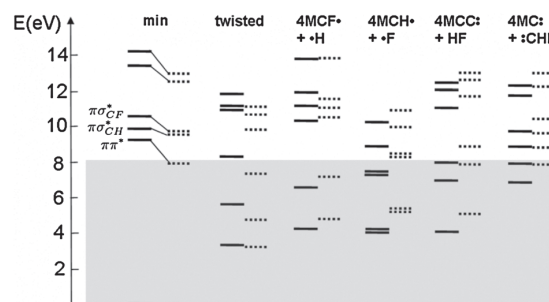


Fig. 3 CASSCF (solid line) and CASPT2 (dotted line) vertical excitation energies for the minimum structure, the HF twisted transition state, and dissociation products optimized at the CASSCF(12,10)/6-31G* level of theory. The grey area denotes the amount of energy available in 4MCF after excitation to the bright $\pi\pi^*$ state (at the CASPT2 level of theory).

is employed. This transition is closely followed by two dark $\pi\sigma^*$ excitations involving the σ_{CH}^* (9.87 (CASSCF)/9.50 (CASPT2) eV) and σ_{CF}^* (10.58/9.78 eV) orbitals, respectively. Note that the $\pi\sigma_{\text{CH}}^*$ and $\pi\sigma_{\text{CF}}^*$ states are mixed in character, as we also found in ref. 44. It is interesting to note that the energy gap between the $\pi\pi^*$ and $\pi\sigma^*$ states is rather sensitive to the method employed (see also ref. 44). With the basis sets used here this gap amounts to 0.59 eV and 1.58 eV, at CASSCF and CASPT2, respectively. Using the best correlated method reported in ref. 44, MS-CASPT2/CASSCF(12,10)/ANO-L, this gap amounts to 0.22 eV, which is comparable to the one obtained with CASSCF(12,10)/6-31G*. Higher excited states have a different electronic nature,⁴⁴ and they are not relevant for the present paper.

Fig. 3 depicts the CASSCF and CASPT2 vertical excitation energies of 4MCF at the equilibrium geometry but also at the twisted conformation. Furthermore, the energies of all the dissociation products, including atomic H and F abstraction, HF elimination, and rupture of the CC double bond are also shown. As it can be seen, upon excitation to the bright $\pi\pi^*$ state all dissociation products are thermodynamically accessible, both from the CASSCF and CASPT2 energy point of view.

Unrelaxed one-dimensional PESs along the dissociation coordinates R , $d(\text{C-H})$ and $d(\text{C-F})$ have been calculated and are shown in Fig. 4a–c. The rupture of a single bond (C–H or C–F) gives a typical ground state Morse potential while excited state potentials show a barrierless decreasing asymptotic behavior. The PESs for HF elimination (Fig. 4a) have been first presented in ref. 44. Here, we just recall the most important features and their implications. At the FC point ($\tau = 0^\circ$) the S_1 ($\pi\pi^*$) and S_2 ($\pi\sigma^*$) states experience an avoided crossing. Assuming that the system is excited to the bright S_1 state, the character of the potential will quickly change from $\pi\pi^*$ to $\pi\sigma^*$ after a small bond elongation. Due to the energy gradient of the lowest excited state, the system is expected to remain in the adiabatic S_1 state, although the $\pi\pi^*$ character is completely lost after a few tenths of Angstroms of elongation. An important consequence is that the diabatic $\pi\pi^*$ state is bound (see the inset of Fig. 4a) and that HF dissociation can take place in a repulsive $\pi\sigma^*$ state competing with a ground state reaction.^{31,34,35} Furthermore, one can see that both the

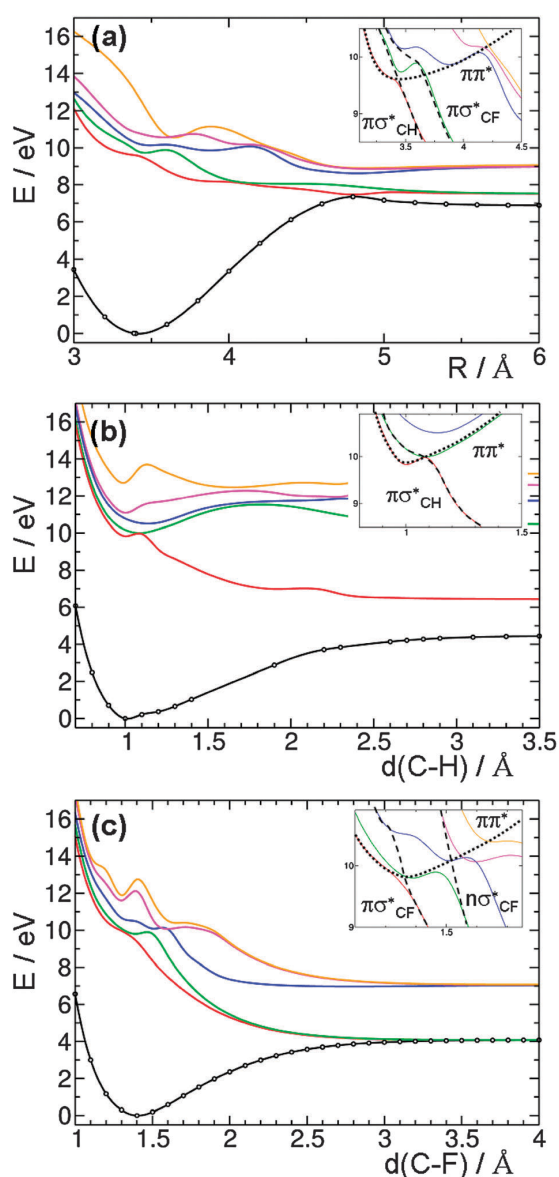


Fig. 4 SA6-CASSCF(12,10)/6-31G* unrelaxed potential energy curves for (a) HF dissociation along R , adapted from ref. 44, (b) atomic H dissociation along $d(\text{C-H})$, and (c) atomic F dissociation along $d(\text{C-F})$. The dashed lines in the insets indicate the schematic diabatic states. The open circles indicate the actual *ab initio* data points calculated.

$\pi\sigma_{\text{CH}}^*$ and the $\pi\sigma_{\text{CF}}^*$ states, initially S_2 and S_3 , are repulsive and thus nicely resemble the low-lying repulsive states obtained for the individual dissociation of either H or F atom (Fig. 4b and c). Similar profiles to those found in the concerted HF elimination are observed in the unrelaxed PES of atomic H and F abstraction. Both potentials show avoided crossings between the bright $\pi\pi^*$ state (S_1) and the $\pi\sigma^*$ states (S_2 and S_3) in the FC window. Therefore, after elongation of the corresponding bond the $\pi\pi^*$ character is lost and dissociation can take place on the repulsive $\pi\sigma^*$ excited state.

Since all dissociation products are energetically accessible and the topology of the PES for the different dissociation possibilities (HF and atomic H/F) is similar, mixed quantum-classical dynamical simulations have been carried out to unveil which of the elimination pathways (or any other) is competitive with *cis-trans* isomerization. The results are presented in the next section.

3.2 Non-adiabatic mixed quantum-classical dynamics

The spectrum generated from the Wigner distribution with scaled energies can be seen in Fig. 5. The overall spectrum centered at 6.5 eV is composed of a $S_0 \rightarrow S_1$ transition centered at 6.2 eV and a $S_0 \rightarrow S_2$ transition centered at 6.8 eV. Both transitions show the same intensities in the center of their bands and thus nicely resemble the strong mixing of the two excited states predicted in ref. 44 with the implication that small geometrical distortions change the degree of mixing of the two lowest lying excited states or even reverse their character.

Fig. 6 shows the time evolution of the adiabatic population in each state averaged for all the trajectories (P_{tot}) during the first 150 fs. Almost all trajectories arrive at the ground state S_0 after 150 fs. The total occupation in S_2 decreases by 90% in less than 20 fs and diminishes further after 80 fs. Concomitantly, the occupation of S_1 increases in the first 20 fs due to direct non-adiabatic $S_2 \rightarrow S_1$ transfer and then decreases at the expense of populating the ground state. At longer times, *i.e.* after 150 fs, some population remains in the S_1 and S_2 states and do not decay to the S_0 . This population is ascribed to atomic F dissociation. At long C-F distances, the three lowest lying electronic states are degenerated (recall Fig. 4c) and therefore population can be freely exchanged among the three states.

The lifetime of each state can be also analyzed looking at the relaxation of the individual subsets of trajectories. The corresponding curves are plotted as insets in Fig. 6: P_{S_1} (top inset) for the set of trajectories started in the S_1 and P_{S_2} (bottom inset) for those started in the S_2 state. We have used these curves to estimate the lifetimes of each of the states by fitting the corresponding population to an exponential decay of the form of $f(t) = e^{-(t-t_0)/T}$, with t_0 as the offset of the fitted function. As a result we estimate a lifetime T in S_1 of 48.8 ± 0.6 fs

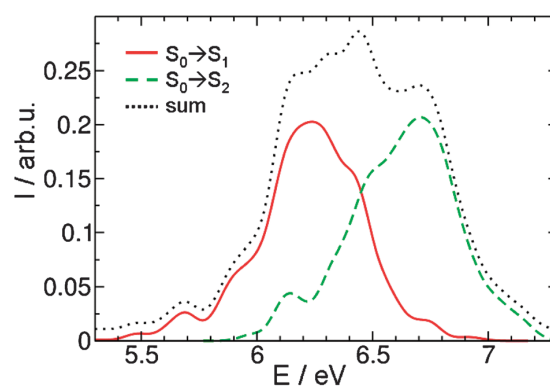


Fig. 5 Total spectrum lifted by 0.01 a.u. (dotted line in black), with the contributions of the $S_0 \rightarrow S_1$ transition (solid line in red) and that of the $S_0 \rightarrow S_2$ transition (dashed line in green). The excitation energies are scaled by 0.7.

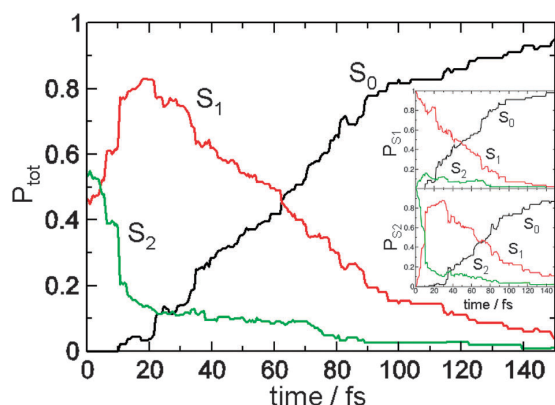


Fig. 6 Time evolution of the average adiabatic population P_{tot} in each state; insets: P_{S_1} and P_{S_2} describing the average occupation of the states for subsets of trajectories starting in S_1 and S_2 , respectively.

($t_0 = 3.7 \pm 0.4$) for P_{S_1} and 56.5 ± 0.6 fs ($t_0 = 30.7 \pm 0.4$) for P_{S_2} . The time constant in S_2 for P_{S_2} on the other hand is very short and amounts to 11.8 ± 0.4 fs ($t_0 = 0.9 \pm 0.2$).

In Table 1 we summarize the number and percentage of the trajectories which follow a particular process in 4MCF. The possible events are classified as: (i) atomic H-dissociation, if the distance $d(\text{C-H})$ is greater than 2.5 \AA ; (ii) atomic F-abstraction, if the distance $d(\text{C-F})$ is greater than 3.0 \AA ; (iii) CHF-dissociation, if the distance $d(\text{C-C})$ is greater than 3.0 \AA ; (iv) pyramidalization, if the angles θ_1 or θ_2 change by more than 10° , while the dihedral angle τ does not change; (v) torsion, if the dihedral angle τ changes by more than 10° , and this change is not an artifact of the pyramidalization angle at C_1 , θ_1 , which then should be around 0° ; (vi) concerted HF elimination, if both $d(\text{C-H})$ and $d(\text{C-F})$ concertedly reach a value of 3.0 \AA ; and finally (vii) others, if there is any other irreversible bond rupture not mentioned above. The values chosen for the events (i), (ii) and (vi) are based on the dissociation plateaus in Fig. 4b and c, respectively. The relaxation of 4MCF is considered complete once the trajectories decayed to S_0 and no further reactions except vibronic motion occur, or one of the events mentioned above takes place.

Inspection of Table 1 shows a striking result. Out of a total of 197 trajectories the main product (78%) is undesired

Table 1 Total number (percentage) of trajectories following one of the deactivation paths starting either from S_1 or S_2

Path	S_1	S_2	Sum
Total	92 (100)	105 (100)	197 (100)
H-Dissociation	67 (73)	46 (44)	113 (57)
F-Dissociation	6 (7)	24 (23)	30 (15)
CHF-Dissociation	3 (3)	9 (9)	12 (6)
Pyramidalization ^a	5 (5)	14 (13)	19 (10)
Torsion ^b	3 (3)	9 (9)	12 (6)
HF-elimination	0 (0)	1 ^c (1)	1 ^c (1)
Others ^d	8 (9)	1 (1)	10 (5)

^a Pyramidalization on both double bond carbons is taken into account. ^b Torsion is strongly connected to the pyramidalization mode. ^c Not concerted; first H- then F-dissociation. ^d Ring opening, insertion, other dissociation products.

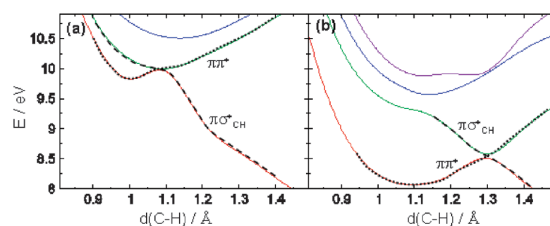


Fig. 7 CASSCF (a) versus CASPT2 (b) potential energy curves along $d(\text{C-H})$ around the avoided crossing between the $\pi\pi^*$ and $\pi\sigma^*$ states. Dashed lines indicate schematically the diabatic states as in Fig. 4.

dissociation instead of *cis-trans* isomerization! The most probable event is atomic H-dissociation (57%), followed by atomic F-abstraction (15%) and irreversible C-C bond breaking (6%). The relative ratio of H versus F dissociation products depends strongly on the initially populated state. We observe significantly more F-dissociation when starting on the S_2 state. This is due to the fact that not only the $\pi\sigma_{\text{CH}}^*$ state but also the $\pi\sigma_{\text{CF}}^*$ state is very close to the spectroscopic $\pi\pi^*$ state (recall Fig. 3). Hence, starting in S_2 and thus being higher in energy facilitates the crossing with the $\pi\sigma_{\text{CF}}^*$ state. Furthermore, we note that only one single trajectory undergoes HF elimination, however in a step-wise manner. Finally, a small amount of trajectories (16%) shows pyramidalization and/or torsion, whereby pyramidalization is dominant. We observe that torsion of the CHF moiety is always coupled with pyramidalization.

Since cleavage of atomic H is clearly the dominant reaction, we considered of interest to recalculate the potential energy curves for C-H dissociation around the $\pi\pi^*$ and $\pi\sigma^*$ avoided crossing with MS-CASPT2. The comparison of the CASSCF and MS-CASPT2 curves is shown in Fig. 7. As it can be seen, the avoided crossing has shifted from *ca.* 1.1 to 1.3 \AA and the barrier to reach the crossing has slightly increased from 0.12 to 0.44 eV. Since the ZPE is included in the simulations and is about 2 eV (*vide infra*), we are confident that the CASSCF model is enough to describe qualitatively the dynamics of 4MCF.

In the following, the nature and character of the trajectories relaxing to the ground state after excitation to the $\pi\pi^*$ state is analyzed in further detail. Fig. 8 highlights the geometrical parameters at which jumps between the different surfaces occur, considering all the trajectories (Fig. 8a and b) and the subset of 41 trajectories that do not undergo dissociation (Fig. 8c). Fig. 9 presents the time evolution of the important internal coordinates changing during the deactivation of 4MCF. Panels a-c display the evolution of the selected distances for all trajectories while panels d-f are devoted to pyramidalization and torsional angles for the trajectories that do not dissociate.

Firstly, it is interesting to observe that the $S_1 \rightarrow S_0$ hopping points (Fig. 8a) are all distributed along a single coordinate. Thus, if dissociation occurs it is only along either the C-H, C-F or the C-C coordinate, but not along a mixture of two. The $S_2 \rightarrow S_1$ hopping (see Fig. 8b) occurs either at geometries very close to the FC point, corresponding to a very fast decay at the equilibrium geometry, or at extended C-F distances, corresponding to a decay at longer times when the states are threefold degenerated at the dissociation limit—the last event being connected to F-abstraction.

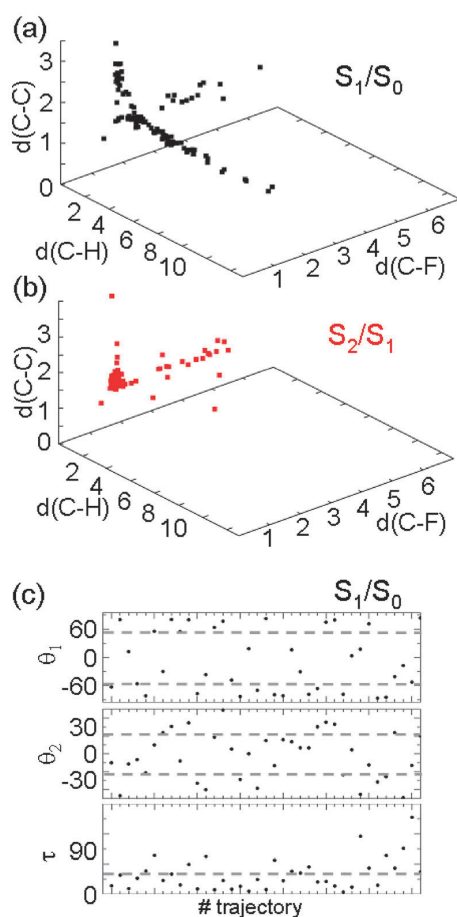


Fig. 8 Geometric parameters at hopping times. S_1/S_0 (a) and S_2/S_1 (b) hoppings vs. distances; (c) S_1/S_0 jumps vs. pyramidalization angles, θ_1 and θ_2 , and torsional angle, τ , respectively, for the subset of 41 trajectories that are not dissociating.

As expected, the dissociation of atomic H is much faster than that of atomic F or the CHF fragment—note the different scale in Fig. 9a–c. The H-abstraction reaction takes place without any significant change in the skeleton of the molecule

prior to dissociation. This means that the potential energy curves that are computed on-the-fly during the MD calculations resemble qualitatively quite well the unrelaxed PES depicted in Fig. 4b. These PESs show no crossing between the S_1 state and the ground state. Hence, the only way the system can relax to the ground state is either through a CI connected to the degrees of freedom of the dissociated 4MCF or by vibrational motion. Since we also observe no significant geometric changes in the molecule after dissociation, we propose that the latter reason must be the main deactivation channel for 4MCF dissociating atomic hydrogen. Interestingly, we see that the S_1 to S_0 crossing points along the C–H dissociation (Fig. 8a) are spread over a large number of distances, supporting the idea that relaxation to the ground state is due to vibrational motion of the 4MCF skeleton. Moreover, the large spread of hops along the C–H coordinate is in agreement with the fact that the lifetime for $S_1 \rightarrow S_0$ is longer than the one for $S_2 \rightarrow S_1$ (*vide supra*). In contrast to H-dissociation, which mostly takes place in the S_1 state, F-abstraction can happen on any of the electronic excited states (see Fig. 8a and b), in agreement with the topology in Fig. 4b and c, respectively.

The trajectories that do not lose atomic H or F show a pronounced stretching of C–C, more intensely connected to $S_1 \rightarrow S_0$ hops (Fig. 8a). The stretching of the double bond is only in a few cases leading to CHF-dissociation (see Fig. 9c), but in most of the trajectories it is linked to pyramidalization and torsion. Note, however, that in the first 10 fs, all the trajectories experience a slight C–C stretch, which is not surprising since each initial condition contains $\pi\pi^*$ character. The 6% of the trajectories which undergo CHF-dissociation (see Table 1) either stay for a long time in the excited state (jump after *ca.* 80 fs) or gain a large momentum along the C–C bond after a hop at early times (*ca.* 40 fs) to be able to dissociate in the electronic ground state (see Fig. 9c).

Disregarding the dissociating trajectories, we have found that the 41 trajectories of this subset experience strong pyramidalization at C_1 up to $\pm 80^\circ$ (Fig. 9d), and some pyramidalization at C_2 of about $\pm 30^\circ$ (Fig. 9e). A total of 12 trajectories undergo torsion, whereby 11 of them, after hopping to the ground state, evolve back to the enantiomer they originally started from (Fig. 9f). With the help of the geometries obtained at the time 4MCF decays to the ground state, we can estimate

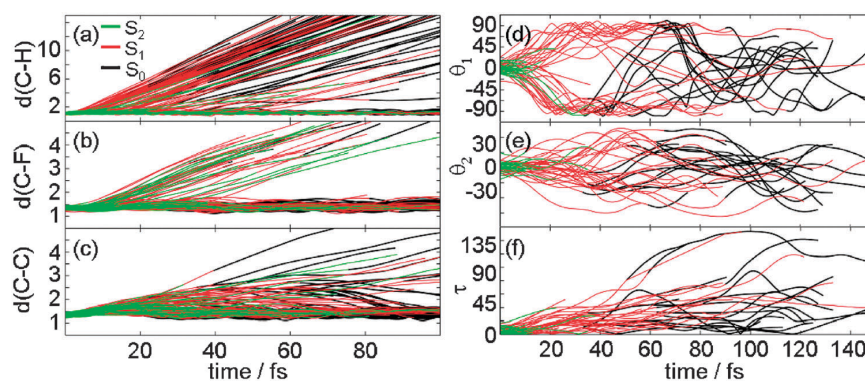


Fig. 9 Selected internal coordinates as a function of time over all trajectories. Distances in panels a–c and pyramidalization and dihedral angles only over trajectories not going through dissociation in panels d–f. Color code refers to the trajectory currently occupying S_0 (black), S_1 (red), or S_2 (green).

average geometrical parameters which later on can be compared with the CIs optimized by quantum chemical methods. Fig. 8c shows the values of the two pyramidalization angles, θ_1 and θ_2 , and the torsional angle, τ , at the point of the last hop to the ground state as well as the predicted averages (indicated by dotted lines). Note that, since 41 trajectories are not statistically representative, these average values should be considered only as rough estimations. Thus, we predict an average pyramidalization angle θ_1 of either $+60^\circ$ or -60° , an angle θ_2 of $+20^\circ$ or -20° and a torsional angle τ of 30° . A detailed analysis shows that torsion is strongly coupled with the pyramidalization mode at both, C_1 and C_2 , as found *e.g.* in ethylene.^{22,39}

It is now appealing to discuss the average geometries at the time of the $S_1 \rightarrow S_0$ hopping in terms of the CIs previously optimized in 4MCF.^{42,43} Recall that a total of five CIs have been found in 4MCF: a twisted CI, two pyramidalized CIs, a H-migration CI and a HF-elimination CI (Fig. 1). Since concerted HF-elimination and H-migration are not observed here (see Table 1), no connection to these CIs can be done. For the rest of the CIs, the most relevant internal coordinates are collected in Table 2. For completeness, we have added the mirror images of each of the CIs reported in ref. 42 (they are indicated by *). A quick inspection of the values obtained at the time of the hop (also in Table 2) shows that the average pyramidalization angle at C_1 (θ_1) is much bigger and θ_2 is much smaller than the corresponding angles of the two optimized pyramidalized CIs, labeled as pyr1 and pyr2 CIs in Table 2. Furthermore, the average torsion angle is much smaller than that of any of the CIs previously optimized, *i.e.* 4MCF deactivates before the twisting of the CHF group is completed and hence the other enantiomer can be obtained. Since none of the CIs optimized until now resemble the average hopping geometry, this geometry has been used as a guess for a new CI optimization search at the SA2-CAS(2,2)/cc-pVDZ level of theory, as in ref. 42. The obtained CI and its enantiomer counterpart (see Fig. 10) are labeled as pyr3/pyr3* and they show strong pyramidalization at C_2 , contrary to pyr1 and pyr2, see Table 2. The similarity between the obtained parameters of this new CI and the average hopping geometry confirms that the pyr3* CI is the one which is accessed by the present MD simulations of the non-dissociate reactions. Indeed, this CI is higher in energy than the previously found ones (3.8 eV) underscoring that it is more probable to access after irradiation.

Fig. 11 shows trajectories exemplifying each of the deactivation pathways observed in 4MCF. To each trajectory the overlap of the geometries at every time step before and after hopping to the ground state, as well as the geometry at the time of crossing is

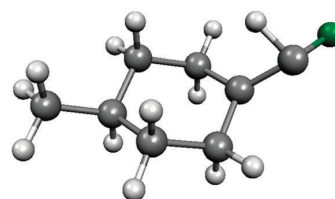


Fig. 10 Geometry of the conical intersection pyr3* optimized at the SA2-CAS(2,2)/cc-pVDZ level of theory.

displayed. As it can be seen the C–H bond breaking reaction takes place in the excited state. At the time of hopping to the ground state, 45 fs, the C–H distance is already longer than 6 Å. As mentioned before, during the ultrafast H-abstraction reaction the molecular scaffolding is little affected, except for light C–H stretching vibrations. Although in this particular trajectory the molecule finally deactivates to the ground state after 45 fs, the S_1 and the S_0 are very close in energy for about 20 fs.

A similar deactivation time is observed in the exemplary F-dissociation trajectory. Although the C–F bond is less extended in this time, the reaction can be considered completed before reaching the electronic ground state. It should be noted that the S_2 and S_1 electronic excited states are very close in energy most of the time. Stretching of the C–F bond brings the S_2 and S_1 degenerated with the S_0 and they remain as a threefold degeneracy until full F-dissociation (recall Fig. 4c).

A comparable S_2 and S_1 degeneracy for about 40 fs is observed in the trajectory illustrating the irreversible rupture of the C=C double bond. The reason is that not only the $\pi\pi^*$ state but, after some C–C elongation, also a $\pi\sigma_{CC}^*$ excitation leads to the irreversible breaking of this bond. The ground state decay takes place after *ca.* 60 fs and at this point the C=C bond is stretched up to 2.45 Å; further dissociation takes place in the electronic ground state.

In the case of pyramidalization we observe an intense movement of the H-atom accompanied with a strong C=C stretch. At the point of the jump after 48 fs, the C=C bond measures 2.42 Å. This value is similar to the one achieved in the CHF-dissociation example at the decay time; however, in the present case, 4MCF recombines to reach the ground state minimum structure once in the S_0 state. At the point of hop the C_1 is strongly pyramidalized ($\theta_1 = 62.7^\circ$) while C_2 is nearly unchanged.

Deactivation to the ground state for the torsion around the C=C bond (coupled with pyramidalization) requires almost double the amount of time (90 fs) as pyramidalization alone. During that excess of time the much heavier fluorine atom can

Table 2 Geometrical parameters of optimized CIs in 4MCF at the SA2-CAS(2,2)/cc-pVDZ level of theory and the corresponding energies relative to the 4MCF equilibrium. The values of tw, pyr1 and pyr2 are taken from ref. 42. The * denotes the corresponding enantiomer. The average hopping values are obtained at the SA3-CAS(12,10)/6-31G* level of theory

	Tw	Tw*	Pyr1	Pyr1*	Pyr2	Pyr2*	Pyr3	Pyr3*	Average hop (no diss.)
θ_1	-1.3	1.3	5.0	-5.0	-6.1	6.1	-56.7	56.7	± 60
θ_2	-12.6	-12.6	-59.7	-59.6	46.5	46.5	12.6	12.6	± 20
τ	82.5	81.9	134.1	114.0	51.4	67.7	143.7	53.1	30
$d(\text{C-H})$	1.082	1.082	1.106	1.106	1.094	1.094	1.177	1.177	1.2
$d(\text{C-F})$	1.729	1.729	1.289	1.289	1.343	1.343	1.380	1.380	1.5
$d(\text{C-C})$	1.260	1.260	1.357	1.357	1.342	1.342	1.447	1.447	1.9
$\Delta E/\text{eV}$	3.74	3.74	3.05	3.05	3.17	3.17	3.82	3.82	—

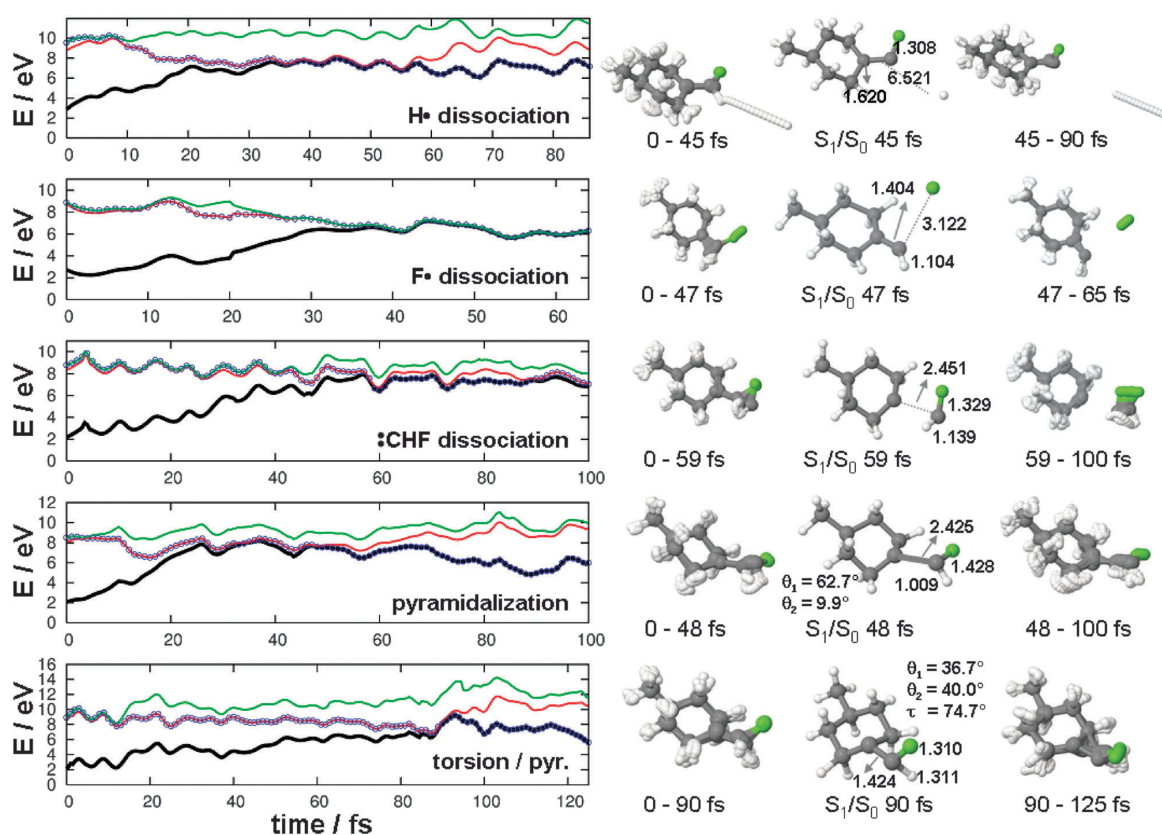


Fig. 11 Selected trajectories for main deactivation paths. Left panel: time evolution of the adiabatic potentials, momentary state indicated by rings; right panel: average geometry before and after the S_1/S_0 hop as well as geometry at the jump.

slowly follow the H atom to a twisting of 74.7° . The C_1 and C_2 achieve pyramidalization angles of 36.7° and 40.0° , respectively. Depending on the momentum direction of fluorine at the point of hopping, the system relaxes either to the opposite enantiomer or to the one it started in. In the present trajectories the latter process is observed. In general, we can say that any observed torsion is strongly connected to pyramidalization at both, C_1 and C_2 . Moreover, we do not observe any rigid torsion of the CHF group—a fact that can be explained by the asymmetry introduced by the large mass of the fluorine atom. Hence, the twisted CI (see Fig. 1b) is not reached by any of the trajectories.

4 Conclusions

The dynamics of the chiral 4MCF has been investigated in full dimensionality by using non-adiabatic molecular dynamics simulations. The on-the-fly electronic structure calculations are performed using the CASSCF method including an active space that not only can describe the $\pi\pi^*$ state—the typical V state for olefins—but also $\pi\sigma^*$ states. The role of $\pi\sigma^*$ states is then investigated here, finding that they are responsible for the major dissociation channel of atomic H and F in the electronic excited state. This finding is striking since in standard olefins, such as ethylene itself or F-ethylene, it is assumed that H- or F-dissociation occurs in the electronic ground state, where

the systems quickly decay first *via* a twisted CI. The torsion around the double bond and therefore *cis-trans* isomerization in such alkenes are then governed by the same CI. In 4MCF, in contrast, we find that torsion around the double bond is not necessary for dissociation. A crossing between the $\pi\pi^*$ and $\pi\sigma^*$ states at the Franck–Condon region allows for ultrafast direct dissociation in the electronic excited $\pi\sigma^*$ state before the system decays to the ground state. Further noticeable is that, among all of the processes observed in 4MCF, torsion is found one of the most rare. The preferred reaction after irradiation to the bright $\pi\pi^*$ state is atomic H-dissociation. A minor amount of molecules undergoes F-dissociation, followed by pyramidalization at the sp^2 carbons and CHF-dissociation. Furthermore, the calculations show that the sparsely observed torsion motion giving rise to both enantiomers is strongly coupled to pyramidalization at both carbons connected to the olefinic double bond.

Acknowledgements

We gratefully thank the Deutsche Forschungsgemeinschaft for financial support in the frame of a trilateral cooperation between Israel, Palestine and Germany (GO-1059/7-3). We thank Dr. Marko Schreiber for digging into the old conical intersection files of 4MCF. The calculations have been performed at the computer center of the Friedrich-Schiller-University of Jena.

References

- M. Klessinger and J. Michl, *Excited states and photochemistry of organic molecules*, VCH, New York, 1995.
- M. Ben-Nun, F. Molnar, K. Schulten and T. J. Martínez, *Proc. Natl. Acad. Sci. U. S. A.*, 2002, **99**, 1769.
- P. Kukura, D. W. McCamant, S. Yoon, D. B. Wandschneider and R. A. Manthies, *Science*, 2005, **310**, 1006.
- N. Koumura, R. W. J. Zijlstra, R. A. van Delden, N. Harada and B. L. Feringa, *Nature*, 1999, **401**, 152.
- N. Koumura, E. M. Geertsema, M. B. van Gelder, A. Meetsma and B. L. Feringa, *J. Am. Chem. Soc.*, 2002, **124**, 5037.
- R. A. van Delden, M. K. J. ter Wiel, M. M. Pollard, J. Vicario, N. Koumura and B. L. Feringa, *Nature*, 2005, **437**, 1337.
- M. M. Pollard, A. Meetsma and B. L. Feringa, *Org. Biomol. Chem.*, 2008, **6**, 507.
- G. Pérez-Hernández and L. González, *Phys. Chem. Chem. Phys.*, 2010, **12**, 12279.
- R. S. Mulliken, *Phys. Rev.*, 1932, **6**, 751.
- M. Ben-Nun and T. J. Martínez, *Chem. Phys.*, 2000, **259**, 237.
- J. Quenneville and T. J. Martínez, *J. Phys. Chem. A*, 2003, **107**, 829.
- L. Serrano-Andrés, M. Merchán, I. Nebot-Gil, R. Lindh and B. O. Roos, *J. Chem. Phys.*, 1992, **98**, 3151.
- R. P. Krawczyk, A. Viel, U. Manthe and W. Domcke, *J. Chem. Phys.*, 2003, **119**, 1397.
- M. Barbatti, J. Paier and H. Lischka, *J. Chem. Phys.*, 2004, **121**, 11614.
- M. Barbatti, A. J. A. Aquino and H. Lischka, *J. Phys. Chem. A*, 2005, **109**, 5168.
- B. G. Levine and T. J. Martínez, *Annu. Rev. Phys. Chem.*, 2007, **58**, 613.
- M. Ben-Nun and T. J. Martínez, *Chem. Phys. Lett.*, 1998, **298**, 57.
- M. Ben-Nun and T. J. Martínez, *J. Phys. Chem. A*, 1999, **103**, 10517.
- M. Ben-Nun, J. Quenneville and T. J. Martínez, *J. Phys. Chem. A*, 2000, **104**, 5161.
- J. Quenneville, M. Ben-Nun and T. J. Martínez, *J. Photochem. Photobiol., A*, 2001, **144**, 229.
- G. Granucci, M. Persico and A. Toniolo, *J. Chem. Phys.*, 2001, **114**, 10608.
- A. Viel, R. P. Krawczyk, U. Manthe and W. Domcke, *J. Chem. Phys.*, 2004, **120**, 11000.
- M. Barbatti, G. Granucci, M. Persico and H. Lischka, *Chem. Phys. Lett.*, 2005, **401**, 276.
- B. A. Balko, J. Zhang and Y. T. Lee, *J. Chem. Phys.*, 1992, **97**, 935.
- E. F. Cromwell, A. Stolow, M. J. J. Vrakking and Y. T. Lee, *J. Chem. Phys.*, 1992, **97**, 4029.
- B. A. Balko, J. Zhang and Y. T. Lee, *J. Phys. Chem. A*, 1997, **101**, 6611.
- J. J. Lin, S. M. Wu, D. W. Hwang, Y. T. Lee and X. Yang, *J. Chem. Phys.*, 1998, **109**, 10838.
- D. A. Blank, W. Sun, A. G. Suits, Y. T. Lee, S. W. North and G. E. Hall, *J. Chem. Phys.*, 1998, **108**, 5414.
- K. Sato, S. Tsunashima, T. Takayanagi, G. Fijisawa and A. Yokoyama, *Chem. Phys. Lett.*, 1995, **242**, 401.
- G. E. Hall, J. T. Muckerman, J. M. Preses, J. Ralph, E. Weston, G. W. Flynn and A. Persky, *J. Chem. Phys.*, 1994, **101**, 3679.
- A. Peña-Gallego, E. Martínez-Núñez and S. A. Vázquez, *Chem. Phys. Lett.*, 2002, **353**, 418.
- E. M. Núñez and S. A. Vázquez, *Struct. Chem.*, 2001, **12**, 95.
- E. Martínez-Núñez, C. M. Estévez, J. R. Flores and S. A. Vázquez, *Chem. Phys. Lett.*, 2001, **348**, 81.
- J. González-Vázquez, A. Fernández-Ramos, E. Martínez-Núñez and S. A. Vázquez, *J. Phys. Chem. A*, 2003, **107**, 1389.
- J. González-Vázquez, A. Fernández-Ramos, E. Martínez-Núñez and S. A. Vázquez, *J. Phys. Chem. A*, 2003, **107**, 1398.
- S. A. Vázquez, F. J. Aoi, L. Banares, J. Santamaria, E. Martínez-Núñez and A. Fernández-Ramos, *J. Chem. Phys.*, 2003, **118**, 9641.
- E. M. Núñez, A. Fernández-Ramos, S. A. Vázquez, F. J. Aoi and L. Banares, *J. Phys. Chem. A*, 2003, **107**, 7611.
- J. González-Vázquez, E. Martínez-Núñez, S. A. Vázquez, J. Santamaria and L. Banares, *Chem. Phys. Lett.*, 2004, **396**, 442.
- D. Kröner and L. González, *Phys. Chem. Chem. Phys.*, 2003, **5**, 3933.
- D. Kröner and L. González, *Chem. Phys.*, 2004, **298**, 55.
- Y. Fujimura, L. González, D. Kröner, J. Manz, I. Mehdaoui and B. Schmidt, *Chem. Phys. Lett.*, 2004, **386**, 248.
- M. Schreiber, M. Barbatti, S. Zilberg, H. Lischka and L. González, *J. Phys. Chem. A*, 2007, **111**, 238.
- S. Zilberg, S. Cogan, Y. Haas, O. Deeb and L. González, *Chem. Phys. Lett.*, 2007, **443**, 43.
- D. Kinzel, J. González-Vázquez and L. González, *Int. J. Quant. Chem.*, 2011, **111**, 3394.
- S. Alfalah, D. Kinzel, J. González-Vázquez and L. González, *Chem. Phys.*, 2010, **369**, 138.
- M. Assmann, C. S. Sanz, G. Pérez-Hernández, G. A. Worth and L. González, *Chem. Phys.*, 2010, **377**, 86.
- M. N. R. Ashfold, G. A. King, D. Murdock, M. G. D. Nix, T. A. A. Oliver and A. G. Sage, *Phys. Chem. Chem. Phys.*, 2010, **12**, 1218.
- A. L. Sobolewski, W. Domcke, C. Dedonder-Lardeux and C. Jouvet, *Phys. Chem. Chem. Phys.*, 2002, **4**, 1093.
- M. Zierhut, W. Roth and I. Fischer, *Phys. Chem. Chem. Phys.*, 2004, **6**, 5178.
- H. Ritze, H. Lippert, E. Samoylova, V. R. Smith, I. V. Hertel, W. Radloff and T. Schultz, *J. Chem. Phys.*, 2005, **122**, 224320.
- B. O. Roos, *Adv. Chem. Phys.*, 1987, **69**, 399.
- W. Hehre, L. Radom, P. v. R. Schleyer and J. Pople, *Ab initio Molecular Orbital Theory*, Wiley, New York, 1986.
- H.-J. Werner, P. J. Knowles, R. Lindh, F. R. Manby, M. Schütz, P. Celani, T. Korona, A. Mitrushenkov, G. Rauhut, T. B. Adler, R. D. Amos, A. Bernhardsson, A. Berning, D. L. Cooper, M. J. O. Deegan, A. J. Dobbyn, F. Eckert, E. Goll, C. Hampel, G. Hetzer, T. Hrenar, G. Knizia, C. Köppl, Y. Liu, A. W. Lloyd, R. A. Mata, A. J. May, S. J. McNicholas, W. Meyer, M. E. Mura, A. Nicklass, P. Palmieri, K. Pflüger, R. Pitzer, M. Reiher, U. Schumann, H. Stoll, A. J. Stone, R. Tarroni, T. Thorsteinsson, M. Wang and A. Wolf, *MOLPRO, version 2006.1, a package of ab initio programs*, 2006, see <http://www.molpro.net>.
- J. Finley, P.-A. Malmqvist, B. O. Roos and L. Serrano-Andrés, *Chem. Phys. Lett.*, 1998, **288**, 299.
- B. O. Roos and K. Andersson, *Chem. Phys. Lett.*, 1995, **245**, 215.
- G. Karlström, R. Lindh, P.-A. Malmqvist, B. O. Roos, U. Ryde, V. Veryazov, P.-O. Widmark, M. Cossi, B. Schimmelpennig, P. Neogrady and L. Seijo, *Comput. Mater. Sci.*, 2003, **28**, 222.
- J. C. Tully, *Faraday Discuss.*, 1998, **110**, 407.
- W. C. Swope, *J. Chem. Phys.*, 1982, **76**, 637.
- J. Butcher, *J. Assoc. Comput. Mach.*, 1965, **12**, 124.
- J. C. Tully, *J. Chem. Phys.*, 1990, **93**, 1061.
- S. Hammes-Schiffer and J. C. Tully, *J. Chem. Phys.*, 1994, **101**, 4657.
- J. González-Vázquez and L. González, *Comput. Phys. Commun.*, 2010, **111**, 3617.
- V. Leyva, I. Corral, F. Feixas, A. Migani, L. Blancafort, J. González-Vázquez and L. González, *Phys. Chem. Chem. Phys.*, 2011, **13**, 14685.
- TURBOMOLE V5.1, a development of University of Karlsruhe and Forschungszentrum Karlsruhe GmbH, 1989.
- R. Ahlrichs, M. Bar, M. Haser, H. Horn and C. Kolmel, *Chem. Phys. Lett.*, 1989, **162**, 165.
- M. Barbatti, G. Granucci, M. Persico, M. Ruckebauer, M. Vazdar, M. Eckert-Maksic and H. Lischka, *J. Photochem. Photobiol., A*, 2007, **190**, 228.
- M. Barbatti, G. Granucci, J. P. M. Ruckebauer, M. Persico and H. Lischka, *NEWTON-X: a package for Newtonian dynamics close to the crossing seam*, 2007, www.newtonx.org.
- H. Lischka, R. Shepard, F. B. Brown and I. Shavitt, *Int. J. Quantum Chem., Quantum Chem. Symp.*, 1981, **15**, 91.
- R. Shepard, I. Shavitt, R. M. Pitzer, D. C. Comeau, M. Peppera, H. Lischka, R. A. P. G. Szalay, F. B. Brown and J. Zhao, *Int. J. Quantum Chem., Quantum Chem. Symp.*, 1988, **22**, 149.
- H. L. R. Shepard, R. M. Pitzer, I. Shavitt, M. Dallos, T. Müller, P. G. Szalay, M. Seth, G. S. Kedziora, S. Yabushita and Z. Zhang, *Phys. Chem. Chem. Phys.*, 2001, **3**, 664.
- H. Lischka, R. Shepard, I. Shavitt, R. M. Pitzer, M. Dallos, T. Müller, P. G. Szalay, F. B. Brown, R. Ahlrichs, H. J. Böhm, A. Chang, D. C. Comeau, R. Gdanitz, H. Dachsels, C. Ehrhardt, M. Ernzerhof, P. Höchtl, S. Irle, G. Kedziora, T. Kovar, V. Parasuk, M. J. M. Pepper, P. Scharf, H. Schiffer, M. Schindler, M. Schüler, M. Seth, E. A. Stahlberg, J.-G. Zhao, S. Yabushita, Z. Zhang, M. Barbatti, S. Matsika, M. Schuurmann, D. R. Yarkony, S. R. Brozell, E. V. Beck and J.-P. Blaudeau, *COLUMBUS, an ab initio electronic structure program, release 5.9.1*, 2006.
- L. M. Frutos, T. Andruniów, F. Santoro, N. Ferré and M. Olivucci, *Proc. Natl. Acad. Sci. U. S. A.*, 2007, **104**, 7764.
- A. Gedanken, M. Duraisamy, J. Huang, J. Rachon and H. M. Walborsky, *J. Am. Chem. Soc.*, 1988, **110**, 4593.

4.4 Control of Molecular Hydrogen Abstraction in 4MCF. A One-dimensional study

The previous results from semiclassical simulations in full dimensionality (section 4.3) indicate that the ultrafast H-dissociation is the most important deactivation channel after laser excitation. In following article “*Stark Control of a Chiral Fluoroethylene Derivative*”, it will be shown how the non-resonance dynamic Stark effect [25] (also, recall sections 1 and 3.2.2) can be utilized to prevent the molecule from being destroyed via atomic hydrogen abstraction.

To this aim quantum dynamical calculations including external electric fields have been employed, i.e. solving the TDSE on coupled surfaces in the presence of laser fields (recall section 3.2.2). As discussed in the previous section H-dissociation is so fast that the rest of the molecular framework can be considered frozen, justifying a one-dimensional model. Hence, one-dimensional PESs along the C-H bond axis coordinate have been calculated using CASSCF. The problem at hand became much simpler compared to the AIMD calculations, where a very flexible quantum chemistry is needed to account for the full dimensionality. Here, it is necessary to include the electronic ground state, the bright $\pi\pi^*$ excited state as well as the distinct $\pi\sigma^*_{CH}$ excited state, which plays the major role in the dissociation of hydrogen only. In order to describe these states an active space including four electrons in four orbitals, namely the π_{CC} , the σ_{CH} and their corresponding antibonding ones, is sufficient here. The resulting PESs resemble very nicely the dissociation scheme depicted in figure 8 and shown again for the special case of 4MCF in figure 11a). In addition to the PESs, dipole moments, polarizabilities and NACTs have been calculated at the same level of theory.

During the quantum dynamical simulations presented in the following paper the amount of population that dissociates is represented as the sum of portions of the initial wavefunction that are cut off when it reaches the end of the grid (see equation 12 in the following article reprint). As a first result of the quantum dynamics in the boundaries of the one-dimensional potential grid using a δ -pulse (i.e. at time $t = 0$ a wavepacket starts on the excited states without using laser fields), it is found that 54% dissociation occurs within the first 50 fs of simulation time. This percentage and timescale is in very good agreement with the AIMD calculation (section 4.3) that show 57% H-dissociation within 50 fs. This finding, on the one hand, justifies the 1D model once more, and, on the other hand, confirms that the crossing between the $\pi\pi^*$ and $\pi\sigma^*_{CH}$ state is very efficient and fast.

As discussed above, in order to prevent the population transfer to the repulsive $\pi\sigma^*$ state one needs to find a control scheme, that e.g. traps the initial wavefunction on the bound $\pi\pi^*$ state by reducing the efficiency of the Franck-Condon CoIn or by shifting it to regions that are not or less accessible for the excited wavefunction. The latter idea is picked up

in this study; a Stark effect control scheme using strong non-resonant laser fields can be employed to shift individual states, here the $\pi\pi^*$ state, so that the CoIn is shifted to larger distances (here, strong fields is meant in a sense that the field is strong enough to shift potentials but weak enough so that ionization is not taking place, sometimes also referred to intermediate fields). In figure 11 the Stark effect using a static external field with a field strength F_0 on the diabatic $\pi\pi^*$ state is illustrated.

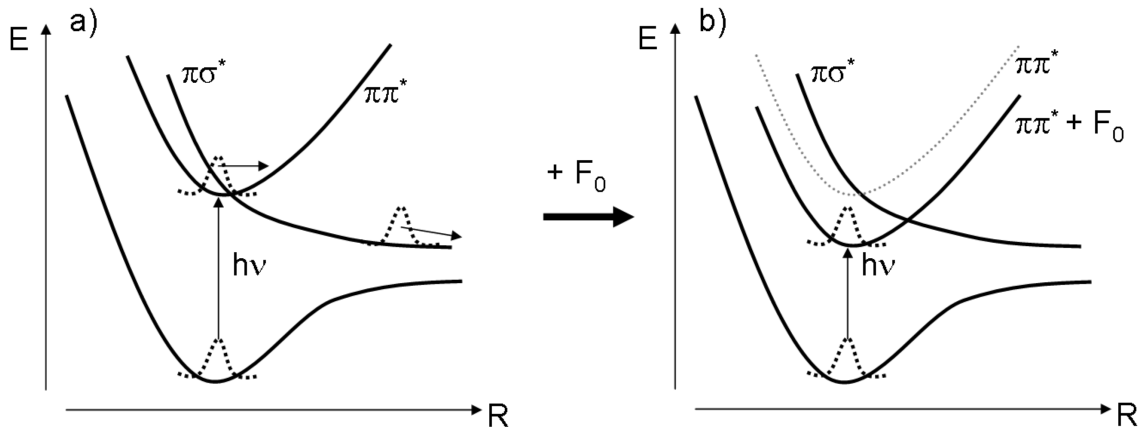


Figure 11: illustration of the Stark effect on the 1D PESs in 4MCF in the diabatic representation: a) field free PESs and b) dressed PESs in the presence of an external electric field with field strength F_0 . The net down shift of the $\pi\pi^*$ state is indicated. The schematic PESs (a and b) resemble the actual calculated ab initio PESs shown in the article. Time evolution of a wavepacket is indicated.

The unperturbed PESs (Figure 11a) show the crossing between the $\pi\pi^*$ and $\pi\sigma^*$ state directly at the Franck-Condon point as found previously in section 4.3, so that excited population can be transferred immediately to the repulsive $\pi\sigma^*$ state leading to almost complete H-dissociation. Including an external field to the potential matrix leads to the shifted or dressed states (Figure 11b), also recall equation 19 in section 3.2.2). Here, the effect of the field is mostly pronounced at the $\pi\pi^*$ state, that shifts to lower energies; the $\pi\sigma^*$ state keeps nearly unchanged due to the lack of dipole coupling. Thus, the crossing between these two states is moved away from the Franck-Condon region to higher C-H bond-distances. While in the unperturbed case the wavefunction can cross to the repulsive $\pi\sigma^*$ state immediately after excitation, in the dressed state picture an effective trapping of the wavefunction can be achieved.

Since the field strength causing the $\pi\pi^*$ state to shift in such a manner is quite high (around 10 GV/m), and because such strong static fields are not accessible experimentally [126], in the following study non-resonant laser fields have been used. Moreover, due to the high field strength it was mandatory to include up to the second term in the dipole field

4.4 Control of Molecular Hydrogen Abstraction in 4MCF. A One-dimensional study 71

interaction, namely the polarizabilities, since the dipole moments alone are not sufficient for a correct description of the dressed states (see equation 19).

The laser fields simulated in the following article are a sum of a non-resonant control laser, which produces the dressed states, and a resonant UV laser, that excites the ground state wavefunction to the excited states. In particular, a control scheme has been considered, where first the control laser interacts with the molecule, and then a UV pulse transfers population to the prepared dressed excited states, here, the bright $\pi\pi^*$ state.

In the following, the field strength, or amplitude, of the control laser, F_0 , is scanned from 1 to 20 GV/m to study the effect of the non-resonant control laser on the amount of population dissociating, i.e. the accumulated flux $I_{\pi\sigma^*}^{acc}$ on the $\pi\sigma^*$ state at the end of the grid. Figure 12 shows the results of this scan. The UV laser, that excites the wavefunction, is adapted for every control field strength to meet the resonance conditions between the ground and resulting dressed state.

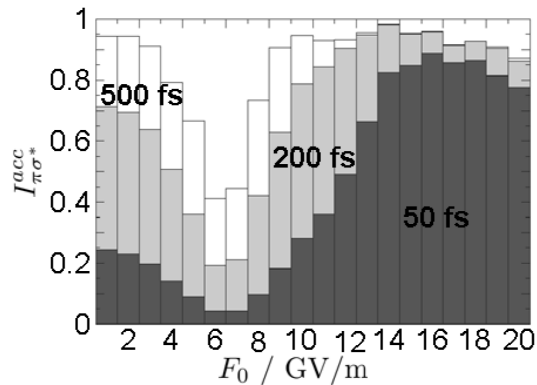


Figure 12: Accumulated flux $I_{\pi\sigma^*}^{acc}$ (amount of H-dissociation) vs. the field amplitude, F_0 , of the control laser at times as indicated.

As the field strength parameter of the control laser increases, the amount of atomic H-dissociation decreases significantly until a control field strength of $F_0 = 7$ GV/m. Hence, the wavepacket is effectively trapped on the dressed $\pi\pi^*$ state, and its lifetime in this state increases. With a field strength of 6 or 7 GV/m almost 95% of the population are still trapped after 50 fs, whereas 54% are already dissociated when the control laser is turned off. Moreover, more than 50% of the population can be preserved in the $\pi\pi^*$ state after 500 fs of simulation time, and thus long enough to, for example, initiate a rotation around the double bond of the molecule, although some portion of the wavepacket can still cross to the dissociative $\pi\sigma^*$ state and a constant loss of population is observed. These results are consistent with the idea that a non-resonant control is the dominant mechanism in the proposed control scheme (Figure 11).

Concluding, the following study could show, that using the Stark effect in 4MCF, the bound state potentials can be distorted such that the potential crossing can be shifted away from the Franck-Condon region in a fashion that the population is mainly trapped in the $\pi\pi^*$ state on time scales long enough to induce the desired torsion, that could drive a potential molecular switch. The non-resonant Stark effect, however, is only effective until an optimal field strength of 8 GV/m, and H-dissociation can be slowed down significantly until that field strength. Other processes, such as resonant transitions, compete with the desired trapping of the wavefunction, when using higher field strengths, and hence H-dissociation is accelerated.

Finally, it can be assumed that the proposed control scheme also works in full dimensionality, i.e. once the excited wavefunction has avoided the undesired Franck-Condon CoIn (at least within 50 fs), the control field can be turned off and other deactivation paths, such as the path through the twisted CoIn, are not affected by the control field anymore.

Next, the original article “*Stark Control of a Chiral Fluoroethylene Derivative*” published in *The Journal of Physical Chemistry A*, Vol. 116, in 2012 is reprinted.

(D. K. contributed to the following study by calculating field-free and field-perturbed one-dimensional PESs along the H-dissociation coordinate in 4MCF, by creating a program code for solving the TDSE on a potential grid in the presence of strong fields, and by setting up, running and analysing the quantum dynamics simulations in the presence of external fields varying several laser parameters.

P. M. and L. G. supervised the research and revised the manuscript.)

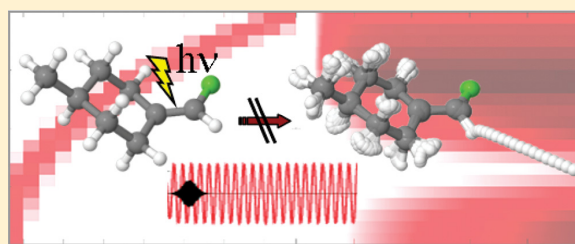
Stark Control of a Chiral Fluoroethylene Derivative

Daniel Kinzel, Philipp Marquetand,^{*,†} and Leticia González[†]

Institute of Physical Chemistry, Friedrich-Schiller-Universität Jena, Helmholtzweg 4, 07743 Jena, Germany

[†]Institute of Theoretical Chemistry, University of Vienna, Währinger Str. 17, 1090 Vienna, Austria

ABSTRACT: Hydrogen dissociation is an unwanted competing pathway if a torsional motion around the C=C double bond in a chiral fluoroethylene derivative, namely (4-methylcyclohexylidene) fluoromethane (4MCF), is to be achieved. We show that the excited state H-dissociation can be drastically diminished on time scales long enough to initiate a torsion around the C=C double bond using the nonresonant dynamic Stark effect. Potential energy curves, dipoles, and polarizabilities for the regarded one-dimensional reaction coordinate are calculated within the CASSCF method. The influence of the excitation and the laser control field is then simulated using wave packet dynamics.



INTRODUCTION

Laser control of chemical reactions has been on the cutting edge of current research for several years, as illustrated in the number of excellent reviews and books in the field, see, for example, refs 1–8. A number of control strategies have been proposed based on the seminal papers of Brumer and Shapiro,^{9–11} Tannor–Kosloff–Rice,^{12,13} and Bergmann.¹⁴ In these papers, control is achieved by manipulating one single parameter, for example, the phase, the time delay or the chirp. In addition to single parameter control, feedback learning algorithms can be used to search the best laser parameters that prepare specific products based on fitness information.¹⁵ Since its first application,¹⁶ this method, also called *close-loop* control, has been used in plenty of cases, see, for example, refs 17–20.

Another control strategy is to make use of the Stark effect²¹ where the molecular potentials are considerably distorted to yield dressed states or light-induced potentials (LIPs).²² With static fields, oriented samples can be prepared, where the eigenstates are called pendar states.²³ Interesting rovibrational dynamics can then be observed after photoexcitation, see, for example, refs 24 and 25. The Stark effect also plays a role in the interaction with oscillating electric fields produced by lasers. If the laser frequency is high enough, the states mainly follow the field envelope. This shift is known as the dynamic Stark effect, which is particularly interesting for quantum control since it works also when the laser is nonresonant.²⁶ Especially the latter case is appealing because no highly specific wavelength sources are required, and this nonresonant dynamic Stark effect (NRDSE) has already been the target of several studies.^{26–35} There, reaction pathways are reversibly changed and, in this way, the NRDSE acts like a photonic catalyst.

A prominent control target is the *cis/trans* photoisomerization of an olefinic double bond because, in this way, chemical properties determined by *E–Z* isomerism can be changed or energy can be transformed into molecular motion.³⁶ The latter

effect is the basis for molecular engineering in nanotechnology, where molecular switches, rotors, and motors are investigated.³⁷

While several studies use simplified models to get insight into the dynamics and control of light driven rotors, see, for example, refs 38–44, we want to point out another aspect that is important in this context: Besides the turning of the rotor, competing processes can play a role but should be avoided. In our case, the turning motion is the rotation (labeled by τ) around the double bond of the chiral fluoroethylene derivative (4-methylcyclohexylidene) fluoromethane (4MCF), see Figure 1. In a series of papers, we have introduced 4MCF as a molecular rotor/switch and investigated different adversary pathways to the desired turning that consist of a switching between the *R/S* enantiomers.^{41,45–49} Interestingly, a recently discovered conical intersection (CI) between a $\pi\pi^*$ and $\pi\sigma^*$ state at the Franck–Condon (FC) geometry allows for different dissociation channels in the electronically excited state.⁴⁸ Our subsequent results from semiclassical simulations in full dimensionality indicate that the ultrafast H-dissociation is the most important reaction channel after laser excitation.⁴⁹ Therefore, in this paper, we will show how Stark control can be employed to prevent the molecule from being destroyed.

COMPUTATIONAL DETAILS

We consider a one-dimensional (1D) model for the dissociation of the hydrogen belonging to the fluoromethane moiety (Figure 1). Surface-hopping trajectories show that the dissociation of this hydrogen proceeds along its bond axis.⁴⁹ H-Dissociation is so fast that the rest of the molecular framework can be considered frozen, justifying the 1D model. The corresponding

Special Issue: Femto10: The Madrid Conference on Femtochemistry

Received: August 18, 2011

Revised: October 14, 2011

Published: November 09, 2011

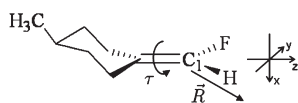


Figure 1. Structural formula of (4-methylcyclohexylidene) fluoromethane; \vec{R} indicates the dissociation vector and τ the torsion around the double bond.

potential energy curves (PECs) are calculated using the state-averaged complete active space self-consistent field method (SA-CASSCF).⁵⁰ The active space employed contains four electrons in four orbitals, namely, the π_{CC} , the σ_{CH} and their corresponding antibonding ones. This active space is sufficient to calculate the three lowest-lying singlet electronic states that correspond to the ground state, the spectroscopic bright $\pi\pi^*$ state, and the $\pi\sigma^*$ state playing a major role in the dissociation process. The basis set used is the double- ζ polarized Pople basis set 6-31G*.⁵¹ This rather small basis set is used intentionally to avoid Rydberg mixing (see ref 52).

When constructing the PECs, the molecule is assumed to be preoriented so that the laboratory z -axis lies within the C=C double bond. The fluorine and hydrogen atom connected to the C_1 of this double bond are then found in the yz -plane. Orientation can be nowadays achieved, for example, by using static fields.^{24,25,53,54} The dissociation coordinate, henceforth labeled R , is defined as the distance between the double bonded carbon C_1 and the attached hydrogen atom, see Figure 1. The rest of the molecular framework is kept frozen at the geometry optimized at the MP2/6-311+G(d,p) level of theory.⁵² A grid of a total of 18 points is calculated along R using the SA3-CASSCF(4,4)/6-31G* protocol as implemented in the MOLPRO program package.⁵⁵ The grid points are equally distributed between $R = 0.6$ and 3.0 Å, with a spacing of 0.2 Å. Additional points were added to describe the crossing around the Franck–Condon point at 1.05 , 1.08 , 1.10 , and 1.15 Å. To ensure a correct asymptotic behavior of the resulting PECs an extra grid point at $R = 50$ Å was added. Furthermore, permanent dipoles μ_{ij} , transition dipole moments between each state μ_{ij} , and polarizabilities α_{ij} have been computed. The polarizabilities have been evaluated numerically according to the MOLPRO manual.⁵⁵ All potentials and corresponding properties were cubic-splined to give 1024 points between $R = 0.6$ and 3.0 Å.

Because at least one CI plays a role during the deactivation process, nonadiabatic coupling terms (NACTs) T_{ij}^R between each state, i and j , with respect to R , defined as

$$T_{ij}^R = \langle \chi_i | \frac{\partial}{\partial R} \chi_j \rangle \quad (1)$$

were calculated at the same level of theory using a three-point formula, as implemented in MOLPRO.⁵⁵

To investigate the dynamics of the dissociation process in 4MCF, we solve the time-dependent Schrödinger equation (TDSE) for the nuclei in each of the three states. In the adiabatic representation, the TDSE for the three-state model is written as

$$i\hbar \frac{\partial}{\partial t} \begin{pmatrix} \psi_0^{\text{ad}}(t) \\ \psi_1^{\text{ad}}(t) \\ \psi_2^{\text{ad}}(t) \end{pmatrix} = \begin{pmatrix} H_{00}^{\text{ad}} & H_{01}^{\text{ad}} & H_{02}^{\text{ad}} \\ H_{10}^{\text{ad}} & H_{11}^{\text{ad}} & H_{12}^{\text{ad}} \\ H_{20}^{\text{ad}} & H_{21}^{\text{ad}} & H_{22}^{\text{ad}} \end{pmatrix} \begin{pmatrix} \psi_0^{\text{ad}}(t) \\ \psi_1^{\text{ad}}(t) \\ \psi_2^{\text{ad}}(t) \end{pmatrix} \quad (2)$$

with approximate matrix elements of the Hamiltonian given as

$$H_{ii}^{\text{ad}} = -\frac{\hbar^2}{2M} \frac{\partial^2}{\partial R^2} + V_i^{\text{ad}} \quad \text{and} \quad H_{ij}^{\text{ad}} = -\frac{\hbar^2}{M} T_{ij}^R \frac{\partial}{\partial R} \quad (3)$$

in which the kinetic couplings are expressed as in eq 1. V_i^{ad} are the electronic adiabatic states computed as described above and M is the reduced mass between the hydrogen atom and the rest of the molecule. The second order kinetic couplings defined as

$$T_{ij}^{\text{RR}} = \langle \chi_i | \frac{\partial^2}{\partial R^2} \chi_j \rangle \quad (4)$$

are neglected because they are much smaller than the first order ones.

Describing kinetic dynamics in the presence of CIs is a difficult task, because the NACTs at these points eventually become singularities. Treating such sudden changes in the character of the wave function numerically is very challenging. To overcome this problem nuclear dynamics is carried out in the diabatic representation. Here, we use a unitary transformation matrix \mathbf{U} to derive the diabatic potentials from the adiabatic ones:

$$\mathbf{V}^{\text{d}} = \mathbf{U}^\dagger \mathbf{V}^{\text{ad}} \mathbf{U} \quad (5)$$

The same applies for the transformation from the adiabatic to the diabatic dipole as well as polarizability matrix, $\mu^{\text{ad/d}}$ and $\alpha^{\text{ad/d}}$, respectively.

The coordinate-dependent transformation matrix $\mathbf{U}(R)$ has been numerically derived by using the Crank–Nicholson-like equation for the transformation matrix propagation, as described in ref 56, which is written as

$$\left(\mathbf{I} + \mathbf{T} \frac{\Delta R}{2} \right) \mathbf{U}(R + \Delta R) = \left(\mathbf{I} - \mathbf{T} \frac{\Delta R}{2} \right) \mathbf{U}(R) \quad (6)$$

where \mathbf{I} is the identity matrix and \mathbf{T} is the matrix containing the nonadiabatic coupling elements T_{ij}^R , see eq 1. Here, the matrix \mathbf{U} is propagated in the spatial coordinate along the 1D potential starting at $R = 3$ Å and evolving until $R = 0.6$ Å. Thus, at $R = 3$ Å, the transformation matrix is set to be the identity matrix, that is, $\mathbf{U}(R = 3 \text{ Å}) = \mathbf{I}$. As in our case \mathbf{U} is propagated backward along R , we set $\Delta R = -\Delta R$.

After transformation, V_i^{d} are then the diabatic potentials for the three states of interest and $V_{ij}^{\text{d}} = V_{ji}^{\text{d}}$ are the potential couplings. Hence, in the diabatic representation, the TDSE is written as

$$i\hbar \frac{\partial}{\partial t} \begin{pmatrix} \psi_0^{\text{d}}(t) \\ \psi_1^{\text{d}}(t) \\ \psi_2^{\text{d}}(t) \end{pmatrix} = \begin{pmatrix} H_{00}^{\text{d}} & H_{01}^{\text{d}} & H_{02}^{\text{d}} \\ H_{10}^{\text{d}} & H_{11}^{\text{d}} & H_{12}^{\text{d}} \\ H_{20}^{\text{d}} & H_{21}^{\text{d}} & H_{22}^{\text{d}} \end{pmatrix} \begin{pmatrix} \psi_0^{\text{d}}(t) \\ \psi_1^{\text{d}}(t) \\ \psi_2^{\text{d}}(t) \end{pmatrix} \quad (7)$$

with

$$H_{ii}^{\text{d}} = -\frac{\hbar^2}{2M} \frac{\partial^2}{\partial R^2} + V_i^{\text{d}} \quad \text{and} \quad H_{ij}^{\text{d}} = V_{ij}^{\text{d}} \quad (8)$$

The elements V_i^{d} and V_{ij}^{d} form the diabatic potential matrix \mathbf{V}^{d} . In the presence of an external electric field $E(t)$, this potential matrix is replaced by a matrix \mathbf{W} whose elements are given by

$$W_{ij} = V_{ij}^{\text{d}} - \mu_{ij}^{\text{d}} E(t) - \alpha_{ij}^{\text{d}} E(t)^2 \quad (9)$$

Diagonalizing the matrix \mathbf{W} results in the so-called dressed states potentials V_i^{dressed} .

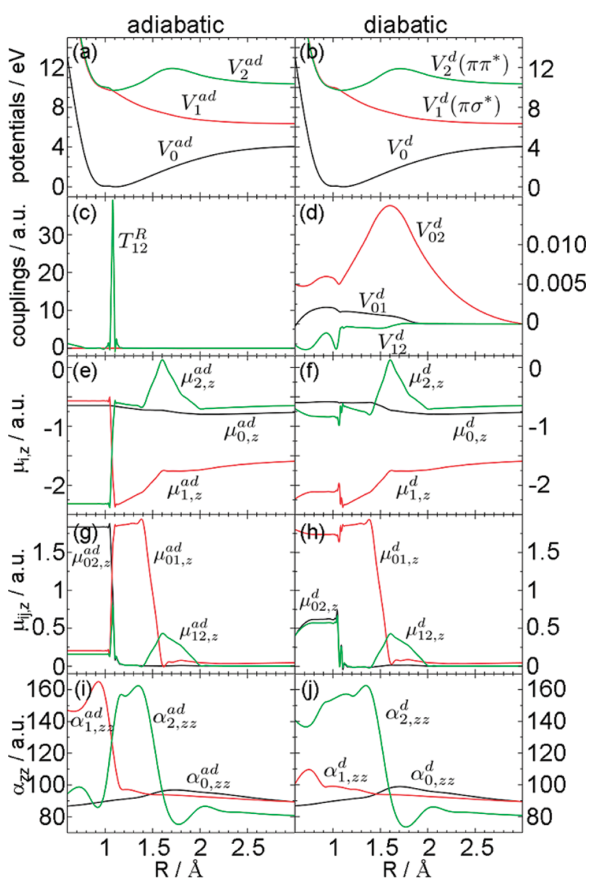


Figure 2. Adiabatic (a) and diabatic (b) potential energy curves, corresponding kinetic (c) and potential (d) couplings, z -polarized adiabatic (e) and diabatic (f) permanent dipole moments, z -polarized adiabatic (g) and diabatic (h) transition dipole moments and zz -polarized adiabatic (i) and diabatic (j) polarizabilities.

In this paper, the total dynamic electric field that affects the molecule is modeled as a sum of a resonant Gaussian-shaped UV pulse and a nonresonant strong field control pulse of approximately rectangular shape,

$$\vec{E}(t) = \vec{\epsilon}^{\text{UV}} E_0^{\text{UV}} G(t) \cos(\omega^{\text{UV}} t) + \vec{\epsilon}^{\text{control}} E_0^{\text{control}} S(t) \cos(\omega^{\text{control}} t) \quad (10)$$

with the polarization vectors $\vec{\epsilon}^{\text{UV/control}}$, the field amplitudes $E_0^{\text{UV/control}}$, the frequencies $\omega^{\text{UV/control}} = (2\pi c)/(\lambda^{\text{UV/control}})$ with c being the speed of light, the Gaussian envelope function $G(t)$, and the analytical shape function $S(t)$ defining the envelope of the control pulse. To mimic a realistic rectangular shape, $S(t)$ is described by a \sin^2 -type function from the beginning of the pulse at t_i until a constant value of $S(t) = 1$ is attained at time t_{c1} . The pulse is switched off in the same fashion from time t_{c2} until the end of the pulse t_f . In the case of a static external field, eq 10 reduces to $\vec{E}(t) = \vec{\epsilon} E_0$.

The diabatic TDSE including the field interaction, eqs 7 and 9, is solved with the help of the split-operator method^{57–60} with a time discretization of $\Delta t = 0.01$ fs.

The system is initially prepared in the vibrational ground state of V_0^{ad} computed with the Fourier–Grid–Hamiltonian method

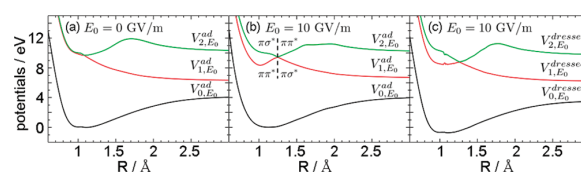


Figure 3. (a) Unperturbed adiabatic PECs; (b) perturbed PECs obtained by adding the field interaction in the electronic Hamiltonian; (c) dressed PECs obtained by diagonalizing $V_{ij}^d - \mu_{ij,z}^d E_0 - \alpha_{ij,zz}^d E_0^2$. The change of the electronic character in the adiabatic states is exemplarily indicated in (b).

(FGH).⁶¹ To prevent artificial reflections of the wave packet from the grid boundary, a cutoff function, $\gamma(R)$, is introduced, which annihilates parts of the outgoing wave function ψ_i in each state at the end of the grid. This function is defined as

$$\gamma(R) = \begin{cases} \cos^2 \left[\frac{\pi}{2} \frac{R_{\text{end}} - R_\gamma - R}{R_\gamma} \right] & \text{if } R > R_{\text{end}} - R_\gamma \\ 1 & \text{otherwise} \end{cases} \quad (11)$$

with $R_{\text{end}} = 3$ Å being the end of the grid and the cutoff parameter R_γ , which we set to 0.5 Å, meaning that the cutoff function starts at $R = 2.5$ Å. At this distance, the C–H bond can be considered broken. Furthermore, we have ensured that the asymptotic behavior of the states involved is correct also for much larger distances (see above).

On the basis of this cutoff function, we define the accumulated flux for each state, $I_i^{\text{acc}}(t)$, as the part of the wave function that has been cut off after the previous time step

$$I_i^{\text{acc}}(t) = \sum_t |\psi_i(t - \Delta t)|^2 - |\psi_i(t)|^2 \quad (12)$$

RESULTS AND DISCUSSION

Field Free Potential Energy Curves. In Figure 2 we present the adiabatic and diabatic potential energy curves (PECs), V_i^{ad} and V_i^d , their corresponding kinetic and potential couplings, T_{ij} and V_{ij}^d , respectively, the adiabatic and diabatic z -polarized permanent and transition dipole moments $\mu_i^{\text{ad/d}}$ and $\mu_{ij}^{\text{ad/d}}$, and the adiabatic and diabatic zz -polarized polarizabilities, $\alpha_i^{\text{ad/d}}$.

The adiabatic potential (Figure 2a) shows a near-degeneracy point between states V_1^{ad} and V_2^{ad} at the Franck–Condon distance of $R = 1.08$ Å. At that point, the nonadiabatic coupling term T_{12}^R amounts to 39.2 a.u., indicating a strong coupling between these states. Furthermore, the character of the electronic wave function of V_1^{ad} switches from $\pi\pi^*$ to $\pi\sigma^*$ and vice versa of that of V_2^{ad} . This switch is also evident in the adiabatic permanent and transition dipole moments, μ_1^{ad} , μ_2^{ad} and μ_{01}^{ad} , μ_{02}^{ad} , respectively, as well as in adiabatic polarizabilities, α_1^{ad} and α_2^{ad} (Figure 2e, g, and i, respectively), which switch their values at the point of degeneracy. These results agree with the fact that the FC geometry is actually a point on the multidimensional seam of CIs between the states V_1^{ad} and V_2^{ad} , as stated in ref 48.

Dressed States in the Presence of an External Field. To prevent H-dissociation, we want to employ the NRDSE to trap the wave packet in the $\pi\pi^*$ state. Because the double bond of the molecule lies in the z -axis, all fields and field interactions are assumed to be z -polarized in the following. As a first attempt to

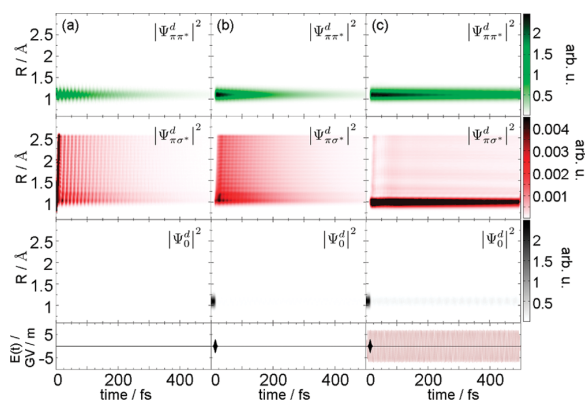


Figure 4. Time evolution of the wave packet in the diabatic representation, $|\Psi_i^d(t)|^2$, in each diabatic state shown for three representative cases: (a) δ -pulse only, (b) UV pulse only, and (c) UV + control-pulse.

study the effect of a strong field on the PECs, a static electric field with a field strength of $E_0 = 10$ GV/m is added to the electronic Hamiltonian as implemented in the MOLPRO program package.⁵⁵ Each point of the PECs is recalculated and the resulting new potentials are shown in Figure 3b. Compared to the unperturbed potentials (Figure 3a), the crossing point has been shifted to longer C–H distances (1.25 Å). This leaves the opportunity to trap a wave packet at smaller distances on the first excited state potential V_{1,E_0}^{ad} after excitation from the ground state. Note that the electronic character in this region is $\pi\pi^*$ (as exemplarily indicated in Figure 3b), and therefore, the majority of the overall population will be excited to this bright state. Static fields at such high field strengths are not accessible experimentally.²⁵ Usually, the dielectric already breaks down at field strengths on the order of 10 MV/m under normal gas-phase experimental conditions. Hence, the only way to achieve the required field strength in a potential experiment is to use laser fields. The approach described above, where the field was included in the electronic Hamiltonian, is computationally too expensive in a dynamical simulation because the field strength entering in the calculations is time dependent, and as such, it is necessary to recalculate the complete PECs in every time step. To circumvent this problem, the field-free potentials are usually changed a posteriori by adding the dipole interaction (first two terms in eq 9). It has to be noted that one uses a Taylor expansion to describe the change of the potential energies with respect to the field strength⁶² and that higher terms like the polarizability may be needed to describe the effects of strong fields. Often, it is difficult to obtain good values for the polarizabilities because tiny errors in the calculation of the energy have a dramatic effect on this second-order property. Particularly at CIs, problems can arise. As we treat the laser interaction according to eq 9, we check for the quality of our curves as follows. We diagonalize the matrix \mathbf{W} for a field of $E_0 = 10$ GV/m and compare the obtained dressed potentials (Figure 3c) to the ones calculated by incorporating the interaction directly into the electronic Hamiltonian (Figure 3b). As we see, the qualitative picture of the dressed states resembles very nicely the field perturbed PECs calculated with MOLPRO. We note that it is mandatory to include terms at least up to the second term of the Taylor expansion in the electric field interaction (the polarizability), because the dipole interaction alone is not sufficient for the regarded field strength.

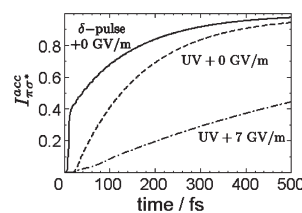


Figure 5. Accumulated wave function flux vs time in the diabatic $\pi\sigma^*$ state for case (a) δ -pulse only, (b) UV pulse only, and (c) UV + control-pulse.

Quantum Dynamics in the Presence of an External Dynamic Field. We now turn to describe the quantum dynamics influenced by a control laser. As discussed above, our goal is to prevent H-dissociation and therefore trap the molecule in a dressed state. We consider a control scheme where first the control laser interacts with the molecule, and then a UV pulse transfers population to the prepared dressed excited states. To understand the underlying processes, the time-dependent probability densities $|\Psi_i^d(t)|^2$ are plotted for three scenarios in Figure 4. There, we use the diabatic representation, first, because it is the natural outcome of our simulation (eq 7), and second, because due to the nonadiabatic coupling the major part of the dynamics takes place in the diabatic states. Note the different scales for the density amplitudes in Figure 4. The three cases are the following:

Case (a). Only a δ -pulse is used to excite population to the adiabatic state potential V_2^{ad} exclusively and no control field is present (Figure 4a). This scenario also serves to compare with previous semiclassical simulations,⁴⁹ therefore, validating our 1D model.

Case (b). No control field is yet present, but a UV pulse of finite duration is employed to transfer population to all the considered excited states. The employed pulse has a Gaussian shape centered at $t = 14$ fs with a full width half maximum (fwhm) of 7 fs, wavelength $\lambda^{UV} = 128$ nm and a field strength $E_0^{UV} = 3$ GV/m. While the choice of these parameters is rather arbitrary, it ensures that all of the population initially located in the ground state is excited so fast that interferences between the pump and the control laser are minimized.

Case (c). A control laser with a wavelength of $\lambda^{control} = 1200$ nm is switched on from $t_i = 0$ fs to $t_{c1} = 7$ fs in a sinusoidal fashion and then stays at a constant field strength $E_0^{control} = 7$ GV/m (Figure 4c). The parameters for the UV pulse are the same as in case (b) except that the wavelength has been changed to $\lambda^{UV} = 132$ nm to accommodate the potential energy shift induced by the control field.

The corresponding time-accumulated wave function flux in the diabatic $\pi\sigma^*$ state for each cases (a), (b), and (c) according to eq 12 is shown in Figure 5. This flux then corresponds to the population that dissociated in this state.

In case (a), the vibrational ground-state wave function is excited to the adiabatic potential V_2^{ad} using a δ -pulse. In the diabatic representation, this is equivalent to approximately 35% population in the spectroscopically dark $\pi\sigma^*$ state at time $t = 0$ fs. A δ -pulse excitation to an adiabatic state is typically employed in semiclassical simulations and the excited-state wave packet here matches the initial conditions for the trajectories run in ref 49. As expected from its repulsive character, the population in the diabatic $\pi\sigma^*$ state dissociates very fast within the first 10 fs

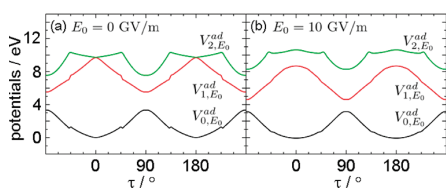


Figure 6. (a) Field-free adiabatic PECs along the torsional coordinate, τ and (b) perturbed PECs obtained by adding the field interaction in the electronic Hamiltonian.

(Figure 4a) The rest of the wave function, initially located on the diabatic bright $\pi\pi^*$ state, is oscillating in R due to the displaced potential minimum with respect to the FC geometry. During every oscillation, the $\pi\pi^*/\pi\sigma^*$ crossing is accessed and a further portion of the wave function is transferred nonadiabatically to the $\pi\sigma^*$ state leading to rapid dissociation. Within the first 50 fs 54% of the initial population is dissociated through the $\pi\sigma^*$ state, in agreement to the trajectory simulations, which showed that 57% of the trajectories undergo atomic hydrogen dissociation within 50 fs.⁴⁹ In the present quantum dynamical simulation, about 90% of the molecules dissociate after 200 fs and after 500 fs almost the complete population has dissociated. From Figure 5 we can also infer time constants \mathcal{T} for the build-up of the dissociated products. We fit the corresponding curves according to $1 - e^{-(t-t_0)/\mathcal{T}}$, where t_0 is the offset from $t = 0$. For the process induced by the δ -pulse, we obtain a biexponential build-up with a fast and a slow component. The corresponding time constants are $\mathcal{T}_{\delta\text{-pulse}}^{\text{fast}} = 9.36 \pm 1.98$ fs with an offset $t_0 = 2.20 \pm 0.82$ fs and $\mathcal{T}_{\delta\text{-pulse}}^{\text{slow}} = 145.25 \pm 0.25$ fs with an offset $t_0 = -62.75 \pm 0.29$ fs.

When a resonant UV pulse (case (b)) is used, 95% of the population in the ground state is excited to the bright $\pi\pi^*$ state. Although less population is initially found in the $\pi\sigma^*$ state compared to case (a), the dissociation proceeds on a similar time scale and to a similar extent. Accordingly, the corresponding time constant is $\mathcal{T}_{\text{UV}} = 159.64 \pm 0.49$ fs with an offset $t_0 = 15.61 \pm 0.30$ fs, which very well agrees with $\mathcal{T}_{\delta\text{-pulse}}^{\text{slow}}$. As the degeneracy is located very close to the FC point, population is almost constantly transferred to the $\pi\sigma^*$ state, which directly leads to dissociation. This process is effective even if the wave packet is not moving considerably. After 50 fs 25%, after 200 fs 70%, and at the end of the propagation time all of the excited population has dissociated.

In case (c), the control laser with a field strength $E_0^{\text{control}} = 7$ GV/m is turned on and as a result the potentials are strongly shifted. A net Stark shift of -0.3 eV is observed between the ground state and the bright excited state compared to the unperturbed case. Hence, the UV pulse needs to have a wavelength of $\lambda^{\text{UV}} = 132$ nm, instead of 128 nm, as in the UV-only case, to match the resonance condition. In the presence of the control field, the wave packet excited to the bright $\pi\pi^*$ state, is indeed trapped for much longer times than in cases (a) and (b). At the end of the propagation time, only 45% of the total population has dissociated. From the build-up of dissociated products (Figure 5), a time constant can be deduced. The obtained value of $\mathcal{T}_{\text{UV+control}} = 811.33 \pm 1.19$ fs with an offset of $t_0 = 21.92 \pm 0.33$ fs is much higher than the previous derived constants. The crossing is shifted to larger distances and the distorted potentials favor the desired trapping. Despite some portion of the wave packet can still cross to the dissociative $\pi\sigma^*$ state and a constant loss of population is observed, more than

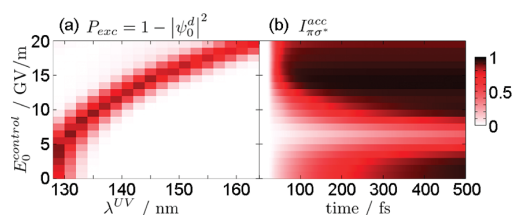


Figure 7. (a) Excited population ($P_{\text{exc}} = 1 - |\Psi_0^{\text{d}}|^2$ at $t = 50$ fs) vs E_0^{control} and λ^{UV} . (b) Accumulated flux in the $\pi\sigma^*$ state vs E_0^{control} and time at $\lambda^{\text{UV,max}}$, where P_{exc} is maximum.

50% of the population can be preserved in the $\pi\pi^*$ state during times long enough to, for example, initiate a rotation around the double bond of the molecule.

To demonstrate that torsion can take place in the Stark shift field, we have computed unrelaxed one-dimensional torsional PECs at the SA3-CASSCF(4,4)/6-31G(d) level of theory, along τ (see Figure 1), both field-free and in the presence of an external field of 10 GV/m. The latter calculation has been done by adding the field interaction directly to the electronic Hamiltonian, as implemented in MOLPRO. The resulting potentials, analogues to the dissociative ones of Figure 3a and b, are shown in Figure 6a and b. The potentials are calculated from -90 to 0° every 5° and then mirrored at 0 and 90° , according to symmetry. A total of 1025 grid points is obtained by cubic splines.

As it can be seen, the field shifts the spectroscopic $\pi\pi^*$ state to lower energies at the Franck–Condon geometry ($\tau = 0$ and 180°), but the overall shape, that is, the energy difference between the maxima and the minima of this state and, thus, its energy gradients, is very similar to the unperturbed potential. Accordingly, the time scales involved in the torsional movement should not change dramatically. The torsional half cycle to go from one enantiomer to the other in the field-free potential is about 150 fs.⁴⁷ An equivalent wave packet simulation in the perturbed adiabatic potentials using a δ -pulse excited at $\tau = 0^\circ$ results in about 140 fs. This simulation also shows that within the first 50 fs the whole wave packet has left the Franck–Condon region.

Fitness Landscapes of Reduced Dimensionality. As we have seen above, introducing a nonresonant strong laser field with a strength of 7 GV/m in the quantum dynamics simulations increases the lifetime of the wave packet in the spectroscopic $\pi\pi^*$ state significantly. To check the influence of the control field strength E_0^{control} , a two-dimensional pulse parameter scan is carried out. The first dimension is the field strength of the control laser scanned from 0 to 20 GV/m using a step size of 1 GV/m. Since the overall Stark effect results in shifted dressed states, where the bright $\pi\pi^*$ state is shifted more extensively than the others, the wavelength of the resonant UV pulse needs to be adjusted in each case. Thus, the second dimension of the scan is λ^{UV} , which is varied from 128 to 164 nm with a step size of 2 nm. All other parameters of the two laser pulses are kept as described above (see “case (c)”).

The result can be visualized in a fitness landscape of reduced dimensionality,^{63–65} where we map the amount of excited-state population $P_{\text{exc}} = 1 - |\Psi_0^{\text{d}}|^2$ after 50 fs (i.e., the UV pulse is over) as a function of the wavelength of the UV pulse λ^{UV} and the field strength of the control laser E_0^{control} , see Figure 7a. We observe an overall shift of the excitation energy of -2.1 eV when going from 0 to 20 GV/m, indicating a strong Stark shift of the spectroscopic $\pi\pi^*$ state.

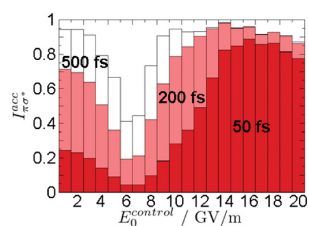


Figure 8. Accumulated flux $I_{\pi\sigma^*}^{acc}$ vs $E_0^{control}$ at times as indicated. The wavelength for the excitation laser is adjusted for each field strength of the control laser according to Figure 7a.

With the information about the required excitation wavelength at hand, we now take a look at the amount of population that dissociates at each particular field strength, that is, the time-accumulated flux in the $\pi\sigma^*$ state versus the strength of the control laser field. Here, we consider only those cases in which the UV laser is in resonance with the dressed $\pi\pi^*$ state. In Figure 7b, the time evolution of the accumulated flux (or dissociated population) is shown depending on the strength of the control laser, $E_0^{control}$.

As the field strength parameter of the control laser increases, the amount of atomic H-dissociation decreases significantly until a field strength of $E_0^{control} = 7$ GV/m. Hence, the wave packet is effectively trapped on the dressed $\pi\pi^*$ state, and its lifetime in this state increases. With a field strength between 6 and 7 GV/m almost 95% of the population are still trapped after 50 fs, whereas 54% are already dissociated when the control laser is turned off. These results are consistent with the idea that the nonresonant control is the dominant mechanism.

Interestingly, we also observe that the dissociation process can also be accelerated if the field strength of the control laser is increased above 7 GV/m. For an easier analysis, cuts through the landscape given in Figure 7b are plotted as a bar chart in Figure 8 at times $t = 50, 200,$ and 500 fs. There, it becomes obvious that at field strengths larger than 14 GV/m the dissociation process is almost completed after the first 50 fs. One explanation for this behavior could be a resonant transition from the $\pi\pi^*$ to the $\pi\sigma^*$ state induced by the control laser. Even if the NRDSE considers a nonresonant field, the resonance condition will almost always be met at some point along the potential energy surfaces.^{66,67} Additionally, the transition dipole moment between the S_1 and S_2 states, μ_{12} (Figure 2g,h) is nonzero around the FC geometry; this, combined with a possibly resonant control laser, could transfer population between these states. Another reason can be inferred from the Landau–Zener theory, which claims that more population is transferred if the momentum of the wave packet at a crossing point is higher. At high field strengths, we are in the impulsive regime where the wave packet experiences a kick due to the shifting potentials, gains a high momentum, and is then more efficiently transferred to the dissociative $\pi\sigma^*$ state.

CONCLUSION

In this paper we have performed quantum dynamical wavepacket propagations in the presence of external fields for (4-methylcyclohexylidene) fluoromethane (4MCF). The potentials, dipole moments, and polarizabilities were computed at the CASSCF level of theory. Polarizabilities are important for the correct modeling of strong laser field interactions.

We have shown that laser control of 4MCF is possible by means of the nonresonant dynamic Stark effect. 4MCF possesses two enantiomers connected by the rotation around the double bond. In previous studies^{41,45–49} we have demonstrated that after excitation several competing pathways to the torsion exist, among which H-dissociation is the most important one.⁴⁹ If the molecule is electronically excited to its first bright $\pi\pi^*$ state, where a rotation around the double bond is enabled, a conical intersection (CI) with a dark $\pi\sigma^*$ state opens up the competitive dissociation channel. Using Stark control, the potentials can be distorted and the potential crossing can be shifted away from the Franck–Condon (FC) region in a fashion that the population is mainly trapped in the $\pi\pi^*$ state on time scales long enough to induce the desired torsion. As a next step, we intend to incorporate also the torsional coordinate in our simulations to devise an efficient laser-induced *cis/trans* isomerization of 4MCF.

AUTHOR INFORMATION

Corresponding Author

*E-mail: philipp.marquetand@univie.ac.at

ACKNOWLEDGMENT

This work has been supported by the Deutsche Forschungsgemeinschaft (DFG) in the frame of a trilateral cooperation between Israel, Palestine, and Germany under the project GO 1059/7-3 and the Friedrich-Schiller-Universität Jena. The authors thank Monika Leibscher and Jesús González-Vázquez for interesting discussions. Generous allocation of computer time at the Computer Center of the Friedrich-Schiller-Universität is gratefully acknowledged.

REFERENCES

- (1) Gordon, R. J.; Rice, S. A. *Annu. Rev. Phys. Chem.* **1997**, *48*, 601–641.
- (2) Rice, S. A. *Adv. Chem. Phys.* **1997**, *101*, 213–283.
- (3) Rice, S. A.; Zhao, M. *Optical Control of Molecular Dynamics*; Wiley: New York, 2000.
- (4) Dantus, M. *Annu. Rev. Phys. Chem.* **2001**, *52*, 639–679.
- (5) Shapiro, M.; Brumer, P. *Principles of Quantum Control of Molecular Processes*; Wiley: New York, 2003.
- (6) Hertel, I. V.; Radloff, W. *Rep. Prog. Phys.* **2006**, *69*, 1897–2003.
- (7) Nuernberger, P.; Vogt, G.; Brixner, T.; Gerber, G. *Phys. Chem. Chem. Phys.* **2007**, *9*, 2470–2497.
- (8) Worth, G. A.; Sanz-Sanz, C. *Phys. Chem. Chem. Phys.* **2010**, *12*, 15570–15579.
- (9) Brumer, P.; Shapiro, M. *Chem. Phys. Lett.* **1986**, *126*, 541–546.
- (10) Brumer, P.; Shapiro, M. *Annu. Rev. Phys. Chem.* **1992**, *43*, 257–282.
- (11) Shapiro, M.; Brumer, P. *Rep. Prog. Phys.* **2003**, *66*, 859–942.
- (12) Tannor, D. J.; Rice, S. A. *J. Chem. Phys.* **1985**, *83*, 5013–5018.
- (13) Tannor, D. J.; Kosloff, R.; Rice, S. A. *J. Chem. Phys.* **1986**, *85*, 5805–5820.
- (14) Bergmann, K.; Theuer, H.; Shore, B. W. *Rev. Mod. Phys.* **1998**, *70*, 1003–1025.
- (15) Judson, R. S.; Rabitz, H. *Phys. Rev. Lett.* **1992**, *68*, 1500–1503.
- (16) Assion, A.; Baumert, T.; Bergt, M.; Brixner, T.; Seyfried, V.; Strehle, M.; Gerber, G. *Science* **1998**, *282*, 919–922.
- (17) Glass, A.; Rozgonyi, T.; Sauerbrey, T. F. R.; Szabó, G. *Appl. Phys. B: Laser Opt.* **2000**, *71*, 267–276.
- (18) Brixner, T.; Gerber, G. *Chem. Phys. Chem.* **2003**, *4*, 418–438.
- (19) Daniel, C.; Full, J.; González, L.; Lupulescu, C.; Manz, J.; Merli, A.; Štefan Vajda; Wöste, L. *Science* **2003**, *299*, 536–539.

4.4 Control of Molecular Hydrogen Abstraction in 4MCF. A One-dimensional study⁷⁹

- (20) Brixner, T.; Damrauer, N. H.; Gerber, G. *Adv. Atmos. Mol. Opt. Phys.* **2001**, *46*, 1–54.
- (21) Stark, J. *Nature* **1913**, *92*, 401.
- (22) Garraway, B. M.; Suominen, K. *Phys. Rev. Lett.* **1998**, *80*, 932–935.
- (23) Stapelfeldt, H.; Seideman, T. *Rev. Mod. Phys.* **2003**, *75*, 543–557.
- (24) Marquetand, P.; Materny, A.; Henriksen, N. E.; Engel, V. *J. Chem. Phys.* **2004**, *120*, 5871–5874.
- (25) Marquetand, P.; Engel, V. *Phys. Chem. Chem. Phys.* **2005**, *7*, 469–474.
- (26) Sussman, B. J.; Townsend, D.; Ivanov, M. Y.; Stolow, A. *Science* **2006**, *314*, 278–281.
- (27) Levis, R. J.; Menkir, G. M.; Rabitz, H. *Science* **2001**, *292*, 709–713.
- (28) González-Vázquez, J.; Sola, I. R.; Santamaria, J.; Malinovsky, V. S. *Chem. Phys. Lett.* **2006**, *431*, 231–235.
- (29) González-Vázquez, J.; Sola, I. R.; Santamaria, J. *J. Phys. Chem. A* **2006**, *110*, 1586–1593.
- (30) Chang, B. Y.; Choi, H.; Shin, S.; Lee, S.; Sola, I. R. *J. Mod. Opt.* **2009**, *56*, 811–821.
- (31) Chang, B. Y.; Shin, S.; Sola, I. R. *J. Chem. Phys.* **2009**, *131*, 204314.
- (32) González-Vázquez, J.; González, L.; Sola, I. R.; Santamaria, J. *J. Chem. Phys.* **2009**, *131*, 104302–104305.
- (33) González-Vázquez, J.; González, L.; Nichols, S. R.; Weinacht, T. C.; Rozgonyi, T. *Phys. Chem. Chem. Phys.* **2010**, *14*, 14203–14216.
- (34) Sussman, B. J. *Am. J. Phys.* **2011**, *79*, 477–484.
- (35) Townsend, D.; Sussman, B. J.; Stolow, A. *J. Phys. Chem. A* **2011**, *115*, 357–373.
- (36) Levine, B. G.; Martínez, T. J. *Annu. Rev. Phys. Chem.* **2007**, *58*, 613–634.
- (37) Balzani, V.; Credi, A.; Venturi, M. *Chem. Soc. Rev.* **2009**, *38*, 1542–1550.
- (38) Hoki, K.; Yamaki, M.; Fujimura, Y. *Angew. Chem., Int. Ed.* **2003**, *42*, 2976–2978.
- (39) Hoki, K.; Sato, M.; Yamaki, M.; Sahnoun, R.; Gonzalez, L.; Koseki, S.; Fujimura, Y. *J. Phys. Chem. B* **2004**, *108*, 4916–4921.
- (40) Hoki, K.; González, L.; Shibl, M. F.; Fujimura, Y. *J. Phys. Chem. A* **2004**, *108*, 6455–6463.
- (41) Fujimura, Y.; González, L.; Kröner, D.; Manz, J.; Mehdaoui, L.; Schmidt, B. *Chem. Phys. Lett.* **2004**, *386*, 248–253.
- (42) Marquetand, P.; Gräfe, S.; Scheidel, D.; Engel, V. *J. Chem. Phys.* **2006**, *124*, 054325.
- (43) Yamaki, M.; Nakayama, S.-i.; Hoki, K.; Kono, H.; Fujimura, Y. *Phys. Chem. Chem. Phys.* **2009**, *11*, 1662–1678.
- (44) Pérez-Hernández, G.; Pelzer, A.; González, L.; Seideman, T. *New J. Phys.* **2010**, *12*, 075007.
- (45) Kröner, D.; González, L. *Phys. Chem. Chem. Phys.* **2003**, *5*, 3933–3942.
- (46) Kröner, D.; González, L. *Chem. Phys.* **2004**, *298*, 55–63.
- (47) Alfalah, S.; Kinzel, D.; González-Vázquez, J.; González, L. *Chem. Phys.* **2010**, *369*, 138–144.
- (48) Kinzel, D.; González-Vázquez, J.; González, L. *Int. J. Quantum Chem.* **2011**, *111*, 3394–3404.
- (49) Kinzel, D.; González-Vázquez, J.; González, L. *Phys. Chem. Chem. Phys.* **2011**, DOI:10.1039/c1cp22646k.
- (50) Roos, B. O. *Adv. Chem. Phys.* **1987**, *69*, 399–445.
- (51) Hehre, W.; Radom, L.; v. R. Schleyer, P.; Pople, J. *Ab Initio Molecular Orbital Theory*; Wiley: New York, 1986.
- (52) Schreiber, M.; Barbatti, M.; Zilberg, S.; Lischka, H.; González, L. *J. Phys. Chem. A* **2007**, *111*, 238–243.
- (53) Holmegaard, L.; Nielsen, J. H.; Nevo, I.; Stapelfeldt, H.; Filsinger, F.; Kúpper, J.; Meijer, G. *Phys. Rev. Lett.* **2009**, *102*, 023001.
- (54) Nevo, I.; Holmegaard, L.; Nielsen, J. H.; Hansen, J. L.; Stapelfeldt, H.; Filsinger, F.; Meijer, G.; Kúpper, J. *Phys. Chem. Chem. Phys.* **2009**, *11*, 9912–9918.
- (55) Werner, H.-J.; Knowles, P. J.; Lindh, R.; Manby, F. R.; Schütz, M.; Celani, P.; Korona, T.; Mitrushenkov, A.; Rauhut, G.; Adler, T. B.; Amos, R. D.; Bernhardsson, A.; Berning, A.; Cooper, D. L.; Deegan, M. J. O. et al. *MOLPRO*, version 2006.1, a package of ab initio programs; 2006; see <http://www.molpro.net>.
- (56) Esry, B. D.; Sadeghpour, H. R. *Phys. Rev. A* **2003**, *68*, 042706.
- (57) Feit, M. D.; Fleck, J. A., Jr.; Steiger, A. *J. Comput. Phys.* **1982**, *47*, 412–433.
- (58) Feit, M. D.; Fleck, J. A., Jr. *J. Chem. Phys.* **1983**, *78*, 301–308.
- (59) Feit, M. D.; Fleck, J. A., Jr. *J. Chem. Phys.* **1984**, *80*, 2578–2584.
- (60) Kosloff, R. *Annu. Rev. Phys. Chem.* **1994**, *45*, 145–178.
- (61) Martson, C. C.; Balint-Kurti, G. G. *J. Chem. Phys.* **1989**, *91*, 3571–3576.
- (62) Atkins, P. W.; Friedman, R. S. *Molecular Quantum Mechanics*; Oxford University Press: Oxford, 2003.
- (63) Chakrabarti, R.; Rabitz, H. *Int. Rev. Phys. Chem.* **2007**, *26*, 671–735.
- (64) Marquetand, P.; Nuernberger, P.; Vogt, G.; Brixner, T.; Engel, V. *Europhys. Lett.* **2007**, *80*, S3001.
- (65) Marquetand, P.; Nuernberger, P.; Brixner, T.; Engel, V. *J. Chem. Phys.* **2008**, *129*, 074303.
- (66) Marquetand, P.; Richter, M.; González-Vázquez, J.; Sola, I.; González, L. *Faraday Discuss.* **2011**, *153*, 261–273.
- (67) Sanz-Sanz, C.; Richings, G. W.; Worth, G. A. *Faraday Discuss.* **2011**, *153*, 275–291.

5 Summary

The present thesis is a theoretical work carried out in the frame of a trilateral research project in cooperation with work groups at Al-Quds university, Palestine, at the Hebrew-University in Israel, and at the Freie Universität Berlin as well as at the Friedrich-Schiller-Universität Jena, Germany. It focuses on a model for a light-triggered molecular rotor or switch based on a fluoroethylene derivative. In particular, (4-methylcyclohexylidene) fluoromethane (4MCF) has been subject of investigation, since it possesses an axial chirality, and thus, its R and S enantiomers can be converted into each other by a torsion around the central carbon-carbon double bond (see Figure 4 in section 1). Moreover, due to the necessity of breaking a double bond, the two isomers are distinct, i.e. at room temperature no racemization occurs, and, although chemically equal, it could be shown, that the R and S enantiomers of 4MCF can be selectively excited, and thus identified, by the use of cleverly chosen laser pulses [77, 78, 83]. Hence, 4MCF has been suggested as a simple model, but also as a functioning example, for a light-induced molecular rotor or switch.

Towards understanding the function of 4MCF, the thesis' author has been trained in electronic structure calculations, reaction dynamics, and laser control strategies. Ground and excited state properties and quantum as well as molecular dynamics have been the subject of investigation yielding a mechanistic insight into 4MCF's photochemistry in gas phase. To this aim, commercial quantum chemical and self-written dynamical codes have been utilized.

As it is the case in all olefinic compounds, the torsion around the C-C double bond in 4MCF is induced by promoting an electron from the C-C π orbital into the corresponding antibonding π^* molecular orbital using a UV light source. Once excited, ultrafast decay is possible through several conical intersections (CoIns) between the $\pi\pi^*$ or V excited state and the electronic ground or N state surfaces, which are connected with the *cis-trans* isomerization. Such a CoIn, for example, is responsible for the ultrafast eye vision process in the animal visual cycle. In 4MCF several CoIns between the V and N states have been found, namely twisted, pyramidalized, hydrogen migration and hydrogen fluoride elimination CoIns (see Figure 6 in section 2). All of these CoIns are connected to a preliminary torsion about the C-C double bond. However, the latter two also connect coordinates that prevent 4MCF to be an efficient switch or rotor. Especially the elimination pathway is on the focus of this thesis. In order to achieve a controlled *cis-trans* isomerization in 4MCF any other competing path upon excitation to the bright $\pi\pi^*$ state, that could lead to a destroyed molecule, needs to be suppressed. Hence, different models for the relaxation of 4MCF after irradiation have been investigated in the present work in order to reveal the competition of isomerization versus dissociation pathways.

In the first study presented in this thesis (section 4.1), a simple model was set up to investigate the chiral interconversion between R and S enantiomers of the 4MCF, obtained upon rotation around the olefinic double bond, versus the competing reaction of eliminating HF. The study of these competing reactions was motivated by (i) the experimental observation that ethylene or halogenated ethylene derivatives show molecular hydrogen or hydrogenhalide fragmentation, and (ii) by the HF-elimination CoIn located for 4MCF, that connects a 90° torsion with the dissociation of HF. Additionally, the HF-elimination CoIn allows for the competition between an excited state versus the previously postulated ground state dissociation process. To this aim, PESs for 4MCF have been calculated using the multiconfigurational method CASSCF, along the torsion around the C-C bond and the HF elimination coordinate describing the concerted dissociation of the HF fragment. For simplicity, only the electronic ground state and the bright $\pi\pi^*$ excited states have been considered. Quantum dynamical wavepacket propagations have been carried out on these PESs, and the calculations showed, that despite the system starts with enough kinetic energy to arrive to the HF-elimination CoIn, no dissociation could be observed, and, moreover, there is no transfer of population to the ground state in a sub-ps time scale. Hence, it has been concluded that, within this simple two-dimensional model, HF elimination does not compete with the isomerization process. However, it was stated that other electronic excited states might need to be included in the description of 4MCF, due to a deceptive mixing of $\pi\pi^*$ and $\pi\sigma^*$ states near the HF-eliminating CoIn.

The subsequent investigation on 4MCF (section 4.2), aimed at discovering the role of the $\pi\sigma^*$ states in the HF dissociation process in 4MCF. In this study it was shown that the HF dissociation indeed involves the presence of $\pi\sigma^*$ states. Moreover, a crossing between the bright $\pi\pi^*$ and the repulsive $\pi\sigma^*$ state occurs already at the FC geometry. As a consequence, it is also plausible that HF fragmentation can take place in the electronic excited state even before torsion is initiated. Additionally, the PESs along the HF dissociation coordinate show two distinct repulsive $\pi\sigma^*$ states, that could each be responsible for either atomic hydrogen or fluorine abstraction.

Consequently, full-dimensional dynamics were needed in order to unravel the most probable relaxation path(s) of 4MCF upon excitation into the bright $\pi\pi^*$ state by employing full-dimensional *ab initio* molecular dynamics (AIMD) on 4MCF (section 4.3). The on-the-fly electronic structure calculations are performed using the CASSCF method including an active space that not only can describe the $\pi\pi^*$ state - the typical V state for olefins - but also the important $\pi\sigma^*$ states. The AIMD simulations showed, that the preferred reaction after irradiation to the bright $\pi\pi^*$ state is atomic H dissociation. A minor amount of molecules undergoes F dissociation, followed by pyramidalization at the

sp² carbons and C-C bond rupture. Furthermore, the calculations show that the sparsely observed torsion motion giving rise to both enantiomers is strongly coupled to pyramidalization at both carbons connected to the olefinic double bond. Most importantly, it could be shown, that the preferred reaction via atomic H or F abstraction is governed by the newly found, and very fast and efficient, crossing from the $\pi\pi^*$ to the repulsive $\pi\sigma^*$ states, identified in the previous investigation.

The AIMD results showed that the main competition to the desired torsion about the C-C double bond in 4MCF is actually atomic H dissociation. Hence, the final study presented in this thesis aimed at avoiding this reaction channel (section 4.4). To this aim, quantum dynamical wavepacket propagations in the presence of external fields on one-dimensional CASSCF PESs have been carried out; the reduced dimensionality was justified by the findings of the AIMD simulations. Using strong non-resonant laser fields, i.e. Stark control, the potentials can be distorted and the $\pi\pi^*/\pi\sigma^*$ potential crossing can be shifted away from the Franck-Condon region so that the population is mainly trapped in the $\pi\pi^*$ state on time scales long enough to induce the desired torsion. Additionally, it has been pointed out, that for the correct modelling of the strong field interactions, the polarizabilities need to be incorporated in the dipole field interaction. Finally, it has been shown, that the proposed Stark control scheme does not effect the torsional cycle, so that it should also work in full dimensionality.

6 Zusammenfassung

“Chemie ist die Wissenschaft der Stoffe, ihren Strukturen, ihren Eigenschaften sowie den Reaktionen, die sie ineinander überführen.” (frei übersetzt nach Linus Pauling [1]) Nach dieser einfachen Definition zeigt sich, dass die Menschheit seit jeher die Chemie nutzt, um ihre eigene Entwicklung voranzutreiben. Zu wissen, wie sich bestimmte Stoffe unter gewissen Bedingungen verhalten, machte es möglich, Dinge zu erschaffen, so zum Beispiel die Extraktion von Metallen aus Erzen, die Herstellung von Keramiken oder die Fermentation von Pflanzen, um Alkohol herzustellen, um nur einige wenige Prozesse zu nennen. Obwohl das Wissen frühzeitiger Zivilisationen über diese Prozesse, durchaus beachtlich sein musste, waren die zugrundeliegenden chemischen Vorgänge allerdings noch nicht bekannt. Daher kann man das damals erlangte Wissen über die Veränderung von Stoffen lediglich als praktikable Regeln bezeichnen. Die Erkenntnis allein jedoch, dass ein Stoff in einen anderen umgeformt werden kann, gestattete es dem Menschen, nach besseren Methoden und Verfahren zu forschen, um zum Beispiel die Ausbeute eines gewünschten Produkts zu erhöhen beziehungsweise zu maximieren, sprich den Prozess zu kontrollieren. Wissenschaftler haben bis zum heutigen Tage eine große Bandbreite von Methoden entwickelt, die einen tiefen Einblick in die Struktur und Eigenschaften von Atomen und Molekülen ermöglichen. Mit diesem Wissen konnte nunmehr eine große Anzahl von Synthesvorschriften erarbeitet werden, um jede erdenkbare chemische Verbindung herzustellen. Der wissenschaftliche und technologische Fortschritt ermisst sich dennoch nach wie vor an der Fähigkeit, den Ausgang eines gegebenen Prozesses kontrollieren zu können [2].

Der Ausgang oder die Ausbeute einer chemischen Reaktion im Besonderen ist abhängig von vielen verschiedenen Parametern. Auf der makroskopischen Ebene können zum Beispiel Temperatur, Druck und/oder Konzentration der beteiligten Stoffe verändert werden, um das chemische Gleichgewicht zwischen Edukten und Produkten zu Gunsten des kinetisch favorisierten Produkts zu beeinflussen. Durch Kontrolle der Reaktion im mikroskopischen Bereich können selbst thermodynamisch ungünstige Produkte durch Zugabe von speziellen Katalysatoren oder Enzymen hergestellt werden. Die Kontrolle auf makroskopischer als auch mikroskopischer Ebene fallen in den Bereich der passiven Kontrolle, da die Rolle des Experimentators lediglich darin liegt, die gewünschte Reaktion zu bestimmten äußeren Bedingungen zu initiieren. Die Kontrolle über die Evolution der an der Reaktion beteiligten chemischen Spezies auf einer molekulardynamischen Zeitskala ist bei Veränderung der oben genannten Parameter allerdings nicht möglich.

Elektromagnetische Strahlung, also Licht, ermöglicht einen anderen und neuen Weg, chemische Reaktionen im Zeitmaßstab von molekularen Veränderungen zu verfolgen, aber auch zu manipulieren. Die Entwicklung und Fortschritte in der Lasertechnologie ma-

chen es möglich, ultrakurze Pulse zu generieren, die mit Substanzen in der Zeit von wenigen molekularen Schwingungen interagieren können. Die Bewegungen der Atome finden dabei typischerweise auf einer Zeitskala im Bereich Pico- bzw. Femtosekunden statt. Diese Entwicklung führte letztendlich zu dem neuen Forschungsbereich *Femtosekundenchemie* [3, 4] und im Jahre 1999 zum Nobelpreis für Chemie für Ahmed Zewail [5]. Ultraschnelle Reaktionen, wie zum Beispiel der sehr schnelle strahlungslose Übergang zwischen verschiedenen elektronisch angeregten Zuständen durch eine konische Überschneidung, können mit Hilfe der Erkenntnisse aus dem Bereich der *Femtosekundenchemie* überwacht und auch aktiv kontrolliert werden. Generell kann jedes molekulare System mittels einer Molekül-Licht-Interaktion so modifiziert werden, dass ein bestimmtes Produkt entsteht. Dies liegt im Besonderen daran, dass die Laserpulse anhand ihrer Parameter, wie zum Beispiel Farbe, Phase, Feldstärke oder Polarisation, in jeder erdenklichen Art und Weise geformt werden können. Daraus ableitend ergeben sich viele verschiedene Kontrollstrategien, wie zum Beispiel die von Brumer und Shapiro eingeführte kohärente Kontrolle von chemischen Reaktionen [6, 8], die sich den Welle-Teilchen-Dualismus der Moleküle zunutze macht, die *pump-dump* Kontrollstrategie, erstmals beschrieben von Tannor, Rice und Kosloff [18, 19], oder die Ausnutzung des Stark-Effekts [23], der die Form ganzer Potenzialhyperflächen verändern kann.

Ein sehr prominentes Beispiel für die Kontrolle einer chemischen Reaktion ist die *cis-trans*-Isomerisierung einer zentralen Kohlenstoff-Kohlenstoff-Doppelbindung. Die relativ hohe Rotationsbarriere, die eine Torsion um die Doppelbindung darstellt, kann leicht durch elektronische Anregung mittels elektromagnetischer Strahlung in einen $\pi\pi^*$ Zustand überwunden werden. Darüber hinaus sind Isomerisierungen typischerweise reversibel. Daher ist eine solche lichtinduzierte *cis-trans*-Isomerisierung eine selektive Überführung von Lichtenergie in molekulare Bewegungen, ohne dabei das System zu zerstören. In den meisten Fällen fällt das System nach der Isomerisierung mittels eines ultraschnellen Übergangs durch eine konische Überschneidung zurück in den elektronischen Grundzustand. Von diesen Eigenschaften selektiver Anregung und molekularen Veränderung profitiert zum Beispiel der erste Schritt im Sehprozess des menschlichen Auges [47, 48]. Während hier der gesamte Sehprozess, also von Signalempfang zu Signalverarbeitung im Gehirn, im Bereich von Millisekunden liegt, bedarf es für die nervensignalauslösende Reaktion des in den Sehzellen befindliche all-*trans*-Retinals zum 11-*cis*-Retinal nur weniger hundert Femtosekunden nach der Aufnahme eines einzelnen Photons [49, 50]. Nach dem Vorbild der Natur, wird die *cis-trans* Isomerisierung einer C-C-Doppelbindung mittels Anregung durch Licht auch als Basis für künstliche molekulare Maschinen, wie molekulare Rotoren oder Schalter verwendet. Beispiele für künstliche lichtinduzierte molekulare Rotoren wurden von Feringa und Mitarbeitern auf Basis von sterisch dicht substituier-

ten Alkenen (“overcrowded alkenes”) vorgestellt und experimentell [40, 41] sowie mit Hilfe von einfachen quantenchemischen Methoden [42, 43, 44] untersucht. Obwohl sich Retinal in der Natur als auch die künstlichen, sterisch anspruchsvollen Olefine als vielversprechende und funktionale molekulare Rotoren und Schalter erwiesen haben, ist die exakte Beschreibung der tatsächlichen Reaktionspfade nach Anregung für diese Beispiele eine sehr herausfordernde Zielstellung. Aufgrund der Größe der Systeme ist eine exakte Beschreibung von komplettdimensionalen Potenzialhyperflächen für verschiedenartig angeregte Zustände eine fast unmöglich zu realisierende Aufgabe. Um den Prozess der lichtinduzierten *cis-trans*-Isomerisierung und die damit verbundenen molekularen aber auch elektronischen Veränderungen quantenchemisch aufzulösen, bedient man sich daher kleinerer Modelle, die die Funktion und elektronischen Eigenschaften der zentralen C-C-Doppelbindung widerspiegeln. Das kleinste denkbare Modell wäre demnach Ethylen [58, 61, 62]. Allerdings weisen unterschiedlich substituierte Ethylenderivate unterschiedliche elektronische Eigenschaften auf, die sich auf die Reaktionspfade nach der Anregung in den elektronisch angeregten $\pi\pi^*$ Zustand zurück in den Grundzustand auswirken können [64, 65]. Darüber hinaus sind die *cis*- und *trans*-Isomere einfacher Ethylenderivate meist ununterscheidbar und daher in der Funktion eines molekularen Schalters als Modell ungeeignet.

Das Ziel der vorliegenden Arbeit ist die quantenchemisch und -dynamisch theoretische Untersuchung für ein Modell eines lichtinduzierten molekularen Rotors oder Schalters auf Basis eines Fluoroethylen Derivats. Speziell die Photochemie nach Anregung von (4-Methylcyclohexyliden) Fluoromethan (4MCF) steht im Mittelpunkt dieser Forschungsarbeit. 4MCF besitzt eine axiale Chiralität, die durch die verschiedenartig substituierte 4-Position des Cyclohexanringes und der Vinylposition der zentralen C-C-Doppelbindung hervorgerufen wird. Die R- und S-Enantiomere von 4MCF können durch die Torsion um die Doppelbindung ineinander überführt werden. Allerdings erfordert eine solche Torsion die Überwindung einer sehr hohen Potentialbarriere, sodass keine Razaemisierung bei Raumtemperatur stattfinden kann. Obwohl chemisch äquivalent, konnte in früheren Studien gezeigt werden, dass unter Verwendung geeigneter Laserpulse, R- und S-Enantiomere selektiv angeregt und somit leicht identifizierbar sind [77, 78, 83]. Darüber hinaus ist das System klein genug, um akkurate quantenchemische Methoden auf hohem Niveau in moderater Computerzeit anwenden zu können. Daher wurde 4MCF als einfaches Modell, aber auch als funktionales Beispiel, für einen molekularen Rotor bzw. Schalter vorgeschlagen.

So wie in allen olefinischen Verbindungen, wird die Torsion um die zentrale C-C-Doppelbindung in 4MCF durch die Anregung eines Elektrons aus dem bindenden π Or-

bital in das korrespondierende π^* Orbital durch eine ultraviolette Lichtquelle induziert. Das angeregte 4MCF kann nun über mehrere verschiedene konische Überschneidungen zwischen dem angeregten $\pi\pi^*$ Zustand und dem Grundzustand strahlungslos relaxieren, namentlich die "verdrehte", die "pyramidalisierte", die "Wasserstoff-Migration" und die "Wasserstofffluorid-Eliminierung" konische Überschneidung (siehe "twisted CoIn", "pyramidalized CoIn", "H-migration CoIn" und "HF-elimination CoIn" in Bild 6 auf Seite 13). All diese konischen Überschneidungen sind untrennbar mit der Drehung um die Doppelbindung verbunden. Die konischen Überschneidungen, die die Migrations- bzw. Eliminierungsreaktion bestimmen, führen allerdings zu einem ineffizienten molekularen Apparat, da das ursprüngliche System zerstört wird. Im Besonderen stehen die zur *cis-trans*-Umlagerung konkurrierenden Eliminierungsreaktionen im Fokus der vorliegenden Studien. Um eine kontrollierte *cis-trans*-Isomerisierung nach Anregung von 4MCF in den spektroskopisch hellen $\pi\pi^*$ Zustand zu erreichen, sind also alle anderen Relaxationskanäle zum Grundzustand, die zu einem funktionsunfähigen System führen, zu vermeiden. Zu diesem Zweck wurden verschiedene theoretische quantenchemische und -dynamische Modelle für das 4MCF System untersucht, um die Konkurrenz zwischen *cis-trans*-Isomerisierung und Dissoziationsreaktionen aufzudecken. Darüber hinaus wurden Laserkontrollstrategien simuliert, die eine unerwünschte Eliminierung verhindern sollen.

In einer ersten Studie wurde ein einfaches zweidimensionales Modell angewandt, welches die chirale Umlagerung von R- nach S-4MCF, induziert durch die Torsion um die zentrale Doppelbindung, und die konkurrierende Eliminierung von Wasserstofffluorid beschreiben kann. Diese Betrachtungsweise wurde durch zwei Erkenntnisse motiviert:

(i) In experimentellen Arbeiten wurde festgestellt, dass Ethylen und Halogenethylen Dissoziation von molekularem Wasserstoff oder Wasserstoffhalogenid nach Photoanregung aufweisen. (ii) In einer kürzlich zuvor erschienenen Publikation [80], wurde die Existenz einer konischen Überschneidung zwischen angeregten $\pi\pi^*$ Zustand und Grundzustand gezeigt, die eine 90° Torsion der Doppelbindung mit der gleichzeitigen konzertierten Eliminierung von HF verbindet. Potenzialhyperflächen für den elektronischen Grund- als auch den angeregten $\pi\pi^*$ Zustand wurden mit Hilfe der quantenchemischen multikonfigurationsalen *complete active space self consistent field* (CASSCF) Methode entlang der Torsions- und der HF-Eliminierungscoordinate berechnet. Auf diesen Potenzialhyperflächen wurden quantendynamische Wellenpaketpropagationen durchgeführt. Dabei zeigen die Dynamiksimulationen, dass keine Dissoziation von HF stattfindet, obwohl das angeregte System genügend kinetische Energie besitzt um die konische Überschneidung für die HF-Eliminierung zu erreichen. Darüber hinaus konnte innerhalb des gewählten Modells und der gewählten Methode kein Populationstransfer in den elektronischen Grundzustand nachgewiesen werden. Aus den Ergebnissen dieser Studie konnte geschlussfol-

gert werden, dass die HF-Eliminierung mit der *cis-trans*-Isomerisierung nicht kompetitiv ist. Allerdings konnte auch festgestellt werden, dass mitunter andere angeregte Zustände in der elektronischen Beschreibung von 4MCF vonnöten sind, da der $\pi\pi^*$ Zustand mit einem angeregten Zustand mit $\pi\sigma^*$ Charakter in der Nähe der konischen Überschneidung der HF-Eliminierung mischt.

Die in dieser Arbeit präsentierte zweite Studie hat daher zur Zielstellung, die Rolle des zuvor gefundenen $\pi\sigma^*$ angeregten Zustandes in der konzertierten HF-Eliminierungsreaktion näher zu beleuchten. Es konnte unter Berücksichtigung verschiedener quantenchemischer Methoden (CASSCF und CASPT2) und Basissätzen, die in der Lage sind eine große Anzahl von verschiedenen angeregten Zuständen genau zu beschreiben, gezeigt werden, dass angeregte Zustände von $\pi\sigma^*$ Charakter entlang der Dissoziationskoordinate tatsächlich präsent und energetisch erreichbar sind. Ferner konnte eine Überschneidung vom spektroskopischen $\pi\pi^*$ mit dem $\pi\sigma^*$ Zustand indentifiziert werden, die sich sehr nahe an der Gleichgewichtsgeometrie von 4MCF befindet. Entlang der HF-Eliminierungscoordinate verhalten sich die $\pi\sigma^*$ Zustände dabei repulsiv, sodass nach einer Anregung in den $\pi\pi^*$ Zustand ein möglicher ultraschneller Populationstransfer in den $\pi\sigma^*$ Zustand sofort zur Dissoziation von HF im angeregten Zustand führen kann. Darüber hinaus zeigen die Potenzialflächen zwei eigenständige $\pi\sigma^*$ Zustände, die die Anregung von dem π in das jeweilige antibindende σ Orbital der C-H beziehungsweise C-F Bindung beschreiben. Aufgrund dieser Tatsache, kann eine ungleichmäßige Bevölkung dieser beiden repulsiven Zustände auch zu einer individuellen Abspaltung atomaren Wasserstoffs bzw. Fluors führen. Diese Untersuchung konnte aufzeigen, dass elektronisch angeregte $\pi\sigma^*$ Zustände über den $\pi\pi^*$ Zustand bevölkert werden können. Dieser Populationstransfer geht dann mit einer sofortigen Eliminierung von H, F, als auch HF einher. Eine solche Dissoziation kann demnach im angeregten Zustand stattfinden, bevor sich überhaupt eine Torsion um die Doppelbindung ereignen kann. Dennoch kann eine Relaxation von 4MCF aus dem angeregten Zustand über die Torsion in Folge dieser Erkenntnisse nicht ausgeschlossen werden.

Als Konsequenz aus den vorangegangenen Studien, sind nach einer Anregung von 4MCF mehrere Reaktionspfade, die alle in Konkurrenz miteinander stehen, denkbar. Die *cis-trans*-Isomerisierung um die C-C-Doppelbindung ist dabei für die Funktionalität als molekularer Rotor oder Schalter die einzig erwünschte Reaktion. Bildung von atomarem Wasserstoff, atomarem Fluor sowie HF, sind sowohl im angeregten Zustand ohne gleichzeitige Torsion, als auch im Grundzustand bei vorheriger 90° Torsion möglich. Eine gleichzeitige Beschreibung aller Prozesse mit Hilfe der Quantendynamik ist aufgrund der hohen Dimensionalität des Problems hier allerdings nur sehr schlecht bzw. nicht zu realisieren. Daher wurden in der Folgestudie, statistische Molekulardynamik-Simulationen mittels

komplettdimensionaler *ab initio molecular dynamics* (AIMD) durchgeführt. Die elektronische Struktur (Energien, Kopplungsterme, etc.) wurde dabei mit der CASSCF Methode für jeden Zeitschritt neu berechnet, während die molekularen Veränderungen über einzelne Trajektorien mittels der Newton'schen Bewegungsgleichungen simuliert werden. Als Resultat der AIMD Simulationen, wurde festgestellt, dass atomare Wasserstoffdissoziation im angeregten Zustand den wichtigsten Reaktionskanal nach Anregung in den $\pi\pi^*$ Zustand darstellt. Fast 60% der simulierten Moleküle dissoziierten auf diesem Wege innerhalb eines sehr kurzen Zeitraums von 50-60 fs. Ein kleinerer Anteil (ca. 15%) zeigt atomare Fluordissoziation im angeregten Zustand. Es ist darüber hinaus wichtig zu erwähnen, dass die erwünschte *cis-trans*-Isomerisierung in nur sehr wenigen Fällen beobachtet werden konnte. Darüber hinaus ist dieser Reaktionspfad sehr stark mit der Pyramidalisierung an den olefinischen Kohlenstoffen verbunden. Die wichtigste Erkenntnis dieser Simulationen ist jedoch, dass sowohl Wasserstoff- als auch Fluordissoziation durch die zuvor indentifizierte, nunmehr reaktive, konische $\pi\pi^*/\pi\sigma^*$ Überschneidung kurz nach der Anregung in den $\pi\pi^*$ Zustand gekennzeichnet werden.

Die AIMD Simulationen haben gezeigt, dass die Hauptkonkurrenzreaktion zur gewünschten *cis-trans*-Isomerisierung nach Anregung von 4MCF die Dissoziation von Wasserstoff darstellt, welche durch einen ultraschnellen strahlungslosen Übergang vom spektroskopischen $\pi\pi^*$ Zustand in einen repulsiven $\pi\sigma^*$ Zustand eingeleitet wird. Die finale Studie, die in dieser Arbeit präsentiert wird, beschäftigt sich mit der Möglichkeit, diesen Reaktionskanal zu vermeiden, um so die gewünschte Torsion um die C-C-Doppelbindung in 4MCF zu initiieren. Zu diesem Zwecke wurden quantendynamische Wellenpaketpropagationen auf eindimensionalen CASSCF Potenzialflächen unter Einbeziehung externer elektromagnetischer Felder durchgeführt. Die geringe Dimensionalität kann mit den Erkenntnissen aus den AIMD Simulationen gerechtfertigt werden; die Dissoziation von Wasserstoff verläuft entlang der C-H Bindungsachse und ereignet sich extrem schnell, sodass der Rest des molekularen Gerüsts kaum auf die Veränderungen reagiert und somit für diesen Reaktionsverlauf als eingefroren gelten kann. Der generelle Ansatz für das Vermeiden der Wasserstoffdissoziation ist die Vermeidung von Populationstransfer vom $\pi\pi^*$ in den $\pi\sigma^*$ Zustand. Sobald das angeregte Wellenpaket im $\pi\pi^*$ Zustand verharren kann bzw. gefangen ist, kann eine effiziente Torsion beginnen, wie in der ersten Studie gezeigt werden konnte. Ziel ist es die extrem reaktive konische Überschneidung in der Nähe der Gleichgewichtsgeometrie zu deaktivieren, damit kein Übergang in den dissoziierenden $\pi\sigma^*$ Zustand geschehen kann. Es konnte in dieser Studie gezeigt werden, dass unter Verwendung von starken, nicht-resonanten Laserfeldern die Potentiale im Sinne des Stark-Effekts so verändert werden können, dass sich die Position des $\pi\pi^*/\pi\sigma^*$ konischen Überschneidung von der Gleichgewichtsgeometrie entfernt. Somit ist es möglich,

dass die angeregten Population im $\pi\pi^*$ Zustand gefangen wird und zwar lange genug, damit die gewünschte Torsion initiiert werden kann. Darüber hinaus konnte in dieser Studie herausgefunden werden, dass für eine korrekte Beschreibung des Stark-Effekts, also der Potenzial-Feld-Interaktion, nicht nur die Dipolmomente der beteiligten elektronischen Zustände sondern auch die Polarisierbarkeiten eine gewichtige Rolle spielen. Abschließend konnte in dieser Studie gezeigt werden, dass die Torsion selbst nicht von starken Feldern beeinflusst wird. Damit kann geschlossen werden, dass die Kontrollstrategie mittels starken, nicht-resonanten Laserfeldern auch in höher dimensionalen Modellen unter Einbeziehung mehrerer Reaktionskoordinaten eine Dissoziation von Wasserstoff effektiv verhindern kann.

Die vorliegende Arbeit erzielte detaillierte Erkenntnisse bezüglich der elektronischen Struktur und Dynamik des chiralen Fluoroethylenderivats, 4MCF, nach Anregung in den spektroskopisch hellen Zustand mit $\pi\pi^*$ Charakter als Modell für einen lichtinduzierten molekularen Rotor bzw. Schalter. Es konnte gezeigt werden, dass die Einbeziehung von repulsiven angeregten Zuständen mit $\pi\sigma^*$ Charakter eine sehr wichtige Rolle in der Beschreibung der Dynamik nach Anregung in das olefinische System spielt. Die Eliminierung von atomarem Wasserstoff stellt den Hauptreaktionspfad nach der Anregung von 4MCF in den $\pi\pi^*$ Zustand dar. Es konnte gezeigt werden, dass mit Hilfe des Stark Effekts die dafür verantwortliche konische Überschneidung auf der Potenzialhyperfläche bewegt und somit weniger leicht erreichbar gemacht werden kann, sodass die unerwünschte Dissoziation von 4MCF effektiv verhindert bzw. verlangsamt wird.

References

- [1] Pauling, L. *General Chemistry*. Freeman, San Francisco, (1970).
- [2] Rice, S. A. and Zhao, M. *Optical Control of Molecular Dynamics*. Wiley, New York, (2000).
- [3] Zewail, A. H. *Femtochemistry, Vols. I, II*. World Scientific, Singapore, (1994).
- [4] Dantus, M. and A. H. Zewail (Eds.). *Chem. Rev.* **104**, 1717 (2004).
- [5] Grenthe, I., editor. *Nobel Lectures, Chemistry 1996-2000*. World Scientific Publishing Co., Singapore, (2003).
- [6] Shapiro, M. and Brumer, P. *Principles of Quantum Control of Molecular Processes*. Wiley, New York, (2003).
- [7] Tannor, D. *Introduction to Quantum Mechanics: A Time-Dependent Perspective*. University Science Books, Sausalito, (2006).
- [8] Brumer, P. and Shapiro, M. *Chem. Phys. Lett.* **126**, 541 (1986).
- [9] Gordon, R. J. and Rice, S. A. *Ann. Rev. Phys. Chem.* **48**, 601 (1997).
- [10] Rice, S. A. *Adv. Chem. Phys.* **101**, 213 (1997).
- [11] Tannor, D. J., Kosloff, R., and Bartana, A. *Faraday Discuss.* **113**, 365 (1999).
- [12] Brixner, T., Damrauer, N. H., and Gerber, G. *Adv. At. Molec. Opt. Phys.* **46**, 1 (2001).
- [13] Shapiro, M. and Brumer, P. *Rep. Prog. Phys.* **66**, 859 (2003).
- [14] Crim, F. F. *Science* **249**, 1387 (1990).
- [15] Rabitz, H., de Vivie-Riedle, R., Motzkus, M., and Kompa, K.-L. *Science* **288**, 824 (2000).
- [16] Shapiro, M., Hepburn, J. W., and Brumer, P. *Chem. Phys. Lett.* **149**, 451 (1988).
- [17] Zhu, L. C., Kleiman, V. D., Li, X. N., Lu, S. P., Trentelman, K., and Gordon, R. J. *Science* **270**, 77 (1995).
- [18] Tannor, D. J. and Rice, S. A. *J. Chem. Phys.* **83**, 5013 (1985).
- [19] Tannor, D. J., Kosloff, R., and Rice, S. A. *J. Chem. Phys.* **85**, 5805 (1986).

- [20] Baumert, T., Grosser, M., Thalweiser, R., and Gerber, G. *Phys. Rev. Lett.* **67**, 3753 (1991).
- [21] Baumert, T., Helbing, J., and Gerber, G. *Adv. Chem. Phys.* **101**, 47 (1997).
- [22] Potter, E. D., Herek, J. L., Pedersen, S., Liu, Q., and Zewail, A. H. *Nature* **355**, 66 (1992).
- [23] Stark, J. *Nature* **92**, 401 (1913).
- [24] Garraway, B. M. and Suominen, K. *Phys. Rev. Lett.* **80**, 932 (1998).
- [25] Sussman, B. J., Townsend, D., Ivanov, M. Y., and Stolow, A. *Science* **314**, 278 (2006).
- [26] Judson, R. S. and Rabitz, H. *Phys. Rev. Lett.* **68**, 1500 (1992).
- [27] Assion, A., Baumert, T., Bergt, M., Brixner, T., Seyfried, V., Strehle, M., and Gerber, G. *Science* **282**, 919 (1998).
- [28] Glass, A., Rozgonyi, T., Sauerbrey, T. F. R., and Szabó, G. *Appl. Phys. B* **71**, 267 (2000).
- [29] Brixner, T. and Gerber, G. *Chem. Phys. Chem.* **4**, 418 (2003).
- [30] Daniel, C., Full, J., González, L., Lupulescu, C., Manz, J., Merli, A., Štefan Vajda, and Wöste, L. *Science* **299**, 536 (2003).
- [31] Kosloff, R., Rice, S. A., Gaspard, P., Tersigni, S., and Tannor, D. J. *Chem. Phys.* **139**, 201 (1989).
- [32] Peirce, A. P., Dahleh, M. A., and Rabitz, H. *Phys. Rev. A* **37**, 4950 (1988).
- [33] Shi, S., Woody, A., and Rabitz, H. *J. Chem. Phys.* **88**, 6870 (1988).
- [34] Levine, B. G. and Martínez, T. J. *Ann. Rev. Phys. Chem.* **58**, 613 (2007).
- [35] Feringa, B. L. *Molecular Switches*. Wiley-VCH, Weinheim, (2003).
- [36] Balzani, V., Credi, A., and Venturi, M. *Chem. Soc. Rev.* **38**, 1542 (2009).
- [37] Lehn, J. M. *Proc. Natl. Acad. Sci. USA* **99**, 4763 (2002).
- [38] Balzani, V., Venturi, M., and Credi, A. *Molecular Devices and Machines*. Wiley-VCH, Weinheim, (2003).

- [39] Yamaki, M., Nakayama, S., Hoki, K., Kono, H., and Fujimura, Y. *Phys. Chem. Chem. Phys.* **11**, 1662 (2009).
- [40] Koumura, N., Zijlstra, R. W. J., van Delden, R. A., Harada, N., and Feringa, B. L. *Nature* **401**, 152 (1999).
- [41] Koumura, N., Geertsema, E. M., van Gelder, M. B., Meetsma, A., and Feringa, B. L. *J. Am. Chem. Soc.* **124**, 5037 (2002).
- [42] Grimm, S., Bräuchle, C., and Frank, I. *Comput. Phys. Commun.* **6**, 1943 (2005).
- [43] Klok, M., Walko, M., Geertsema, E. M., Ruangsapapichat, N., Kistemakea, J. C. M., Meetsma, A., and Feringa, B. L. *Chem. Eur. J.* **14**, 11183 (2008).
- [44] Pérez-Hernández, G. and González, L. *Phys. Chem. Chem. Phys.* **12**, 12279 (2010).
- [45] Feringa, B. L., van Delden, R. A., and ter Wiel, M. K. J. *Pure Appl. Chem.* **75**, 563 (2003).
- [46] Feringa, B. L. *J. Org. Chem.* **72**, 6635 (2007).
- [47] Schoenlein, R. W., Peteanu, L. A., Mathies, R. A., and Shank, C. V. *Science* **254**, 412 (1991).
- [48] Dugave, C. and Demange, L. *Chem. Rev.* **103**, 2475 (2003).
- [49] Kim, J. E., McCamant, D. W., Zhu, L., and Mathies, R. A. *J. Phys. Chem. B* **105**, 1240 (2001).
- [50] Ben-Nun, M., Molnar, F., Schulten, K., and Martínez, T. J. *Proc. Natl. Acad. Sci. USA* **99**, 1769 (2002).
- [51] Kaczmarek, M. S., Ma, Y., and Rohlfing, M. *Phys. Rev. B* **81**, 115433 (2010).
- [52] González-Luque, R., Garavelli, M., Bernardi, F., Merchán, M., Robb, M. A., and Olivucci, M. *Proc. Natl. Acad. Sci. USA* **97**, 9379 (2000).
- [53] Vogt, G., Nuernberger, P., Brixner, T., and Gerber, G. *Chem. Phys. Lett.* **433**, 211 (2006).
- [54] Ohtsuki, Y., Ohara, K., Abe, M., Nakagami, K., and Fujimura, Y. *Chem. Phys. Lett.* **369**, 525 (2003).
- [55] Abe, M., Ohtsuki, Y., Fujimura, Y., and Domcke, W. *J. Chem. Phys.* **123**, 144508 (2005).

- [56] Marquetand, P., Nuernberger, P., Vogt, G., Brixner, T., and Engel, V. *Europhys. Lett.* **80**, 53001 (2007).
- [57] Mulliken, R. S. *Phys. Rev.* **6**, 751 (1932).
- [58] Ben-Nun, M. and Martínez, T. J. *Chem. Phys.* **259**, 237 (2000).
- [59] Quenneville, J. and Martínez, T. J. *J. Phys. Chem. A* **107**, 829 (2003).
- [60] Quenneville, J., Ben-Nun, M., and Martínez, T. J. *Journal of Photochemistry and Photobiology A: Chemistry* **144**, 229 (2001).
- [61] Ben-Nun, M. and Martínez, T. J. *Chem. Phys. Lett.* **298**, 57 (1998).
- [62] Ben-Nun, M. and Martínez, T. J. *J. Phys. Chem. A* **103**, 10517 (1999).
- [63] Viel, A., Krawczyk, R. P., Manthe, U., and Domcke, W. *J. Chem. Phys.* **120**, 11000 (2004).
- [64] Barbatti, M., Aquino, A. J. A., and Lischka, H. *J. Phys. Chem. A* **109**, 5168 (2005).
- [65] González-Vázquez, J. and González, L. *Chem. Phys.* **349**, 287 (2008).
- [66] Balko, B. A., Zhang, J., and Lee, Y. T. *J. Chem. Phys.* **97**, 935 (1992).
- [67] Cromwell, E. F., Stolow, A., Vrakking, M. J. J., and Lee, Y. T. *J. Chem. Phys.* **97**, 4029 (1992).
- [68] Hall, G. E., Muckerman, J. T., Preses, J. M., Ralph E. Weston, J., Flynn, G. W., and Persky, A. *J. Chem. Phys.* **101**, 3679 (1994).
- [69] Balko, B. A., Zhang, J., and Lee, Y. T. *J. Phys. Chem. A* **101**, 6611 (1997).
- [70] Blank, D. A., Sun, W., Suits, A. G., Lee, Y. T., North, S. W., and Hall, G. E. *J. Chem. Phys.* **108**, 5414 (1998).
- [71] Sato, K., Tsunashima, S., Takayanagi, T., Fijisawa, G., and Yokoyama, A. *Chem. Phys. Lett.* **242**, 401 (1995).
- [72] Peña-Gallego, A., Martínez-Núñez, E., and Vázquez, S. A. *Chem. Phys. Lett.* **353**, 418 (2002).
- [73] Martínez-Núñez, E., Estévez, C. M., Flores, J. R., and Vázquez, S. A. *Chem. Phys. Lett.* **348**, 81 (2001).

- [74] González-Vázquez, J., Fernández-Ramos, A., Martínez-Núñez, E., and Vázquez, S. A. *J. Phys. Chem. A* **107**, 1389 (2003).
- [75] González-Vázquez, J., Fernández-Ramos, A., Martínez-Núñez, E., and Vázquez, S. A. *J. Phys. Chem. A* **107**, 1398 (2003).
- [76] González-Vázquez, J., Martínez-Núñez, E., Vázquez, S. A., Santamaria, J., and Banares, L. *Chem. Phys. Lett.* **396**, 442 (2004).
- [77] Kröner, D. and González, L. *Phys. Chem. Chem. Phys.* **5**, 3933 (2003).
- [78] Kröner, D. and González, L. *Chem. Phys.* **298**, 55 (2004).
- [79] Fujimura, Y., González, L., Kröner, D., Manz, J., Mehdaoui, I., and Schmidt, B. *Chem. Phys. Lett.* **386**, 248 (2004).
- [80] Zilberg, S., Cogan, S., Haas, Y., Deeb, O., and González, L. *Chem. Phys. Lett.* **443**, 43 (2007).
- [81] Gedanken, A., Duraisamy, M., Huang, J., Rachon, J., and Walborsky, H. M. *J. Am. Chem. Soc.* **110**, 4593 (1988).
- [82] van Steenis, J. H. and van der Gen, A. *J. Chem. Soc., Perkin Trans. 1*, 2117 (2002).
- [83] Kröner, D., Shibl, M. F., and González, L. *Chem. Phys. Lett.* **372**, 242 (2003).
- [84] Serrano-Andrés, L., Merchán, M., Ignacio Nebot-Gil, Lindh, R., and Roos, B. O. *J. Chem. Phys.* **98**, 3151 (1992).
- [85] Schreiber, M., Barbatti, M., Zilberg, S., Lischka, H., and González, L. *J. Phys. Chem. A* **111**, 238 (2007).
- [86] Krawczyk, R. P., Viel, A., Manthe, U., and Domcke, W. *J. Chem. Phys.* **119**, 1397 (2003).
- [87] Barbatti, M., Paier, J., and Lischka, H. *J. Chem. Phys.* **121**, 11614 (2004).
- [88] McQuarrie, D. A. *Quantum Chemistry*. University Science Books, Sausalito, CA, USA, (2007).
- [89] Jensen, F. *Introduction to Computational Chemistry*. Wiley, Hoboken, NJ, USA, (2006).
- [90] Hehre, W., Radom, L., Schleyer, P., and Pople, J. *Ab Initio Molecular Orbital Theory*. Wiley, New York, (1986).

- [91] Levine, I. N. *Quantum Chemistry*. Prentice Hall, (1999).
- [92] Born, M. and Oppenheimer, R. *Annalen der Physik* **84**, 457 (1927).
- [93] Hartree, D. R. *Proc. Cambridge Phil. Sc.* **24**, 111 (1928).
- [94] Roothaan, C. C. J. *Reviews of Modern Physics* **23**, 69 (1951).
- [95] Hall, G. G. *Proc. R. Soc. London A* **205**, 541 (1951).
- [96] Roos, B. O. and Widmark, P. In *European Summerschool in Quantum Chemistry*, volume 2, 287. (2005).
- [97] Roos, B. O. *Advances in Chemical Physics* **69**, 399 (1987).
- [98] Möller, C. and Plesset, M. S. *Physical Review* **46**, 618 (1934).
- [99] Andersson, K., Malmqvist, P. A., Roos, B. O., Sadlej, A. J., and Wolinski, K. *The Journal of Physical Chemistry* **94**(14), 5483 (1990).
- [100] Finley, J., Malmqvist, P., Roos, B., and Serrano-Andrés, L. *Chem. Phys. Lett.* **288**, 299 (1998).
- [101] Yarkony, D. R. *J. Phys. Chem.* **105**, 277 (2001).
- [102] Bernardi, F., Olivucci, M., and Robb, M. A. *Chemical Society Reviews* **25**, 321 (1996).
- [103] Pacher, T., Cederbaum, L. S., and Köppel, H. *Adv. Chem. Phys.* **84**, 293 (1993).
- [104] Domcke, W., Yarkony, D. R., and Köppel, H., editors. *Conical Intersections: Electronic Structure, Dynamics and Spectroscopy*. World Scientific, Singapore, (2004).
- [105] Baer, M. *Beyond Born-Oppenheimer: Electronic Nonadiabatic Coupling Terms and Conical Intersections*. John Wiley & Sons, Hoboken, (2006).
- [106] Tal-Ezer, H. and Kosloff, R. *J. Chem. Phys.* **81**, 3967 (1984).
- [107] Park, T. J. and Light, J. C. *J. Chem. Phys.* **85**, 5870 (1986).
- [108] Feit, M. D., Fleck Jr., J. A., and Steiger, A. *J. Comput. Phys.* **47**, 412 (1982).
- [109] Feit, M. D. and Fleck Jr., J. A. *J. Chem. Phys.* **78**, 301 (1983).
- [110] Feit, M. D. and Fleck Jr., J. A. *J. Chem. Phys.* **80**, 2578 (1984).

- [111] Kosloff, R. *Ann. Rev. Phys. Chem.* **45**, 145 (1994).
- [112] Martson, C. C. and Balint-Kurti, G. G. *J. Chem. Phys.* **91**, 3571 (1989).
- [113] Kosloff, R. *Dynamics of Molecules and Chemical Reactions*. MerceL Dekker, (1996).
- [114] Tully, J. C. *Faraday Discussions* **110**, 407 (1998).
- [115] Tully, J. C. *J. Chem. Phys.* **93**, 1061 (1990).
- [116] Ashfold, M. N. R., Mordaunt, D. H., and Wilson, S. H. S. *Advances in Photochemistry*, volume 21. John Wiley and Sons, New York, (1996).
- [117] Robin, M. B. *Higher Excited States in Polyatomic Molecules*, volume 1 and 2. Academic Press, New York, (1974).
- [118] Schinke, R. *Photodissociation Dynamics*. Cambridge University Press, Cambridge, (1993).
- [119] Ashfold, M. N. R., King, G. A., Murdock, D., Nix, M. G. D., Oliver, T. A. A., and Sage, A. G. *Phys. Chem. Chem. Phys.* **12**, 1218 (2010).
- [120] Sobolewski, A. L. and Domcke, W. *Chem. Phys. Lett.* **315**, 293 (1999).
- [121] Sobolewski, A. L. and Domcke, W. *Chem. Phys. Lett.* **321**, 479 (2000).
- [122] Sobolewski, A. L. and Domcke, W. *Chem. Phys.* , 181 (2000).
- [123] Perun, S., Sobolewski, A., and Domcke, W. *Chem. Phys.* **313**, 107 (2005).
- [124] Vallet, V., Lan, Z., Mahapatra, S., Sobolewski, A. L., and Domcke, W. *Faraday Discuss.* **127**, 283 (2004).
- [125] Peric, M., Dohmann, H., Pyerimhoff, S. D., and Buenker, R. J. *Z. Phys. D. At. Mol. Clusters* **5**, 65 (1987).
- [126] Marquetand, P. and Engel, V. *Phys. Chem. Chem. Phys.* **7**, 469 (2005).

List of Figures

1	a) Brumer-Shapiro control scheme: A preliminary pulse (not shown) excites two vibrational states. From there, the transfer to the two degenerate final states is steered by the relative phase of the two control lasers with frequencies ω_1 and ω_2 ; b) Tannor-Rice-Kosloff pump-dump control scheme shown for a molecule ABC: At time t_0 a pump pulse creates a wavepacket in the excited state $[ABC]^*$. A dump pulse at either time t_1 or time t_2 then leads to population transfer to different exit channels in the ground state to produce either $AB + C$ or $A + BC$; c) Scheme for the NRDSE in 1D: A state crossing in the unperturbed PESs acts as a funnel for fast population transfer to a different state. Employing a strong field moves the crossing to another point on the PESs, creating a barrier for the fast decay. (For all cases wavepacket movement is indicated.)	4
2	Illustration of the ultrafast light-triggered <i>cis-trans</i> isomerization of 11- <i>cis</i> -retinal to all- <i>trans</i> -retinal along the reaction coordinate mediating through a CoIn between the electronic ground and excited state. Wavepacket movement is indicated.	6
3	Symmetrical photoisomerization of a double bond. After excitation to the spectroscopic V state, both directions are equally probable. When relaxing to the ground state, N , the situation is analogous. Wavepacket motion and branching is indicated.	7
4	R- and S-enantiomers of 4MCF: mirror images, which are connected by a torsion, τ , around the double bond.	9
5	Scheme for the synthesis of R-4MCF	11
6	a) Structure of R-4MCF in the electronic ground state optimized at the MP2/6-31G* level of theory [85]; b) V/N CoIns in 4MCF: twisted CoIn, two pyramidalized CoIns, H-migration CoIn (all from Ref. [85]) and HF-elimination CoIn [80].	13
7	Scheme of the two competing paths, (i) <i>cis-trans</i> isomerization and (ii) dissociation of hydrogenfluoride via the HF-elimination CoIn.	32
8	Schematic illustration of an excited state photodissociation in an exemplary A-B system: A wavepacket excited to a bound state $[A-B]^*$ experiences a coupling to a repulsive state, which leads to a partial dissociation to $A\bullet^* + \bullet B$	42
9	Deactivation paths in the HF photodissociation of 4MCF along dissociation coordinates R in a): two-state model ground state path and b): competing paths in the many-states model including $\pi\sigma^*$ states, i.e. excited state path vs. ground state path after torsion. Time evolution and branching of a wavepacket is indicated.	44
10	Selected trajectories and percentages of trajectories following main deactivation paths. Left panel: time evolution of the adiabatic potentials, momentary state indicated by rings; right panel: overlap of geometries before the crossing to the ground state.	58

- 11 illustration of the Stark effect on the 1D PESs in 4MCF in the diabatic representation: a) field free PESs and b) dressed PESs in the presence of an external electric field with field strength F_0 . The net down shift of the $\pi\pi^*$ state is indicated. The schematic PESs (a and b) resemble the actual calculated ab initio PESs shown in the article. Time evolution of a wavepacket is indicated. 70
- 12 Accumulated flux $J_{\pi\sigma^*}^{acc}$ (amount of H-dissociation) vs. the field amplitude, F_0 , of the control laser at times as indicated. 71

List of Abbreviations

4MCF	(4-methylcyclohexylidene) fluoromethane
AIMD	<i>ab initio</i> molecular dynamics
CASPT2	complete active space perturbation theory of 2nd order
CASSCF	complete active space self-consistent field
CD	circular dichroism
CI	configuration interaction
CoIn	conical intersection
CSF	configuration state function
FC	Franck-Condon
HaFo	Hartree-Fock
IR	infra-red
IUPAC	The International Union of Pure and Applied Chemistry
LIPS	light-induced potential surface
MCSCF	multi-configurational self-consistent field
MO	molecular orbital
MR-CASPT2	multi-reference CASPT2
MR-CI	multi-reference CI
MS-CASPT2	multi-state CASPT2
N	neutral (ground) state
NACT	non-adiabatic coupling term
NRDSE	non-resonant dynamic Stark effect
OCT	optimal control theory
PES	potential energy surface
Ref	reference
RI-CC2	coupled cluster of 2nd order with resolution of identity
SA-CASSCF	state averaged CASSCF
TD-DFT	time-dependent density functional theory
TDSE	time-dependent Schrödinger equation
TISE	time-independent Schrödinger equation
TOF	time of flight
UV	ultra-violet
V	valence state
vs.	versus

Acknowledgements

At this point, I want to take the opportunity to thank the vast amount of people, that contributed to the present thesis and the underlying research. This thesis was prepared in the working group of **Prof. Dr. Leticia González** at the Friedrich-Schiller-Universität Jena in the time from June 2008 until February 2013. The research and studies, which are the basis for this thesis, have been performed in the frame of a trilateral cooperation between the Al-Quds University in Al-Quds, Palestine, the Hebrew University in Jerusalem, Israel and the Freie Universität Berlin as well as the Friedrich-Schiller-Universität in Jena, Germany, funded by the German Research Council (DFG). I am very thankful for being part of this cooperation, and hence, I want to thank very much the leaders of the different working groups. First and most importantly, I thank **Prof. Dr. Jörn Manz** from the Freie Universität Berlin for initiating and running this corporation from the bottom of his heart. I want to thank **Prof. Dr. Yehuda Haas** and **Prof. Dr. Shmuel Zilberg** from the Hebrew University in Jerusalem for the possibility of staying and working in their work group for several times. I also want to thank **Prof. Dr. Omar Deeb** from the Al-Quds University for making many things possible. Of course, I am specially grateful to my boss **Prof. Dr. Leticia González**, who not only has given me the opportunity to be in her AG, but has as well invested much of her time in guiding, correcting, supporting and helping me throughout this work. Moreover, I am especially thankful for her never ending patience during the last steps of writing this thesis.

I am grateful for the nice working atmosphere that all of the above groups provided, yet I want to specially thank my fellow office mates and colleagues from the AG *González*, **Hartmut “Harry” Preuß**, **Dr. Guillermo Pérez-Hernández**, **Dr. Daniel Escudero**, **Anna Hauser**, **Dr. Mariana Aßmann**, **Dr. Stephan Kupfer**, **Martin Richter** and **Federico Latorre**, as well as **Dr. Shiren Alfalah** for working together, help, support, and fun conversations during and outside working hours. I thank very much **Dr. Jesús González-Vázquez** and **Dr. Philipp Marquetand**, who were ready to spend their time supervising parts of my research, providing useful comments regarding computing issues or quantum chemistry and dynamics questions.

Furthermore, I would like to thank **Dr. Dirk Bender** and **Dr. Markus Opperl** for support concerning technical issues.

I am very thankful for the generous help from **John “Beau” Griffith**, who assisted me with corrections and valuable discussions about this work, about chemistry in general, about time planning and about distinguishing between important and urgent things.

Moreover, I thank all of my friends who made my life much easier with endless hours in the *Alster* in Jena or the *Rock Pub* in Vienna. Beyond that, I thank them for all kinds of support and discussions especially while I was working on this thesis.

Finally, I would like to thank my family. This thesis would not have been possible without their support for many, many years. Thank you for arousing my interest in science, and especially in chemistry. Thank you for financial support, whenever times requested it. Thank you for your kindness and warmth. Thank you for your laughter even in bad times. Simply, thank you for everything...

Curriculum vitae

Personal data

Name	Daniel Kinzel
Birth	October 2 nd 1982, in Erfurt
Citizenship	Federal Republic of Germany
Nationality	Germany
Personal status	single
Current working address	Universität Wien Institut für Theoretische Chemie Währinger Straße 17, 1090 Wien, Österreich
E-mail	daniel.kinzel@univie.ac.at

Working experience

2012–present	Research Assistant in the group of Prof. Dr. Leticia González at the Institute of Theoretical Chemistry, University of Vienna, Vienna, Austria
2008–2012	Doctoral studies in the group of Prof. Dr. Leticia González at the Institute of Physical Chemistry, Friedrich-Schiller-University Jena, Germany

Degrees and education

June 2008	Diploma in Chemistry Thesis: “A theoretical study of the thermal rearrangement of <i>cis</i> - and <i>trans</i> -pinane”
2003–2008	Studies of Chemistry, Friedrich-Schiller-University Jena, Germany
June 2002	Abitur
2000–2002	Grammar School, specialized in Mathematics and Natural Sciences in Erfurt, Germany
1999–2000	West-Potomac High-School in Alexandria, VA, USA
1997–1999	Grammar School, specialized in Mathematics and Natural Sciences in Erfurt, Germany
1993–1997	Grammar School in Erfurt, Stadtilm and Arnstadt, Germany
1989–1993	Elementary School in Erfurt, Germany

Community service

2002-2003 Marienstift, Arnstadt, Children's home for mentally and physically handicapped children

Attended conferences and symposia

July 2011 The Madrid Conference on Femtochemistry (FEMTO10), Madrid Spain

July 2010 Gordon Research Conference on Atomic and Molecular Interactions, New London, NH, USA

September 2009 45th Symposium on Theoretical Chemistry, Neuss, Germany

April 2009 EPSRC CoCoChem Summerschool, London, Great Britain

March 2009 Saxonian Theoretical Seminar, Leipzig, Germany

February 2009 10th French-Israeli Symposium on Non-linear and Quantum Optics, Ein Gedi, Israel

July 2008 22nd IUPAC Symposium on Photochemistry, Gothenburg, Sweden

Oral Presentations

December 2011 "Photochemistry and -dynamics on 4-methylcyclohexylidene fluoromethane" and "Electrophilic Aromatic Substitutions - A theoretician's point of view", invited by Prof. Dr. Yehuda Haas, The Hebrew University of Jerusalem, Jerusalem, Israel

February 2010 "4MCF - torsion vs. dissociation? Insights from molecular dynamics simulations", invited by Prof. Dr. Jörn Manz, Freie Universität Berlin, Berlin, Germany

February 2009 "Quantum chemical and dynamical calculations for photoisomerization and photodissociation in a fluoroethylene derivative", Saxonian Theoretical Seminar, Leipzig, Germany

February 2009 "Photoisomerisation vs. photodissociation of a chiral olefin - a two dimensional study of 4-methylcyclohexylidene fluoromethane", invited by Prof. Dr. Yehuda Haas, The Hebrew University of Jerusalem, Jerusalem, Israel

Poster Presentations

- July 2011 “Torsion or Dissociation? - Dynamics on a chiral fluoroethylene derivative”, Daniel Kinzel, Philipp Marquetand, Jesús González-Vázquez, Leticia González, The Madrid Conference on Femtochemistry (FEMTO10), Madrid Spain
- July 2010 “TORSION VS. DISSOCIATION IN A FLUOROETHYLENE DERIVATE”, Daniel Kinzel, Leticia González, Gordon Research Conference on Atomic and Molecular Interactions, New London, NH, USA
- September 2009 “CONTROL OF PHOTOISOMERIZATION VS. PHOTODISSOCIATION IN A CHIRAL OLEFIN; A TWO-DIMENSIONAL APPROACH”, Daniel Kinzel, Sherin Alfalah, Jesús González-Vázquez, Leticia González, 45th Symposium on Theoretical Chemistry, Neuss, Germany
- April 2009 “Towards control of uni-directional torsion avoiding photodissociation in a chiral olefin two-dimensional quantum chemistry and quantum dynamical study of 4-methylcyclohexylidene fluoromethane”, Daniel Kinzel, Sherin Alfalah, Jesús González-Vázquez, Leticia González, EPSRC CoCoChem Summerschool, London, Great Britian
- February 2009 “PHOTOISOMERIZATION VERSUS PHOTODISSOCIATION; QUANTUM DYNAMICAL SIMULATIONS ON A CHIRAL OLEFIN”, Daniel Kinzel, Sherin Alfalah, Jesús González-Vázquez, Leticia González, 10th French-Isreali Symposium on Non-linear and Quantum Optics, Ein Gedi, Israel
- September 2008 “PHOTOISOMERIZATION VERSUS PHOTODISSOCIATION IN CHIRAL OLEFINS; quantum chemical and dynamical simulations for 4-methylcyclohexylidene fluoromethane (4MCF)”, Daniel Kinzel, Sherin Alfalah, Jesús González-Vázquez, Leticia González, 22nd IUPAC Symposium on Photochemistry, Gothenburg, Sweden

Complementary training in foreign laboratories

- December 2011 Two weeks staying in the group of Prof. Dr. Yehuda Haas and Prof. Dr. Shmuel Zilberg, at the Institute of Chemistry, The Hebrew University of Jerusalem, Jerusalem, Israel

April 2010 Four weeks staying in the group of Prof. Dr. Yehuda Haas and Prof. Dr. Shmuel Zilberg, at the Institute of Chemistry, The Hebrew University of Jerusalem, Jerusalem, Israel

Teaching experience

2011–2012	Supervision of an advanced physical chemistry research topic (Forschungspraktikum PC-V; Felix Pröhl and Jan Dworschak)
2010–2011	Supervision of a Diploma-thesis (Leon Freitag)
2009–2010	Supervision of an advanced physical chemistry research topic (Forschungspraktikum PC-V; Sebastian Mai and Martin Thomas)
2008–2009	Supervision of an advanced physical chemistry research topic (Forschungspraktikum PC-V; Robert Kretschmer)
2011	Exercise in Theoretical Chemistry (Wahlpflichtfach, 6 th semester)
2010	Supervision of practical courses in Theoretical Chemistry, (Vertiefungsfach, 8 th semester)
2009–2010	Exercise in Physical Chemistry (PC-V, 7 th semester)
2008–2009	Exercise in Theoretical Chemistry (Vertiefungsfach; 7 th and 8 th semester)

Language skills

German	Mother tongue
English	Fluent in writing and speaking
French	Basic knowledge

IT skills

Scientific	Quantum chemistry suites (Gaussian 09, Molcas, Molpro, Columbus, Turbomole), Newton-X, Fortran and shell programming, molecular and scientific visualization software, L ^A T _E X
General	Office suites, Windows and UNIX/Linux based OSs

List of Publications

1. Stolle, A., Bonrath, W., Ondruschka, B., Kinzel, D., and González, L.
Kinetic Model for the Thermal Rearrangement of *cis*- and *trans*-Pinane
J. Phys. Chem. A **112**, 5885 (2008)
2. Alfalah, S., Kinzel, D., González-Vázquez, J., and González, L.
Non-adiabatic photoisomerization versus photodissociation dynamics of the chiral fluoroethylene derivative (4-methylcyclohexylidene) fluoromethane
Chem. Phys. **369**, 138 (2010)
3. Kinzel, D., Stolle, A., Ondruschka, B., and González, L.
Quantum chemical investigation of the thermal rearrangement of *cis*- and *trans*-pinane
Phys. Chem. Chem. Phys. **12**, 9884 (2010)
4. Kinzel, D., González-Vázquez, J., and L. González
The role of $\pi\sigma^*$ states in the photochemistry of the chiral fluoroethylene derivative (4-methylcyclohexylidene)fluoromethane
Int. J. Quant. Chem. **111**, 3394 (2011)
5. Kretschmer, R., Kinzel, D., and González, L.
The Role of Hydrogen Bonds in Protein-Ligand Interactions. DFT Calculations in 1,3-Dihydrobenzimidazole-2 Thione Derivatives with Glycinamide as Model HIV RT Inhibitors
Int. J. Quant. Chem. **112**, 1786 (2012)
6. Kinzel, D., González-Vázquez, J., and González, L.
H-abstraction is more efficient than *cis-trans* isomerization in (4-methylcyclohexylidene) fluoromethane. An ab initio molecular dynamics study
Phys. Chem. Chem. Phys. **14**, 6241 (2012)
7. Kinzel, D., Marquetand, P., and González, L.
Stark Control of a Chiral Fluoroethylene Derivative
J. Phys. Chem. A, **116**, 2743, (2012)
8. Belz, S., Deeb, O., González, L., Grohmann, T., Kinzel, D., Leibscher, M., Manz, J., Obaid, R., Oppel, M., Xavier, G., and Zilberg, S.,
Nuclear Spin Selective Torsional States: Implications of Molecular Symmetry
Zeitschr. f. Phys. Chem., (accepted), (2013)

9. Almeida, D., Kinzel, D., Ferreira da Silva, F., Puschnigg, B., Gschliesser, D., Scheier, P., Denifl, S., García, G., González, L., and Limão-Vieira, P.

N-site de-methylation in pyrimidine bases as studied by low energy electrons and *ab initio* calculations

Phys. Chem. Chem. Phys., (accepted), (2013)

Selbstständigkeitserklärung

Hiermit erkläre ich, dass ich diese Arbeit selbstständig und ohne Zuhilfenahme weiterer als der angegebenen Hilfsmittel angefertigt habe. Alle verwendeten Textausschnitte, Zitate oder Inhalte anderer Verfasser wurden ausdrücklich als solche gekennzeichnet.

Daniel Kinzel